

Utah State University

DigitalCommons@USU

All Graduate Theses and Dissertations

Graduate Studies

5-2023

The Concept of Multicenter Bonds in Chemistry and Materials Science

Nikolay V. Tkachenko
Utah State University

Follow this and additional works at: <https://digitalcommons.usu.edu/etd>

 Part of the [Chemistry Commons](#)

Recommended Citation

Tkachenko, Nikolay V., "The Concept of Multicenter Bonds in Chemistry and Materials Science" (2023). *All Graduate Theses and Dissertations*. 8732.
<https://digitalcommons.usu.edu/etd/8732>

This Dissertation is brought to you for free and open access by the Graduate Studies at DigitalCommons@USU. It has been accepted for inclusion in All Graduate Theses and Dissertations by an authorized administrator of DigitalCommons@USU. For more information, please contact digitalcommons@usu.edu.



THE CONCEPT OF MULTICENTER BONDS IN CHEMISTRY
AND MATERIALS SCIENCE

by

Nikolay V. Tkachenko

A dissertation submitted in partial fulfillment
of the requirements for the degree

of

DOCTOR OF PHILOSOPHY

in

Chemistry

Approved:

Alexander I. Boldyrev, Ph.D.
Major Professor

Steve Scheiner, Ph.D.
Committee Member

Yi Rao, Ph.D.
Committee Member

Tuan Trinh, Ph.D.
Committee Member

Xiaojun Qi, Ph.D.
Committee Member

D. Richard Cutler, Ph.D.
Vice Provost of Graduate Studies

UTAH STATE UNIVERSITY
Logan, Utah

2023

Copyright © Nikolay V. Tkachenko, 2023

All Rights Reserved

ABSTRACT

The Concept of Multicenter Bonds in Chemistry and Materials Science

by

Nikolay V. Tkachenko, Doctor of Philosophy

Utah State University, 2023

Major Professor: Dr. Alexander I. Boldyrev

Department: Chemistry and Biochemistry

More than 100 years ago G. N. Lewis proposed the shared electron-pair bonding model that may be considered the most successful and generally accepted theory of chemical bonding. However, the Lewis model is not comprehensive, and it cannot describe the entire diversity of chemical species. A vivid illustration of the limitation of Lewis's theory is the diborane molecule (B_2H_6), for which it is impossible to describe chemical bonding pattern only in terms of one-center two-electron (1c-2e) and two-center two-electron (2c-2e) bonding elements. However, *the electron-pair bonding model can be completed with the inclusion of multicenter bonding elements* where the number of centers can reach the number of atoms in the described system.

This dissertation includes six research projects, that investigate and expand the applicability of the concept of multicenter bonds in 3D clusters and cluster-based materials. Firstly, the dissertation introduces the theoretical background of the Adaptive Natural Density Partitioning (AdNDP) algorithm - a method that we extensively employed. During my Ph.D. study, I updated and expanded the applicability of this method, which resulted in the AdNDP 2.0 software. Using this updated program, we showed that multicenter bonds

can explain the structure, stability, and several physical properties of various novel clusters and solids. Thus, we were the first who introduced the concept of multicenter bonds in application to nonagermanide ($[\text{Ge}_9]^{4-}$) clusters. After that finding, similar bonding patterns were further found in other novel germanium and tin clusters synthesized by our collaborators. Finally, we showed how the concept of multicenter bonds can be useful in materials science, and how it helped us to design a new superoctahedral two-dimensional metallic boron material with unique physical properties.

The main advancement of this dissertation is the introduction of the delocalized bonding model in 3D clusters. The studied cases include $[\text{Ge}_9]^{4-}$, $[\text{Ge}_{16}\text{Zn}_6]^{4-}$, $[\text{Ge}_{16}\text{Cd}_6]^{4-}$, $[\text{Ge}_{24}]^{4-}$ and $\{[\text{K}_2\text{ZnSn}_8(\text{ZnMes})]_2\}^{4-}$. In addition to that, we also extended this concept to novel magnetic boron material. We believe that the idea of multicenter bonds will advance in the future and help to create novel 3D materials and molecules with the desired physical and chemical properties.

(209 pages)

PUBLIC ABSTRACT

The Concept of Multicenter Bonds in Chemistry and Materials Science

Nikolay V. Tkachenko

Chemical bonds are components of a universal and compact language of chemistry that was empirically developed before the modern concepts of quantum physics. This language explains how molecules and solids keep together. In particular, Lewis's shared electron-pair bonding model may be considered the most successful and generally accepted theory of chemical bonding due to its simplicity and predictive power. However, there is an entire world of chemical species where the classical Lewis bonding language fails to describe the bonding pattern adequately. Those cases include but are not limited to compounds with a significant electron delocalization (where electron density spread on a region that spans more than 2 atoms) such as so-called aromatic and anti-aromatic compounds. In this dissertation, we are showing that there are some essential "words" missing in the "vocabulary" of classical Lewis's chemical bonds language. To cover most of the chemical species, the electron-pair bonding model *can be extended with the inclusion of multicenter bonds* where the number of centers can reach the number of atoms in the described system. This dissertation includes six research projects, that investigate and expand the applicability of the concept of multicenter bonds in chemistry and materials science. We showed that such a developed chemical bonding model has great predictive power and can explain the structure, stability, and several physical properties of various unusual clusters and solids. Since the chemical bonding pattern can be related to reactivity, structure, and

physical properties, we believe, that the concept of multicenter bonds could be developed in the future up to the level where we will be able to design novel materials with ever-wanted physical and chemical properties.

ACKNOWLEDGMENTS

First of all, I would like to express my sincerest appreciation to my scientific supervisor and major Professor Alexander Boldyrev. He is an exceptional person who supported me during the entire Ph. D. program. Alexander Ivanovich is an excellent scientist, a true professional in his field who works with dedication. He inspired and motivated me to develop further and stay on this thorny path of academic research. I learned a lot from him, and I cherish every conversation with him. Each talk with Alexander Ivanovich included a ton of inspiration, an ocean of great ideas, and a huge portion of useful career advice based on his enormous academic experience. He is a great person, mentor, and teacher.

I would like to thank members of my dissertation committee: Yi Rao, Steve Scheiner, Xiaojun Qi, David Farrelly, and Tuan Trinh, for their valuable comments, fruitful discussions, support, and encouragement.

I am grateful to all the collaborators with whom I had a chance to work during my Ph.D. study. It was a pleasure for me to work with such talented and exceptional scientists as Zhong-Ming Sun (Nankai University, China), Ivan Popov (The University of Akron, USA), Alvaro Munoz-Castro (Universidad San Sebastián, Chile), Li-Ming Yang (Huazhong University of Science and Technology, China), Vladimir Minkin (Southern Federal University, Russia), Artem Oganov (Skolkovo Institute of Science and Technology, Russia), Jean-Marie Lehn (Supramoléculaires Université de Strasbourg, France), Henry F. Schaefer III (University of Georgia, USA), Sergei Tretiak (Los Alamos National Laboratory, USA), Pavel Dub (Los Alamos National Laboratory, USA), and many others.

I appreciate the members and alumni of Boldyrev's group: Dmitry Zubarev, Katie Lundell, Maksim Kulichenko, Nikita Fedik, Pavel Rublev, and Anton Pozdeev for the productive discussions, interesting suggestions, mental tonus, and healthy competition.

During my Ph.D. study at Utah State University, I have been supported by the National Science Foundation (grant CHE-1664379 to Prof. Alexander I. Boldyrev), R. Gaurth Hansen Professorship funds (to Prof. Alexander I. Boldyrev), Teaching Assistantships (Department of Chemistry and Biochemistry, Utah State University), Stephen Bialkowski Award in Environmental Chemistry (Department of Chemistry and Biochemistry, Utah State University), and Los Alamos National Laboratory. I also would like to acknowledge the Center for High Performance Computing at the University of Utah for the access to the computing resources.

I am grateful to my beloved wife Anastasiia Tkachenko, who helped and supported me all the time. I would not have gotten this far without her. She is the most amazing person in the world and I love her very much. She is my soulmate and my best friend.

I dedicate this dissertation to my loving parents Vadim and Marina, to my younger brothers Sasha and Misha, to my sister Katya and to my grandparents Nina Kozyreva, Evgeny Kozyrev, Irina Tkachenko, and Oleg Tkachenko. They teach, support, and inspire me all my life. They are the most precious people I have and I love them very much.

Nikolay V. Tkachenko

CONTENTS

	Page
ABSTRACT.....	iii
PUBLIC ABSTRACT	v
ACKNOWLEDGMENTS	vii
LIST OF TABLES	xii
LIST OF FIGURES	xiii
CHAPTER 1 INTRODUCTION	1
1.1 Development of Chemical Bonding Models.....	1
1.2 Quantum Chemical Tools for Analyzing Chemical Bonding	3
1.3 Multicenter Bonding in Zintl Clusters	5
1.4 Chemical Bonding in Materials Science.....	6
References.....	7
CHAPTER 2 CHEMICAL BONDING ANALYSIS OF EXCITED STATES USING THE ADAPTIVE NATURAL DENSITY PARTITIONING METHOD	11
Abstract.....	11
2.1 Introduction.....	11
2.2 Computational Methods.....	14
2.2.2 <i>Symmetric direct search</i>	17
2.2.3 <i>Bonding analysis of unrestricted and open shell systems</i>	18
2.2.4 <i>Excited states bonding analysis</i>	18
2.3 Results and discussion	19
2.3.1 <i>H₂O molecule</i>	19
2.3.2 <i>B₅⁺ cluster</i>	20
2.3.3 <i>C₂H₄⁺ species</i>	21
2.4 Conclusions.....	22
References.....	22
Tables and figures.....	27

CHAPTER 3 MULTIPLE LOCAL σ -AROMATICITY OF NONAGERMANIDE CLUSTERS 30

Abstract.....	30
3.1 Introduction.....	30
3.2 Computational methods	32
3.3 Results and discussion	32
3.3 Conclusions.....	36
References.....	37
Tables and figures.....	41

CHAPTER 4 SYMMETRY COLLAPSE DUE TO THE PRESENCE OF MULTIPLE LOCAL AROMATICITY IN Ge_{24}^{4-} 55

Abstract.....	55
4.1 Introduction.....	55
4.2 Results.....	57
4.2.1 Preparation of the anionic Ge_{24}^{4-} cluster.....	57
4.2.2 Experimental characterization of Ge_{24}^{4-} cluster.....	58
4.2.3 Computational Studies	61
4.3 Conclusions.....	65
4.4 Methods	65
4.4.1 Materials	65
4.4.2 Synthesis of $[\text{K}(2,2,2\text{-crypt})]_4\text{Ge}_{24} (1)$	66
4.4.3 X-ray diffraction.....	66
4.4.4 Electrospray ionization mass spectrometry (ESI-MS).....	66
4.4.5 Energy dispersive X-ray (EDX)	67
4.4.6 Powder X-ray diffraction	67
4.4.7 Magnetic response analysis	67
4.4.8 Chemical bonding analysis.....	68
References.....	68
Tables and figures.....	76

CHAPTER 5 $[\text{Sn}_8]^{6-}$ -BRIDGED MIXED-VALENCE $\text{Zn}^{\text{I}}/\text{Zn}^{\text{II}}$ IN $\{[\text{K}_2\text{ZnSn}_8(\text{ZnMes})]_2\}^{4-}$ INVERSE SANDWICH-TYPE CLUSTER SUPPORTED BY A $\text{Zn}^{\text{I}}-\text{Zn}^{\text{I}}$ BOND..... 82

Abstract.....	82
5.1 Introduction.....	82
5.2 Results and Discussions.....	84
5.3 Quantum Chemical Methods.....	90
5.3 Conclusions.....	91
References.....	91
Tables and figures.....	98
CHAPTER 6 σ -AROMATICITY-INDUCED STABILIZATION OF HETEROMETALLIC SUPERTETRAHEDRAL CLUSTERS $[\text{Zn}_6\text{Ge}_{16}]^{4-}$ AND $[\text{Cd}_6\text{Ge}_{16}]^{4-}$	104
Abstract.....	104
6.1 Introduction.....	104
6.2 Results and Discussions.....	105
6.3 Conclusions.....	111
References.....	111
Tables and figures.....	115
CHAPTER 7 SUPEROCTAHEDRAL TWO-DIMENSIONAL METALLIC BORON WITH PECULIAR MAGNETIC PROPERTIES.....	120
Abstract.....	120
7.1 Introduction.....	121
7.2 Computational methods.....	122
7.3 Results and discussion.....	123
7.4 Conclusions.....	129
References.....	130
Tables and figures.....	136
CHAPTER 8 SUMMARY.....	148
APPENDICES.....	152
Appendix A: Permission Letters for Journal Copyright Release.....	153
Appendix B: Permission Letters from Coauthors.....	169
CURRICULUM VITAE.....	181

LIST OF TABLES

Table	Page
Table 3-1. Relative energies with ZPE corrections (kcal mol^{-1}) of D_{3h} and C_{4v} $[\text{Ge}_9]^{4-}$ structures at various levels of theory.	41
Table 3-2. Cartesian coordinates of points for NICS calculation.	42
Table 3-3. NICS_{zz} and NICS_{iso} indices calculated at chosen points for D_{3h} and C_{4v} $[\text{Ge}_9]^{4-}$ clusters.....	43
Table 7-1. Lattice constants, atomic positions and total energies of the NM and FM 2D- B_6 monolayers.....	136
Table 7-2. The calculated elastic constants (c_{ij} , in N m^{-1}), Young's modulus (Y_{2D} , in N m^{-1}), and Poisson's ratio (ν) of the 2D- B_6 monolayer.....	137

LIST OF FIGURES

Figure	Page
Figure 2-1. Optimized structures of the water molecule in the ground electronic state (A top) and in the first excited electronic state (B top); the results of the extended AdNDP analysis of the ground state (A bottom) and the first excited state (B bottom) at the ground state optimized geometry.	27
Figure 2-2. Optimized structures of the B_5^+ cluster in the ground electronic state (A top) and in the first excited electronic state (B top); the results of the extended AdNDP analysis of the ground state (A bottom) and the first excited state (B bottom) at the ground state optimized geometry.	28
Figure 2-3. Optimized structures of the $C_2H_4^+$ molecule in the ground electronic state (A top) and in the first excited electronic state (B top); the results of the extended AdNDP analysis of the ground state (A bottom) and the first excited state (B bottom) at the ground state optimized geometry.	29
Figure 3-1. Side and top views of a (a) tricapped trigonal prism (D_{3h} symmetry) and (b) capped square antiprism (C_{4v} symmetry).	44
Figure 3-2. Overall chemical bonding picture obtained for the C_{4v} capped square antiprism $[Ge_9]^{4-}$ cluster. ON denotes the occupation number (equal to 2.00 e in an ideal case). Lines between atoms help in visualization and do not represent 2c–2e bonds here and elsewhere.	45
Figure 3-3. Overall chemical bonding picture obtained for the D_{3h} tricapped trigonal prism $[Ge_9]^{4-}$ cluster.	46
Figure 3-4. Points that were chosen for the NICS indices calculation.	47
Figure 3-5. Chemical bonding picture of C_{4v} $[Si_9]^{4-}$ cluster.	48
Figure 3-6. Chemical bonding picture of D_{3h} $[Si_9]^{4-}$ cluster.	49
Figure 3-7. Chemical bonding picture of C_{4v} $[Sn_9]^{4-}$ cluster.	50
Figure 3-8. Chemical bonding picture of the core Ge_9 fragment obtained for the $[Ge_9\{P(NH_2)_2\}_3]^-$ cluster.	51
Figure 3-9. Chemical bonding picture of $Cu[Ge_9\{P(NH_2)_2\}_3]$ cluster.	52
Figure 3-10. Chemical bonding picture of $Cu(NHC)[Ge_9\{P(NH_2)_2\}_3]$ cluster.	53

Figure 3-11. Chemical bonding of the Cu atom in the $\text{Cu}(\text{NHC})[\text{Ge}_9\{\text{P}(\text{NH}_2)_2\}_3]^-$ cluster..... 54

Figure 4-1. Structures of the Ge_{24}^{4-} cluster and its selected fragments. (a) Ge_{24}^{4-} cluster (1a) (thermal ellipsoids are drawn at 50 % probability). (b) The contrast of bowl-shaped Ge_6 fragment (top, Ge10-Ge15) with bowl depth of 0.93 Å and corannulene $\text{C}_{20}\text{H}_{10}$ (bottom) with ~0.88 Å. (c) The bowl-shaped Ge_6 fragment shown from a vertical view. (d) View of Ge_9 cage (Ge10-Ge18). (e) The distorted prism Ge_6 fragment consisting of a triangle of Ge7–9 and an extended triangle of Ge10–12. All selected bond lengths are given in Å. The Ge and C atoms are drawn in yellow and blue, respectively. 76

Figure 4-2. The selected valence molecular orbitals and chemical components of the electron density of Ge_{24}^{4-} . (a) Selected lowest-lying and frontier valence molecular orbitals in the Ge_{24}^{4-} cluster. Different phases of molecular orbitals are represented with different colors. Positive: magenta; negative: purple. (b) The chemical components of the valence-electron density of Ge_{24}^{4-} with the corresponding electron populations from the EDDB method. Isosurface value is set at $\pm 0.015 |e|$ 77

Figure 4-3. Chemical bonding pattern of the Ge_{24}^{4-} cluster. Different phases of bonding elements are represented with different colors. Positive: red; negative: blue. 78

Figure 4-4. AdNDP analysis of Ge_8 antiprism fragment of Ge_{24}^{4-} (a) and $\text{C}_{4v}\text{-Ge}_9^{4-}$ (b) clusters..... 79

Figure 4-5. Contour plots and isosurfaces of magnetic response of the Ge_{24}^{4-} cluster and various Ge_9^{4-} units. (a) Isosurface and contour plot representation for NICS_{iso} and certain orientations of the external field for Ge_{24}^{4-} . Isosurface value is set at ± 3.0 ppm. (b) Isosurface representation for NICS_{iso} and certain orientations of the external field for the three isolated Ge_9^{4-} units, as found in Ge_{24}^{4-} . Isosurface value is set at ± 3.0 ppm. Blue surface: shielding; Red surface: deshielding..... 80

Figure 4-6. Isosurface representation for the induced magnetic field for $[\text{Ge}_{24}]^{4-}$ under different orientations of the external field, noted by arrows. Isosurface value set at ± 3.0 ppm. 81

Figure 5-1. a) The cluster anion $\{[\text{K}_2\text{ZnSn}_8(\text{ZnMes})]_2\}^{4-}$ (thermal ellipsoids are drawn at 50 % probability). b) The structure of fragment $[\text{K}_4\text{Zn}_2\text{Sn}_8]$ is shown by a rotation of 90 degrees. The Zn-Zn bond length is given in Å. c) The contrast of *closo*- $[\text{Zn}_2\text{Sn}_8]$ moiety in anion 1a and *closo*- $[\text{Li}_2\text{Sn}_8]^{4-}$ in the Zintl phase $\text{K}_4\text{Li}_2\text{Sn}_8$. The average bond lengths are given in Å..... 98

- Figure 5-2. Plots of HOMO/HOMO-1 molecular orbitals and their energy (Hartree) for $\{[\text{K}_2\text{ZnSn}_8(\text{ZnMes})]_2\}^{4-}$ cluster..... 99
- Figure 5-3. The results of AdNDP analysis for $\{[\text{K}_2\text{ZnSn}_8(\text{ZnMes})]_2\}^{4-}$ cluster. Bonding elements are plotted at an iso-value of 0.03 a.u. Different phases of a wave function represented with different colors. Positive: red; negative: blue. For figure compactness, two multicentered bonds are plotted for each structure..... 100
- Figure 5-4. The complete chemical bonding pattern of $[\text{Sn}_8]^{6-}$ cluster..... 101
- Figure 5-5. Three-dimensional (left) and contour-plot (right) representation of the magnetic response B^{ind} for $\{[\text{K}_2\text{ZnSn}_8(\text{ZnMes})]_2\}^{4-}$. Isosurface values are set at ± 2.0 ppm. Blue: shielding, red, deshielding regions..... 102
- Figure 5-6. ELF plots of $\{[\text{K}_2\text{ZnSn}_8(\text{ZnMes})]_2\}^{4-}$ cluster. A) plot is built in the plane of C_6 rings; B) plot is built in the plane of K_4 square. 103
- Figure 6-1. A) Formation scheme of $[\text{M}_6\text{Ge}_{16}]^{4-}$ (M=Zn or Cd); B) Ellipsoid plot (50 % level) of the crystal structure of $[\text{Zn}_6\text{Ge}_{16}]^{4-}$ (the same structure for $[\text{Cd}_6\text{Ge}_{16}]^{4-}$); C) The experimental and computed geometries of the Ge-Ge₂-M unit in $[\text{M}_6\text{Ge}_{16}]^{4-}$ and the average distances of Ge-M and Ge-Ge are given in Å..... 115
- Figure 6-2. The assembly mechanism of tetrahedral cluster $[\text{Zn}_6\text{Ge}_{16}]^{4-}$. Species that have been observed in the mass spectra are boxed (c, d, e, f, 1a)..... 116
- Figure 6-3. A) 3c-2e Ge-Ge-Ge σ -bonds of $[\text{Zn}_6\text{Ge}_{16}]^{4-}$ shown superimposed on the molecular framework (three bonds per Ge_4); B) 3c-2e Zn-Ge-Ge σ -bonds of $[\text{Zn}_6\text{Ge}_{16}]^{4-}$ shown superimposed on the molecular framework (three bonds per Ge_4); C) ELF distribution in rectangular Ge_4Zn fragment (right) and square Zn_4 fragment (left). ON denotes occupation number. The same AdNDP and ELF pictures are identified for $[\text{Cd}_6\text{Ge}_{16}]^{4-}$, both are omitted for clarity..... 117
- Figure 6-4. Localized lone pairs of $[\text{Zn}_6\text{Ge}_{16}]^{4-}$ 118
- Figure 6-5. Magnetic response properties of $[\text{Zn}_6\text{Ge}_{16}]^{4-}$, given by isotropic term ($B^{\text{ind}}_{\text{iso}}$), and under specific orientations of the external field (B^{ind}_z , B^{ind}_x , and B^{ind}_y). Isosurfaces at ± 5 ppm; Blue: shielding; Red: deshielding. The same features are found for $[\text{Cd}_6\text{Ge}_{16}]^{4-}$ 119
- Figure 7-1. (a) The top view of the 2D- B_6 structure. The unit cell is shown with a green dashed square. (b) The side view of the 2D- B_6 structure. The two different types of boron atoms are labeled B_I and B_{II} . (c) The angle view of the 2D- B_6 structure. 138

Figure 7-2. Spin charge density distribution with isosurface $0.002 \text{ e}/\text{\AA}^{-3}$ for the ferromagnetic 2D-B ₆	139
Figure 7-3. Magnetic ordering and relative total energies for the $2 \times 2 \times 1$ supercell of the 2D-B ₆ sheet.	140
Figure 7-4. Calculated phonon dispersion curves along the Γ -M-X- Γ path and phonon density of states for the ferromagnetic 2D-B ₆ material.	141
Figure 7-5. Calculated phonon dispersion curves along the Γ -M-X- Γ path and phonon density of states for the nonmagnetic 2D-B ₆ material.	142
Figure 7-6. Calculated electronic band structure along the Γ -M-X- Γ path and density of states for ferromagnetic 2D-B ₆ . The red curves correspond to the spin up electrons, while the spin down electrons are illustrated with blue curves. The Fermi level is shown as a horizontal dotted black line.	143
Figure 7-7. Calculated fluctuations of the total magnetic moment and temperature vs. simulation time step at 100 K (left column), 300 K (center column) and 450 K (right column).	144
Figure 7-8. Top and side views of final frames of each MD simulation test at different temperatures.	145
Figure 7-9. Overall chemical bonding picture obtained for the B ₆ H ₄ cluster in the triplet state. The abbreviation ON denotes the occupation number of a certain bond....	146
Figure 7-10. Overall chemical bonding picture obtained for the 2D-B ₆ sheet. The results for the spin up and spin down electrons are presented separately.....	147

CHAPTER 1

INTRODUCTION

1.1 Development of Chemical Bonding Models

The term "chemical bond" is the basis of the universal language of chemistry. Although there is no exact definition of a chemical bond in terms of a quantum mechanical observable (there is no quantum mechanical operator for the chemical bond), this concept is useful and essential component of chemistry. The predictive power of various models based on the concept of chemical bonds is very high. Even the simplest valence-shell electron-pair repulsion (VSEPR) model, which all of us learned in schools and universities, predicts the molecular structure of many compounds. One may state that with the development of quantum chemical methods and modern computing resources there is no need to use the language of chemical bonds. I would argue with that statement. While the ground state electronic wavefunction of the chemical system within the Born-Oppenheimer approximation can indeed be used to calculate many of the physical properties of the system, the multidimensional nature of the many-body wavefunction frequently renders this model as a computational tool rather than a model that provides a simple explanation and understanding of the chemical system. As Eugene Wigner said: *"It is nice to know that the computer understands the problem. But I would like to understand it too."*

The key idea of shared electron-pair as a building block of chemical bonds was introduced by Gilbert Lewis in 1916,¹ even before quantum mechanics was developed. Based only on the experimental chemical data available in those days, Lewis built an elegant model with great predictive power that can be considered the most successful and generally accepted theory of chemical bonding even now. The Lewis model is describing

a completely localized picture, since the main building elements of this model are localized electrons that form chemical bonds and lone pairs.

Later in 1925² and 1926,³ Werner Heisenberg and Erwin Schrödinger published their groundbreaking pioneering works, which later became the basis of quantum mechanics. Heisenberg's matrix mechanics and Schrödinger's wave mechanics provided the mathematical framework for understanding the behavior of small particles including electrons. Shortly after this discovery, in 1927 Walter Heitler and Fritz London published their work⁴ where they applied the principles of quantum mechanics to the study of chemical bonding in the hydrogen molecule. The main idea that they stated was that the origin of chemical bonding may come from the phase combination (constructive overlap) of separate electronic wavefunctions. The ideas of this work were expanded by other scientists, leading to the development of advanced quantum chemical methods and tools that are widely used today.

In 1927, Robert Mulliken and Friedrich Hund developed a molecular orbital (MO) theory^{5,6} that introduced a delocalized description of electrons in chemical systems. This point of view significantly contradicted the earlier Lewis description that focused on localized electron pairs. Nevertheless, molecular orbital theory showed its predictive and descriptive power by solving the problems (e.g., the explanation of the triplet state of the O₂ molecule) that the Lewis model cannot solve. Nowadays the MO theory is a basis for many modern quantum chemical calculations. Interestingly, over time, various electron localization techniques were developed that convert the delocalized molecular orbitals into localized Lewis-like structures, connecting two worlds.

In an attempt to connect the Lewis model and quantum theory, Linus Pauling proposed an alternative valence bond (VB) theory.^{7,8} The VB approach was based on a linear combination of localized two-center product function of one-center atomic orbitals and naturally integrates important bonding concepts such as resonance structures and hybridization. Although this approach can be outperformed by other theories, for many cases, the VB model provides a more intuitive and easily interpretable description of chemical bonding than MO theory (although the concept of resonance must be invoked when describing the system with significant electron delocalization), and it can be very helpful for the explanation of the systems with multireference character.

1.2 Quantum Chemical Tools for Analyzing Chemical Bonding

It may seem that nowadays chemists know everything about chemical bonds. However, this is a big misconception. The development of new chemical bonding models is an active and evolving direction of physical chemistry. To illustrate it, in this subsection, I will review the recent quantum chemical tools for chemical bonding analysis. There are currently several fundamentally different approaches that exist to analyze chemical bonds. One large branch of quantum chemical tools is based on the analysis of MOs and bond lengths. These techniques associate a particular number (bond index) with a selected atomic combination. The general definition of the bond index was given by Wiberg.⁹ Since then, numerous bond indices have been proposed to describe chemical bonding in various systems including three-center bond index proposed by Giambiagi *et al.* and Kar *et al.*,^{10,11} bond index of a system calculated in nonorthogonal basis sets proposed by Mayer,^{12,13} electron sharing index (ESI) proposed by Fulton,^{14,15} delocalization indexes (DI),^{16,17} and other.¹⁸

Methods that do not directly reveal the concept of chemical bond have made significant contributions to the description of chemical systems and chemical bonding.¹⁹⁻³⁵ These techniques are based on different types of electron density distribution analysis. A quantum theory of atoms in molecules (QTAIM)¹⁹ based on the topology of the electron density is one of these methods. Other examples are methods based on the Pauli exclusion principle such as electron localization function (ELF)²⁷ and Fermi Hole (FH) function analysis. Various electron density partitioning algorithms such as electron density of delocalized bonds (EDDB) were also introduced recently.³⁵

The localized Lewis description of chemical bonding in molecules can be obtained after application of various electron density localization techniques based on wave function invariance with respect to the unitary transformation.³⁶⁻⁴⁰ Those methods have been used successfully to interpret chemical bonding of many molecular systems. A particularly interesting and useful localization technique, Natural Bond Orbitals (NBOs) analysis was proposed by Winhold.⁴¹ NBOs are localized few-center orbitals that optimally describe the Lewis-like molecular bonding pattern of electron pairs. The method is based on the diagonalization of blocks of first-order reduced density matrix in natural atomic orbitals basis.

Following the general ideas of the NBO analysis, Alexander Boldyrev and Dmitry Zubarev developed Adaptive Natural Density Partitioning (AdNDP) algorithm,⁴² a tool capable of deciphering bonding in molecules, clusters, and solids. Being formally a generalization of NBO technique, the AdNDP is an electron-localization technique that partitions the natural density of the system and reproduces the most occupied localized bonding elements. The main advantage of this method is that we can represent a chemical

bonding pattern in terms of both Lewis bonding elements (lone pairs, two-center two-electron (2c-2e) bonds) and delocalized bonding elements (nc-2e bonds). The latter is associated with the concepts of aromaticity and antiaromaticity. Invoking the delocalized bonding elements allows the method to avoid the resonance structure description. As a result, the obtained chemical bonding patterns are consistent with the symmetry and electron counting of a system. Chapter 2 describes recent advances of the method that were developed during this Ph.D. study. The new features of the algorithm were introduced, and the capability of the software was expanded so the chemical bonding of excited state molecules can be analyzed with the AdNDP method.⁴³

New theoretical techniques and novel experiments allow us to improve our understanding of the chemical bond, requiring us to revise and expand currently available models. The next two subsections summarize the main areas that were studied in this Ph.D. work.

1.3 Multicenter Bonding in Zintl Clusters

Zintl clusters are many-atom multiply charged ions composed of Group 13, 14, and 15 elements that exhibit a wide diversity of unusual structures starting from tetrahedral $[\text{Ge}_4]^{4-}$ to worm-like largest isolated Tin nanorod $[\text{Sn}_{36}]^{4-}$.⁴⁴⁻⁴⁶ Zintl clusters have unusual chemical activity and there are several examples of their use in catalysis. Due to their peculiar chemistry and unique structure, Zintl clusters are also widely utilized as precursors for the synthesis of novel compounds in inorganic chemistry. Importantly, the chemical bonding of most Zintl clusters is difficult to describe by the standard models used in chemistry. Without a chemical bonding description, it is hard to explain their unusual structures and chemical reactivity. In this dissertation, I developed a model of chemical bonding for a series of 3D clusters, synthesized and experimentally characterized by our collaborators.

Using the AdNDP analysis, I introduced a multi-center bonding description, showing that the major contribution to the chemical bonding in studied Zintl clusters came from the delocalized bonding elements (chemical bonds that are associated with more than two atomic centers). Thus, Chapter 3 introduces a new description of the chemical bonding in nonagermanide clusters.⁴⁷ Whereas in Chapters 4-6 I further develop the idea introduced in Chapter 3, showing the similar delocalized chemical bonding motifs in newly synthesized $[\text{Ge}_{24}]^{4-}$, $\{[\text{K}_2\text{ZnSn}_8(\text{ZnMes})]_2\}^{4-}$, $[\text{Ge}_{16}\text{Zn}_6]^{4-}$, and $[\text{Ge}_{16}\text{Cd}_6]^{4-}$ clusters.⁴⁸⁻⁵⁰

1.4 Chemical Bonding in Materials Science

Designing new materials has always been a very attractive topic for both the scientific community and industry. Success in materials design often includes most of the scientific imagination and huge experience in physics and chemistry. Methods aimed at the rational design of new materials are paid more attention nowadays. The description of solids in terms of chemical bonding is an effective tool for generating new materials with specific properties. Developed in Alexander Boldyrev's group, Solid State Adaptive Natural Density Partitioning (SSAdNDP)⁵¹ method is an effective way to describe solids in a chemically intuitive way.⁵²⁻⁵⁴ Similar to non-periodic AdNDP algorithm, this method yields localized and inherently chemical interpretation of bonding in periodic systems involving both the concept of Lewis bonding elements (lone pairs and two-centered two-electron bonds) and the concept of delocalized bonding elements. The SSAdNDP method gives insights into the structure, reactivity, and physical properties of bulk materials. Based on this methodology, we predicted novel boron ferromagnetic materials (2D-B₆) that potentially can be used in spintronic devices. The result of this study is summarized in Chapter 7 of this dissertation.⁵⁵

References

- (1) G. N. Lewis, *J. Am. Chem. Soc.*, **1916**, 38, 762.
- (2) W. Heisenberg, *Z. Phys.*, **1925**, 33, 879.
- (3) E. Schrodinger, *Ann. Physik*, **1926**, 79, 361.
- (4) W. Heitler and F. London, *Z. Phys.*, **1927**, 44, 455.
- (5) F. Hund, *Z. Phys.*, **1931**, 73, 1.
- (6) R. S. Mulliken, *Phys. Rev.*, **1932**, 41, 49.
- (7) L. Pauling, *J. Am. Chem. Soc.*, **1931**, 53, 1367.
- (8) L. Pauling, *J. Am. Chem. Soc.*, **1931**, 53, 3225.
- (9) K. B. Wiberg, *Tetrahedron*, **1968**, 24, 1083.
- (10) M. Giambiagi, M. S. Giambiagi and K. C. Mundim, *Struct. Chem.*, **1990**, 1, 423.
- (11) A. B. Sannigrahi and T. Kar, *Chem. Phys. Lett.*, **1990**, 173, 569.
- (12) I. Mayer, *Chem. Phys. Lett.*, **1983**, 97, 270.
- (13) I. Mayer, *Int. J. Quantum Chem.*, **1986**, 29, 73.
- (14) R. L. Fulton and S. T. Mixon, *J. Phys. Chem.*, **1993**, 97, 7530.
- (15) R. L. Fulton, *J. Phys. Chem.*, **1993**, 97, 7516.
- (16) X. Fradera, M. A. Austen and R. F. W. Bader, *J. Phys. Chem. A*, **1999**, 103, 304.
- (17) R. F. W. Bader and M. E. Stephens, *J. Am. Chem. Soc.*, **1975**, 97, 7391.
- (18) E. Matito, M. Sola, P. Salvador and M. Duran, *Faraday Discuss.*, **2007**, 135, 325.
- (19) R. F. W. Bader, *Atoms in Molecules: A Quantum Theory*, Oxford University Press, Oxford, **1990**.
- (20) V. K. Artman, *Z. Naturforsch.*, **1946**, 1, 426.
- (21) J. E. Lenard-Jones, *Proc. R. Soc. London, Ser. A*, **1949**, 198, 14.

- (22) J. E. Lenard-Jones, *Proc. R. Soc. London, Ser. A*, **1949**, 198, 1.
- (23) R. Daudel, *Quantum Theory of the Chemical Bond*, Reidel, Dordrecht, **1974**.
- (24) R. F. W. Bader and M. E. Stephens, *J. Am. Chem. Soc.*, **1975**, 97, 7391.
- (25) W. L. Luken and J. C. Culberson, *Int. J. Quantum Chem.*, **1982**, 22, 265.
- (26) A. D. Becke and K. E. Edgecombe, *J. Chem. Phys.*, **1990**, 92, 5397.
- (27) B. Silvi and A. Savin, *Nature*, **1994**, 371, 683.
- (28) P. A. Fuentealba, *Int. J. Quantum Chem.*, **1998**, 69, 559.
- (29) R. Ponec and D. L. Cooper, *J. Phys. Chem. A*, **2007**, 111, 11294.
- (30) F. Fantuzzi and M. A. C. Nascimento, *J. Chem. Theory Comput.*, **2014**, 10, 2322.
- (31) J. H. Lange and I. Cukrowski, *J. Comput. Chem.*, **2018**, 39, 1517.
- (32) B. G. Janesko, G. Scalmani and M. J. Frisch, *J. Chem. Phys.*, **2014**, 141, 144104.
- (33) E. Ramos-Cordoba, P. Salvador and M. Reiher, *Chem. Eur. J.*, **2013**, 19, 15267.
- (34) D. L. Cooper, R. Ponec and M. Kohout, *Mol. Phys.*, **2016**, 114, 1270.
- (35) D. W. Szczepanik, M. Andrzejak, J. Dominikowska, B. Pawełek, T. M. Krygowski, H. Szatyłowicz and M. Solà, *Phys. Chem. Chem. Phys.*, **2017**, 19, 28970.
- (36) J. M. Foster and S. F. Boys, *Rev. Mod. Phys.*, **1960**, 32, 300.
- (37) C. Edmiston and K. Ruedenberg, *Rev. Mod. Phys.*, **1963**, 35, 457.
- (38) J. Pipek and P. G. Mezey, *J. Chem. Phys.*, **1989**, 90, 4916.
- (39) J. P. Foster and F. Weinhold, *J. Am. Chem. Soc.*, **1980**, 102, 7211.
- (40) A. E. Reed, L. A. Curtiss and F. Weinhold, *Chem. Rev.*, **1988**, 88, 899.
- (41) F. Weinhold and C. R. Landis, *Valency and Bonding: A Natural Bond Orbital Donor–Acceptor Perspective*, Cambridge University Press, Cambridge, UK, **2005**.
- (42) D. Y. Zubarev and A. I. Boldyrev, *Phys. Chem. Chem. Phys.*, **2008**, 10, 5207.

- (43) N. V. Tkachenko and A. I. Boldyrev, *Phys. Chem. Chem. Phys.*, **2019**, *21*, 9590.
- (44) N. V. Tkachenko, W. X. Chen, H. W. T. Morgan, A. Muñoz-Castro, A. I. Boldyrev and Z. M. Sun, *Chem. Commun.*, **2022**, *58*, 6223.
- (45) N. V. Tkachenko, X. W. Zhang, L. Qiao, C. C. Shu, D. Steglenko, A. Munoz-Castro, Z. M. Sun and A. I. Boldyrev, *Chem. Eur. J.*, **2020**, *26*, 2073-2079.
- (46) H. L. Xu, N. V. Tkachenko, Z. C. Wang, W. X. Chen, L. Qiao, A. Munoz-Castro, A. I. Boldyrev and Z. M. Sun, *Nat. Commun.*, **2020**, *11*, 5286.
- (47) N. V. Tkachenko and A. I. Boldyrev, *Chem. Sci.*, **2019**, *10*, 5761.
- (48) H. L. Xu, I. A. Popov, N. V. Tkachenko, Z. C. Wang, A. Munoz-Castro, A. I. Boldyrev and Z. M. Sun, *Angew. Chem. Int. Ed.*, **2020**, *59*, 17286.
- (49) H. L. Xu, N. V. Tkachenko, A. Munoz-Castro, A. I. Boldyrev and Z. M. Sun, *Angew. Chem. Int. Ed.*, **2021**, *60*, 9990.
- (50) H. L. Xu, N. V. Tkachenko, D. Szczepanik, I. A. Popov, A. Muñoz-Castro, A. I. Boldyrev, Z. M. Sun, *Nat. Commun.*, **2022**, *13*, 2149.
- (51) T. R. Galeev, B. D. Dunnington, J. R. Schmidt and Alexander I. Boldyrev, *Phys. Chem. Chem. Phys.*, **2013**, *15*, 5022.
- (52) N. V. Tkachenko, B. Song, D. Steglenko, R. M. Minyaev, L. M. Yang and A. I. Boldyrev, *Phys. Status Solidi B*, **2019**, *257*, 1900619.
- (53) D. Steglenko, N. V. Tkachenko, A. I. Boldyrev, R. M. Minyaev and V. I. Minkin, *J. Comp. Chem.*, **2020**, *41*, 1456.
- (54) I. V. Getmanskii, V. V. Koval, N. V. Tkachenko, S. A. Zaitsev and A. I. Boldyrev, *MRS Bull.*, **2022**, DOI: 10.1557/s43577-022-00383-6.

- (55) N. V. Tkachenko, D. Steglenko, N. Fedik, N. M. Boldyreva, R. M. Minyaev, V. I. Minkin and A. I. Boldyrev, *Phys. Chem. Chem. Phys.*, **2019**, *21*, 19764.

CHAPTER 2

CHEMICAL BONDING ANALYSIS OF EXCITED STATES USING THE ADAPTIVE
NATURAL DENSITY PARTITIONING METHOD¹**Abstract**

A novel approach to chemical bond analysis for excited states has been developed. Using an extended adaptive natural density partitioning method (AdNDP) as implemented in AdNDP 2.0 code, we obtained chemically intuitive bonding patterns for the excited states of H₂O, B₅⁺, and C₂H₄⁺ molecules. The deformation pathway in the excited states could be easily predicted based on the analysis of the chemical bond pattern. We expect that this new method of chemical bonding analysis would be very helpful for photochemistry, photoelectron spectroscopy, electron spectroscopy and other chemical applications that involved excited states.

2.1 Introduction

The theoretical study of excited states is an important, developing part of modern physical chemistry. Due to the intensive development of computational methods, more and more accurate tools for analyzing excited molecules appear in the hands of chemists. Various predictive models are widely used in modern photochemistry and spectrometry. However, there are still very few methods to analyze chemical bonding of the excited state using basic chemical concepts.

The theory of chemical bonding is still an ambiguous area of physical chemistry. Before the formulation of quantum mechanics, Lewis proposed the most generally

¹ Coauthored by Nikolay V. Tkachenko and Alexander I. Boldyrev. Reproduced from *Phys. Chem. Chem. Phys.* **2019**, *21*, 9590-9596 with permission. Copyright © 2019, Royal Society of Chemistry.

accepted theory of chemical bonding.¹ His empirical model emphasized the key idea that the electron pair is the main element of a chemical bond, becoming an essential part of modern “chemistry language”. However, during the development of quantum mechanics, new approaches were proposed. In 1931, Hund² and in 1932 Mulliken³ introduced a theory of molecular orbitals (MO) which provided a new delocalized way of describing electrons in the chemical system. Chemical bonding theory based on the alternative to MO way was proposed by Pauling,^{4,5} Heitler, London⁶ and Slater.^{7,8} They introduced a valence bond theory which was built on the concept of hybrid orbitals and perfectly predicts the chemical bond of the first two rows of the periodic table.

A great contribution to the description of chemical systems and chemical bonding was made by methods that do not directly reveal the concept of chemical bond. Those methods are based on the various forms of electron density distribution analysis.^{9–24} One example of these methods includes a quantum theory of atoms in molecules (QTAIM)⁹ that is based on the topology of the electron density. Another example is an electron localization function (ELF)¹⁶ that is based on the local quantum-mechanical function, related to the Pauli exclusion principle. Bonds in a chemical system can also be defined using various bond indexes. The general definition of the bond index was given by Wiberg.²⁵ Since then, a plenty of different bond indices were proposed for describing chemical bonding patterns.^{26–37}

Electron density localization methods based on the invariance of the wave function with respect to the unitary transformation are successfully used to obtain an exhaustive chemical bonding interpretation of ground state systems. In the second half of 20th century, a variety of localization methods were proposed.^{38–43} The extraction of localized bonding

pattern from an electron-density function served as a bridge linking two paradigms (quantum chemistry and classical approaches) that are completely distinct from each other. The applicability of some aforementioned methods can be extended for use for electronic excited states. The technique associated with the analysis of molecular orbitals is the most widely used since a lot of computational methods have been developed to accurately predict an electronic structure of excited state compounds.⁴⁴ Several approaches based on localization functions have also been proposed.^{45,46} Thus, introduced by Burnus and coworkers time-dependent ELF⁴⁶ provides a visual understanding of the dynamics of excited electrons. However, those approaches are limited since molecular orbitals are not well defined in the excited states due to the multiconfigurational nature of the wave function. Recently proposed computational methods that can describe molecular orbitals of electronic excited states are not widely available.^{47,48} Another way to analyze excited states is Interacting Quantum Atoms (IQA) method⁴⁹ based on the QTAIM. That method was successfully applied to describe basic reaction mechanisms including excitation processes as well as bonding in excited states of small molecules.⁵⁰⁻⁵³ Likewise, a new tool (the density overlap region indicator) for visualizing interactions in the excited states was proposed.⁵⁴ That method depends only on electron density and its derivatives, which can bypass restrictions associated with multiconfigurational wave function.

Previously, we introduced the Adaptive Natural Density Partitioning algorithm^{55,56} (AdNDP), a powerful approach for the analysis of electron density function. This method allows us to obtain a compact, intuitively simple description of the chemical bonding in molecules with a non-classical bonding pattern. Due to the extension of the Lewis description, AdNDP is a good implementation to search for delocalized n -center 2 electron

bonds ($n > 2$). In the course of our work, we expanded the applicability of the AdNDP method and proposed an approach for studying chemical bonds in the excited state to predict the deformation of the structure under vertical excitation.

2.2 Computational Methods

For the geometry optimization and electron-density calculations, CASSCF method⁵⁷ was used. For each molecule different size of an active space as well as different basis set were chosen (CASSCF(8,10)/aug-cc-pvdz⁵⁸ for H₂O, CASSCF(14,10)/6-311G**⁵⁹ for B₅⁺ and CSSSCF(7,9)/aug-cc-pvdz for C₂H₄⁺). Excited state calculations were performed at the same level of theory using the second root of the CASSCF calculations, thus the first singlet (or doublet in case of C₂H₄⁺) excited state was studied for each molecule. To check the vibrational structure and calculate an energy barrier of the rotation along the C–C bond for C₂H₄⁺ species, CCSD(T)/cc-pvqz^{60,61} level of theory was used. Chemical bonding analysis was performed *via* extended adaptive natural density partitioning algorithm as implemented in AdNDP 2.0 code. The new version was written using Python3.7 programming language.

From a computational point of view, the main bond search algorithm remains the same in AdNDP 2.0 as in the original AdNDP code. In the current version of the AdNDP we are partitioning one-electron density matrix. In the initial design of the AdNDP method, we followed general ideas of the NBO analysis proposed by Weinhold.⁴³ The complete description of the AdNDP algorithm can be found elsewhere.⁵⁶ Nonetheless, for a better understanding of the new features of the AdNDP algorithm, we need to introduce some terms and definitions. We will call $\gamma(\bar{r}_1|\bar{r}'_1)$ the spinless first-order reduced density operator:

$$\gamma(\bar{r}_1|\bar{r}'_1) = N \int \psi(\bar{r}_1, \bar{r}_2, \dots, \bar{r}_N) \psi^*(\bar{r}'_1, \bar{r}_2, \dots, \bar{r}_N) d^3\bar{r}_2 \dots d^3\bar{r}_N \quad (\text{I})$$

where ψ is any N -electron wave function, $\bar{r}_1, \bar{r}_2, \dots, \bar{r}_N$ are generalized coordinates of i^{th} electron. For any complete orthonormal basis set of atomic orbitals $\{\chi_k\}$, the spinless first-order reduced density operator can be expanded as:

$$\gamma(\bar{r}_1|\bar{r}'_1) = \sum_{k,l} P_{kl} \chi_k(\bar{r}_1) \chi_l^*(\bar{r}'_1) \quad (\text{II})$$

The coefficients P_{kl} are elements of the density matrix \mathbf{P} defined as:

$$P_{kl} = \int \chi_k^*(\bar{r}_1) \gamma(\bar{r}_1|\bar{r}'_1) \chi_l(\bar{r}'_1) d^3\bar{r}_1 d^3\bar{r}'_1 \quad (\text{III})$$

Each diagonal matrix element P_{kk} corresponds to the occupation number (ON) of the k^{th} orbital function in the basis set $\{\chi_k\}$. Density matrix \mathbf{P} can be represented in the block form (IV) by splitting a basis $\{\chi_k\}$ into subsets of functions associated with a particular atomic center.

$$\mathbf{P} = \begin{bmatrix} \mathbf{P}_{11} & \dots & \mathbf{P}_{1N} \\ \vdots & \ddots & \vdots \\ \mathbf{P}_{N1} & \dots & \mathbf{P}_{NN} \end{bmatrix} \quad (\text{IV})$$

where \mathbf{P}_{ij} is a submatrix of \mathbf{P} and indices i, j correspond to the i^{th} and the j^{th} atomic center.

By solving eigenproblem (V) for sub-blocks $\mathbf{P}^{(i_1, i_2, \dots, i_n)}$ of block matrix \mathbf{P} we can obtain eigenvectors $\mathbf{v}^{(i_1, i_2, \dots, i_n)}$ and eigenvalues $\lambda^{(i_1, i_2, \dots, i_n)}$ that describe particular bonding interaction between chosen atomic centers i_1, i_2, \dots, i_n .

$$\mathbf{P}^{(i_1, i_2, \dots, i_n)} \mathbf{v}^{(i_1, i_2, \dots, i_n)} = \lambda^{(i_1, i_2, \dots, i_n)} \mathbf{S}^{(i_1, i_2, \dots, i_n)} \mathbf{v}^{(i_1, i_2, \dots, i_n)} \quad (\text{V})$$

Here and below we will call the square matrix $\mathbf{P}^{(i_1, i_2, \dots, i_n)}$ composed of n sub-blocks of i_1^{th} , i_2^{th} , ..., i_n^{th} centers as n -center sub-block matrix. An example of 3-center sub-block matrix for atomic centers i_1, i_2, i_3 is shown below:

$$\mathbf{P}^{(i_1 i_2 i_3)} = \begin{bmatrix} \mathbf{P}_{i_1 i_1} & \mathbf{P}_{i_1 i_2} & \mathbf{P}_{i_1 i_3} \\ \mathbf{P}_{i_2 i_1} & \mathbf{P}_{i_2 i_2} & \mathbf{P}_{i_2 i_3} \\ \mathbf{P}_{i_3 i_1} & \mathbf{P}_{i_3 i_2} & \mathbf{P}_{i_3 i_3} \end{bmatrix} \quad (\text{VI})$$

The search for bonds occurs sequentially starting from one-center elements (lone pairs) and ending at n -center bonds. Bonding elements found by the algorithm are checked for satisfaction of the condition $\lambda^{(i_1, i_2, \dots, i_n)} \geq 2 - t_n$, where t_n is a threshold value that is set individually for each n . It is necessary to deplete density matrix \mathbf{P} from the density associated with found bonds. Equation (VII) demonstrates the depletion process implemented in the AdNDP algorithm.

$$\tilde{\mathbf{P}} = \mathbf{P} - \lambda^{(i_1, i_2, \dots, i_n)} \mathbf{V}^{(i_1, i_2, \dots, i_n)} \mathbf{V}^{(i_1, i_2, \dots, i_n)T} \quad (\text{VII})$$

where $\tilde{\mathbf{P}}$ is the depleted density matrix. The main improvements of the AdNDP 2.0 algorithm are listed below.

2.2.1 Distance restrictions

For the multi-center bond analysis, the original AdNDP algorithm investigates all possible n -center combinations in a molecule. For instance, for searching 6c-2e delocalized bonds in anthracene ($\text{C}_{14}\text{H}_{10}$) one needs to find eigenvalues and eigenvectors for 1.3×10^5 6-center sub-block matrices. However, from a chemical point of view, we know that most of those 6-atoms combinations are meaningless. In order to increase computational efficiency of the method, we decided to introduce distance restriction parameters in the AdNDP analysis. Initially, a list of all possible n -atoms combinations is created. After that,

the algorithm reads the distance matrix of the system and checks each pair of atoms in each combination from the list, so that the distance between them is less than the given restriction parameter. Thus, the most distant atoms in each combination must be closer than the restriction value. This restriction can be defined as follows: a set of atoms is taken into consideration only if all elements of the set lie in the intersection of all spheres of radius R centered on the atoms of the selected fragment, where R is distance restriction parameter that selected by the researcher. Described restriction parameters significantly reduce the number of considered sub-block matrices. Thus, for the anthracene we can reduce the number of analyzed 6-center sub-block matrices from 1.3×10^5 to three by setting a 3 Å limit. Thereby, the new feature of the algorithm noticeably reduces computational time.

2.2.2 *Symmetric direct search*

However, even with distance restriction parameters, one could face difficulties with obtaining a reasonable bonding pattern. For obscure cases, the density matrix could be analyzed by the “direct search” procedure, which allows searching multicentered bonds on given atomic centers. When specifying a fragment with the i_1^{th} , i_2^{th} , ..., i_n^{th} atomic centers, the eigenproblem is solved only for chosen n -center subblock matrices. The found eigenvector corresponding to the maximum eigenvalue are assigned to the nc -2e bond. Also, more than one fragment could be chosen at once. In this case the symmetry of the bonding picture preserves, since the search is conducted simultaneously on all the fragments. The densities associated with the found bonds are then subtracted from the full density matrix *via* equation (VII).

2.2.3 Bonding analysis of unrestricted and open shell systems

For the bonding analysis of an unrestricted case, two different density matrices in the natural atomic orbitals (NAO) basis set (for alpha and beta electrons) should be calculated. The maximum occupancy number that can be obtained for those matrices is $1.0 |e|$. The AdNDP 2.0 code allows us to conduct a separate analysis of alpha and beta electron density matrices. In this case the bonding pattern could be presented in terms of $nc-1e$ bonds. Thus, the analysis for open shell systems or multiplet spin excited states now can be done *via* ADNDP 2.0 code.

2.2.4 Excited states bonding analysis

Analysis of the excited state electron density matrix in NAO basis set was implemented in the AdNDP 2.0 code. The density matrix should be calculated with CASSCF, since the feature is currently compatible only with this method. In the course of our work we used the second root of the CASSCF calculations, thus the density matrix of the first excited state is obtained. However, electron density for higher excited states can be analyzed. By using the flexibility of the AdNDP 2.0 method as well as new features of the algorithm one could easily obtain a bonding pattern for the excited states of the molecule and predict subsequent geometric transformations occurring due to vertical excitation of the molecule.

The new AdNDP 2.0 code is available free of charge and can be downloaded through the Github source (<https://zenodo.org/record/2648092#.XLwJdpnQhPY>). The “User's Manual” could be found through the following links: <http://ion.chem.usu.edu/~boldyrev/>, and <http://ion.chem.usu.edu/~boldyrev/nikolay.html>. The visualization of the calculation results was performed using ChemCraft 1.8 software.

2.3 Results and discussion

In our study, we conducted an extended AdNDP analysis of the excited state of three different molecules: H_2O , B_5^+ , and C_2H_4^+ . The choice of these systems was made to illustrate the flexibility of the method in the analysis of various cases. Thus, the water molecule was chosen as the simplest case due to its classical bonding pattern and well-studied properties. Since AdNDP is widely used for the analysis of the clusters, we chose a boron cluster B_5^+ to show the way, how AdNDP 2.0 can describe non-classical chemical bonding patterns of the excited electronic state. A C_2H_4^+ species was chosen to show the ability of the algorithm to analyze open shell systems. The results of the analysis for each molecule are shown below.

2.3.1 H_2O molecule

The application of the AdNDP method to the water molecule in ground state (C_{2v} , $1a^2_1 2a^2_1 1b^2_2 3a^2_1 1b^2_1$, 1A_1) led us to a classical valence bonding pattern with two $2c-2e$ σ O–H bonds with $\text{ON} = 1.97 |e|$ and two s - and p -type lone pairs on the oxygen with occupation numbers 1.98 and 1.97 $|e|$ respectively (Fig. 2-1, A bottom). To understand the bonding structure after the vertical excitation, we perform an analysis of the excited state of the water molecule (C_{2v} , $1a^2_1 2a^2_1 1b^2_2 3a^2_1 1b^1_1 4a^1_1$, 1B_1) at the geometry of the ground electronic state. We noticed that one electron from p -type lone pair of the oxygen transfers to a $3c-1e$ antibonding orbital. The shape of this orbital is similar to the shape of the canonical molecular $4a_1$ orbital (Fig. 2-1, B bottom). By analyzing the phase sign of this $3c-1e$ bond we can observe a binding region between two hydrogen atoms and an anti-binding region between hydrogen and oxygen atoms. Using this information, one can predict that the O–H bond will lengthen, and the H–O–H angle will decrease upon the

subsequent transformation of the molecular geometry. By performing the optimization of water geometry in the first excited state (the second root of the CASSCF calculations was considered), we can check that our predictions were correct. Indeed, the O–H bonds lengthened from 0.967 Å to 1.066 Å and the H–O–H angle decreased from 104.17° to 103.03° (Fig. 2-1, A top, B top).

2.3.2 B_5^+ cluster

According to previous computational works,⁶² the global minimum structure of B_5^+ cluster belongs to C_{2v} symmetry group and has slightly distorted from the regular pentagon geometry (Fig. 2-2, A top). The main electronic configuration of the ground state at CASSCF/6-311G** level of theory is $1a^2_1 2a^2_1 1b^2_2 3a^2_1 2b^2_2 4a^2_1 3b^2_2 5a^2_1 6a^2_1 4b^2_2 1b^2_1 7a^2_1$, 1A_1 . The application of the AdNDP method to the valence MOs of ground electronic state of B_5^+ led us to five peripheral 2c-2e σ B–B bonds with ON = 1.99–1.96 |e|. Additionally, we found two delocalized 5c-2e bonds with ON = 1.92 and 1.88 |e| that are responsible for the σ and π -aromaticity of the system. According to the extended AdNDP analysis of the valence MOs of the B_5^+ cluster in the first excited state (C_{2v} , $1a^2_1 2a^2_1 1b^2_2 3a^2_1 2b^2_2 4a^2_1 3b^2_2 5a^2_1 6a^2_1 4b^2_2 1b^2_1 7a^1_1 1a^1_2$, 1A_2), the molecule preserves five peripheral 2c-2e σ B–B bonds with ON = 1.95–1.91 |e| and delocalized 5c-2e π bond with ON = 1.92 |e|. However, one electron from 5c-2e σ -bond transfers to an excited 5c-1e π^* -bond. By analyzing this bonding pattern, one can expect that distances between B1–B2 and B3–B4 will increase. Moreover, the distance B1–B2 will increase more than the distance B3–B4 due to the greater electron density on atoms B1 and B2. In contrast, distances B1–B3, B2–B4 will not change. Indeed, after the geometry optimization of the excited state using the second root of the CASSCF calculations, one could see that B1–B2 and B3–B4

distances increase from 2.778 Å to 2.854 Å and from 1.553 Å to 1.621 Å, respectively. Also, B1–B3 and B2–B4 distances remain almost unchanged ($\Delta_{(B1-B2)} = 0.076$ Å, $\Delta_{(B3-B4)} = 0.068$ Å; $\Delta_{(B1-B3)} = \Delta_{(B2-B4)} = -0.009$ Å).

2.3.3 $C_2H_4^+$ species

It has been shown that the ground state geometry of the $C_2H_4^+$ species is not planar and exhibits twisted geometry with the dihedral angle H–C–C–H about 20° (D_2 symmetry).^{63,64} However, spectral data obtained by Willitsch *et al.* suggested that the molecular symmetry may be regarded as D_{2h} rather than D_2 .⁶⁵ We conduct an optimization of twisted and planar geometries at CCSD(T)/cc-pvqz level of theory. We found that the planar geometry is the first order stationary point with one imaginary frequency and has the total electronic energy higher than the twisted structure by $0.23 \text{ kcal mol}^{-1}$. With the inclusion of ZPE corrections, the planar geometry became lower by energy than the twisted isomer ($\Delta E = -0.01 \text{ kcal mol}^{-1}$). Thus, the average vibrational structure has D_{2h} symmetry. Here and below we will investigate bonding structure only for the planar isomer of $C_2H_5^+$ since it is irrelevant in terms of chemical bonding.

Optimized ground state geometry of $C_2H_4^+$ obtained at CASSCF(7,9)/aug-cc-pvdz level of theory is slightly distorted from D_{2h} symmetry (Fig. 2-3, A top). The ground state has the $1a_g^2 1b_u^2 2a_g^2 2b_u^2 3b_u^2 3a_g^2 4a_g^2 1a_u^1$ main electron configuration and the 2A_u electronic term. Due to the vertical excitation, one electron transfers from $4a_g^2$ orbital to $1a_u^1$ orbital. So the main electron configuration of the first excited state in the geometry of the ground state is $1a_g^2 1b_u^2 2a_g^2 2b_u^2 3b_u^2 3a_g^2 4a_g^1 1a_u^2$ with the term 2A_g . The AdNDP analysis of the ground state electron configuration shows a classical bonding pattern (Fig. 2-3, A bottom)

with four 2c-2e σ C–H bonds (ON = 1.99–1.97 |e|), one 2c-2e σ C–C bond (ON = 1.97 |e|) and one electron sitting on 2c-1e π C–C bond (ON = 0.99 |e|).

2.4 Conclusions

An updated AdNDP 2.0 algorithm was introduced. New features of the algorithm such as distance restrictions, symmetric direct search, analysis of open shell systems, and excited states bonding analysis greatly expand the applicability of the method. We showed that the chemical bonding patterns of the excited state molecules, obtained by an updated AdNDP 2.0 code, are comprehensive and consistent with the chemical intuition. Moreover, by analyzing a bonding pattern of the excited state molecule in the geometry of the ground state, one can easily predict the subsequent geometry transformation upon an electronic excitation. We hope that our new AdNDP method will become a useful tool in photochemistry, photoelectron spectroscopy, electron spectroscopy, and other areas of chemistry where excited states are involved.

References

- (1) G. N. Lewis, *J. Am. Chem. Soc.*, 1916, **38**, 762.
- (2) F. Hund, *Z. Phys.*, 1931, **73**, 1.
- (3) R. S. Mulliken, *Phys. Rev.*, 1932, **41**, 49.
- (4) L. Pauling, *J. Am. Chem. Soc.*, 1931, **53**, 1367.
- (5) L. Pauling, *J. Am. Chem. Soc.*, 1931, **53**, 3225.
- (6) W. Heitler and F. London, *Z. Phys.*, 1927, **44**, 455.
- (7) J. C. Slater, *Phys. Rev.*, 1931, **37**, 481.
- (8) J. C. Slater, *Phys. Rev.*, 1931, **38**, 1109.

- (9) R. F. W. Bader, *Atoms in Molecules: A Quantum Theory*, Oxford University Press, Oxford, 1990.
- (10) V. K. Artman, *Z. Naturforsch.*, 1946, **1**, 426.
- (11) J. E. Lenard-Jones, *Proc. R. Soc. London, Ser. A*, 1949, **198**, 14.
- (12) J. E. Lenard-Jones, *Proc. R. Soc. London, Ser. A*, 1949, **198**, 1.
- (13) R. Daudel, *Quantum Theory of the Chemical Bond*, Reidel, Dordrecht, 1974.
- (14) R. F. W. Bader and M. E. Stephens, *J. Am. Chem. Soc.*, 1975, **97**, 7391.
- (15) W. L. Luken and J. C. Culberson, *Int. J. Quantum Chem.*, 1982, **22**, 265.
- (16) A. D. Becke and K. E. Edgecombe, *J. Chem. Phys.*, 1990, **92**, 5397.
- (17) B. Silvi and A. Savin, *Nature*, 1994, **371**, 683.
- (18) P. A. Fuentealba, *Int. J. Quantum Chem.*, 1998, **69**, 559.
- (19) R. Ponec and D. L. Cooper, *J. Phys. Chem. A*, 2007, **111**, 11294.
- (20) F. Fantuzzi and M. A. C. Nascimento, *J. Chem. Theory Comput.*, 2014, **10**, 2322.
- (21) J. H. Lange and I. Cukrowski, *J. Comput. Chem.*, 2018, **39**, 1517.
- (22) B. G. Janesko, G. Scalmani and M. J. Frisch, *J. Chem. Phys.*, 2014, **141**, 144104.
- (23) E. Ramos-Cordoba, P. Salvador and M. Reiher, *Chem. Eur. J.*, 2013, **19**, 15267.
- (24) D. L. Cooper, R. Ponec and M. Kohout, *Mol. Phys.*, 2016, **114**, 1270.
- (25) K. B. Wiberg, *Tetrahedron*, 1968, **24**, 1083.
- (26) I. Mayer, *Chem. Phys. Lett.*, 1983, **97**, 270.
- (27) I. Mayer, *Int. J. Quantum Chem.*, 1986, **29**, 73.
- (28) M. Giambiagi, M. S. Giambiagi and K. C. Mundim, *Struct. Chem.*, 1990, **1**, 423.
- (29) A. B. Sannigrahi and T. Kar, *Chem. Phys. Lett.*, 1990, **173**, 569.

- (30) F. Feixas, M. Sola, J. M. Barroso, J. M. Ugalde and E. Matito, *J. Chem. Theory Comput.*, 2014, **10**, 3055.
- (31) R. L. Fulton, *J. Phys. Chem.*, 1993, **97**, 7516.
- (32) R. L. Fulton and S. T. Mixon, *J. Phys. Chem.*, 1993, **97**, 7530.
- (33) X. Fradera, M. A. Austen and R. F. W. Bader, *J. Phys. Chem. A*, 1999, **103**, 304.
- (34) I. Mayer, *J. Quantum Chem.*, 1984, **26**, 151.
- (35) I. Mayer, *J. Quantum Chem.*, 1985, **28**, 419.
- (36) I. Mayer, *J. Quantum Chem.*, 1986, **29**, 477.
- (37) E. Matito, M. Sola, P. Salvador and M. Duran, *Faraday Discuss.*, 2007, **135**, 325.
- (38) J. M. Foster and S. F. Boys, *Rev. Mod. Phys.*, 1960, **32**, 300.
- (39) C. Edmiston and K. Ruedenberg, *Rev. Mod. Phys.*, 1963, **35**, 457.
- (40) J. Pipek and P. G. Mezey, *J. Chem. Phys.*, 1989, **90**, 4916.
- (41) J. P. Foster and F. Weinhold, *J. Am. Chem. Soc.*, 1980, **102**, 7211.
- (42) A. E. Reed, L. A. Curtiss and F. Weinhold, *Chem. Rev.*, 1988, **88**, 899.
- (43) F. Weinhold and C. R. Landis, *Valency and Bonding: A Natural Bond Orbital Donor–Acceptor Perspective*, Cambridge University Press, Cambridge, UK, 2005.
- (44) L. Gonzalez, D. Escudero and L. Serrano-Andres, *ChemPhysChem*, 2012, **13**, 28.
- (45) E. S. Kadantsev and H. L. Schmider, *Int. J. Quantum Chem.*, 2008, **108**, 1.
- (46) T. Burnus, M. A. L. Marques and E. K. U. Gross, *Phys. Rev. A: At., Mol., Opt. Phys.*, 2005, **71**, 010501.
- (47) J. Cullen, M. Krykunov and T. Ziegler, *Chem. Phys.*, 2011, **391**, 11.
- (48) T. Ziegler, M. Krykunov and J. Cullen, *J. Chem. Phys.*, 2012, **136**, 124107.

- (49) M. A. Blanco, A. Martin Pendas and E. Francisco, *J. Chem. Theory Comput.*, 2005, **1**, 1096.
- (50) J. Jara-Cortés, J. M. Guevara-Vela, A. M. Pendás and J. Hernández-Trujillo, *J. Comput. Chem.*, 2017, **38**, 957.
- (51) F. Feixas, E. Matito, J. Poater and M. Solà, *Chem. Soc. Rev.*, 2015, **44**, 6434.
- (52) L. Gutiérrez-Arzaluz, F. Cortés-Guzmán, T. Rocha-Rinza and J. Peón, *Phys. Chem. Chem. Phys.*, 2015, **17**, 31608.
- (53) M. Estévez-Fregoso and J. Hernández-Trujillo, *Phys. Chem. Chem. Phys.*, 2016, **18**, 11792.
- (54) L. Vannay, E. Bremond, P. Silva and C. Corminboeuf, *Chem. Eur. J.*, 2016, **22**, 18442.
- (55) D. Y. Zubarev and A. I. Boldyrev, *J. Org. Chem.*, 2008, **73**, 9251.
- (56) D. Y. Zubarev and A. I. Boldyrev, *Phys. Chem. Chem. Phys.*, 2008, **10**, 5207.
- (57) P. J. Knowles and H.-J. Werner, *Chem. Phys. Lett.*, 1985, **115**, 259.
- (58) T. H. Dunning, *J. Chem. Phys.*, 1989, **90**, 1007.
- (59) K. Raghavachari, J. S. Binkley, R. Seeger and J. A. Pople, *J. Chem. Phys.*, 1980, **72**, 650.
- (60) K. Raghavachari, G. W. Trucks, J. A. People and M. Head-Gordon, *Chem. Phys. Lett.*, 1989, **157**, 479.
- (61) J. D. Watts, J. Gauss and R. J. Bartlett, *J. Chem. Phys.*, 1993, **98**, 8718.
- (62) A. N. Alexandrova, A. I. Boldyrev, H.-J. Zhai and L.-S. Wang, *Coord. Chem. Rev.*, 2006, **250**, 2811.

- (63) B. Joalland, T. Mori, T. J. Martinez and A. G. Suits, *J. Phys. Chem. Lett.*, 2014, **5**, 1467.
- (64) M. L. Abrams, E. F. Valeev and C. D. Sherrill, *J. Phys. Chem. A*, 2002, **106**, 2671.
- (65) S. Willitsch, U. Hollenstein and F. Merkt, *J. Chem. Phys.*, 2004, **120**, 1761.

Tables and figures

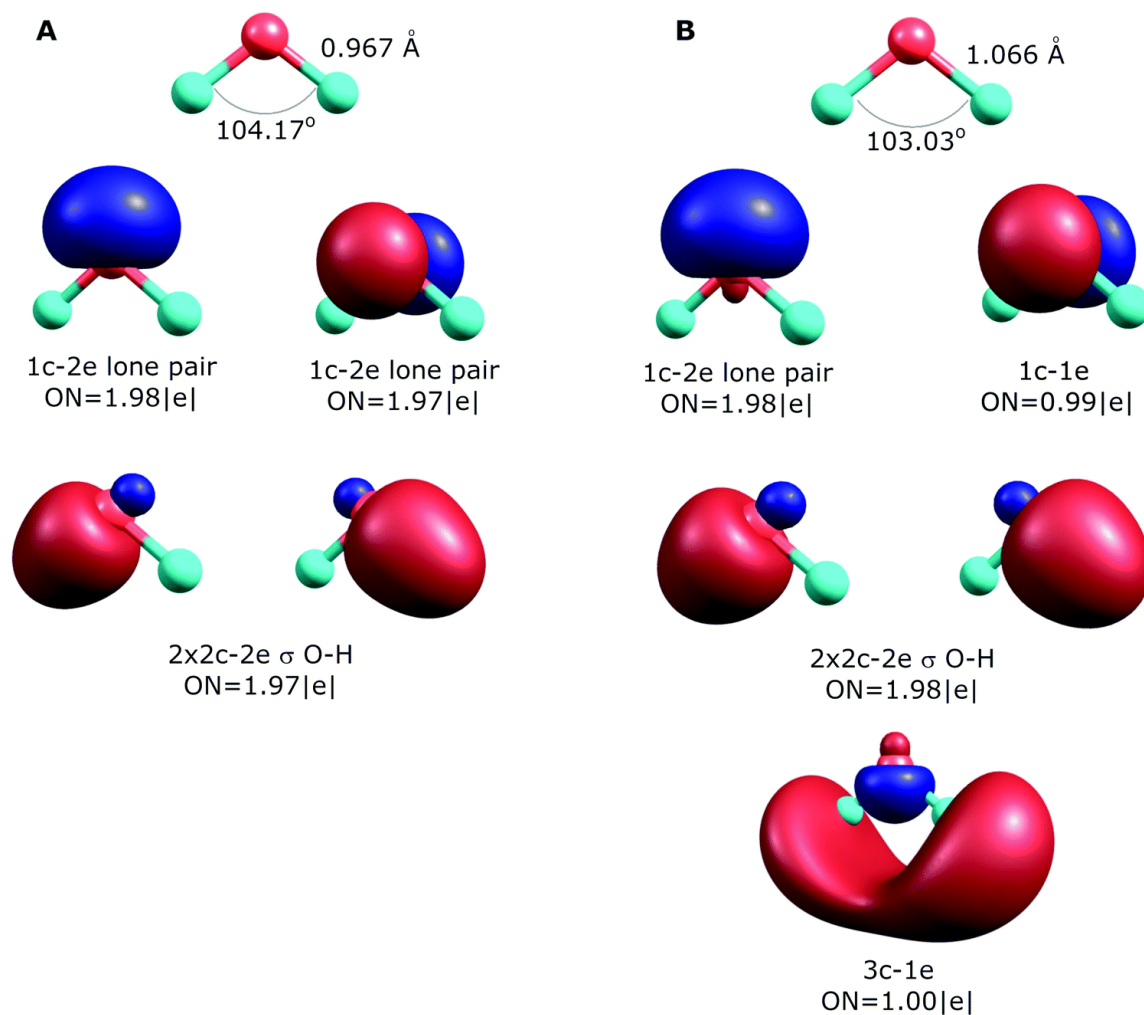


Figure 2-1. Optimized structures of the water molecule in the ground electronic state (A top) and in the first excited electronic state (B top); the results of the extended AdNDP analysis of the ground state (A bottom) and the first excited state (B bottom) at the ground state optimized geometry.

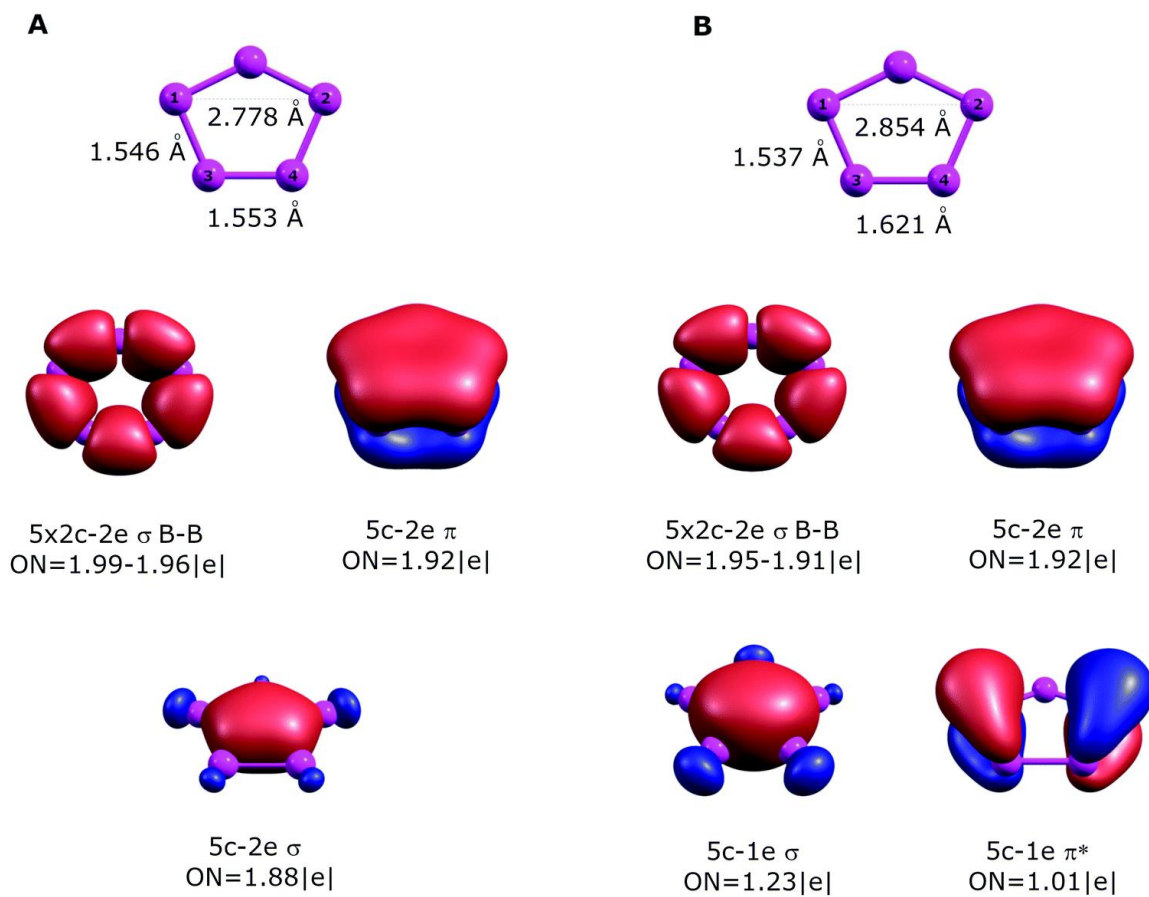


Figure 2-2. Optimized structures of the B_5^+ cluster in the ground electronic state (A top) and in the first excited electronic state (B top); the results of the extended AdNDP analysis of the ground state (A bottom) and the first excited state (B bottom) at the ground state optimized geometry.

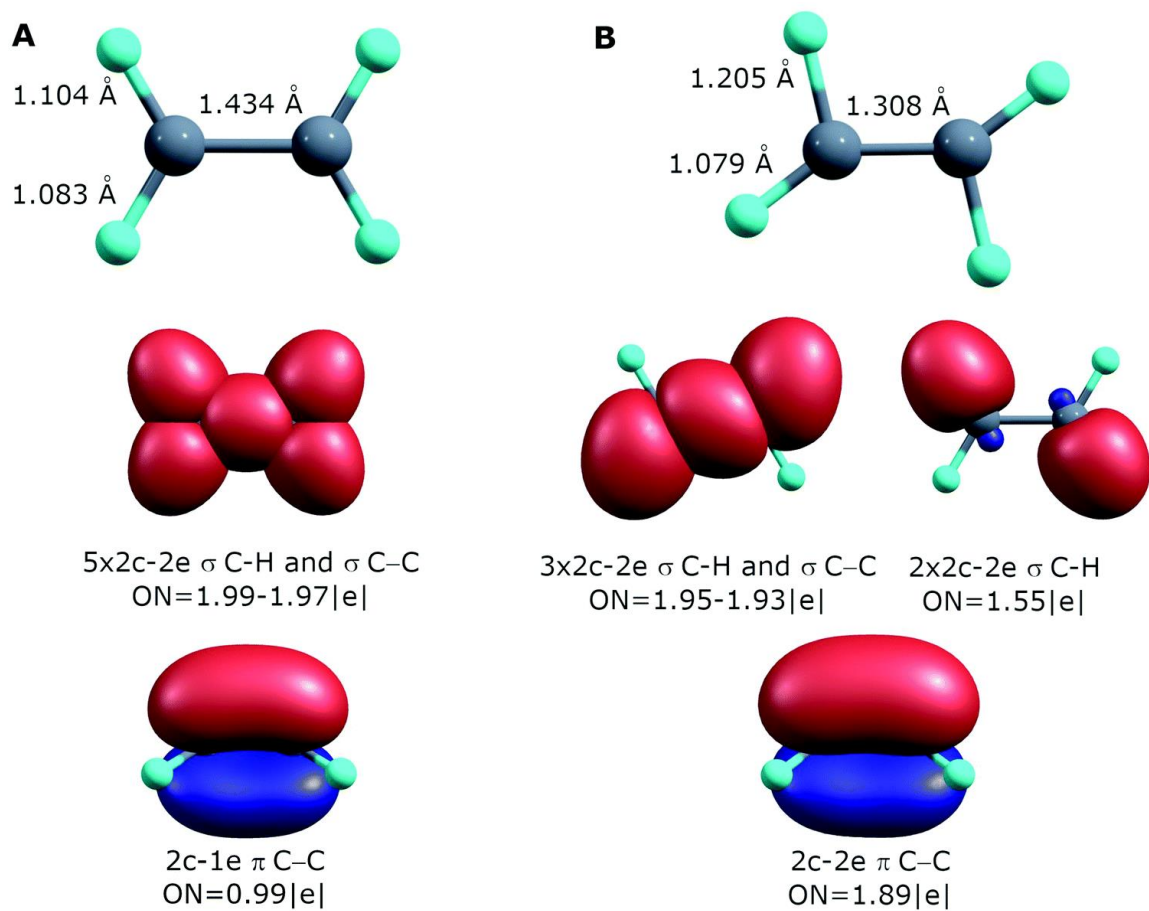


Figure 2-3. Optimized structures of the $C_2H_4^+$ molecule in the ground electronic state (A top) and in the first excited electronic state (B top); the results of the extended AdNDP analysis of the ground state (A bottom) and the first excited state (B bottom) at the ground state optimized geometry.

CHAPTER 3

MULTIPLE LOCAL σ -AROMATICITY OF NONAGERMANIDE CLUSTERS¹**Abstract**

Nonagermanide clusters are widely used in inorganic synthesis and are actively studied by experimentalists and theoreticians. However, chemical bonding of such versatile species is still not completely understood. In our work, we deciphered a bonding pattern for various experimentally obtained nonagermanide species. We localized the electron density *via* the AdNDP algorithm for the model structures $[\text{Ge}_9]^{4-}$, $[\text{Ge}_9\{\text{P}(\text{NH}_2)_2\}_3]^-$, $\text{Cu}[\text{Ge}_9\{\text{P}(\text{NH}_2)_2\}_3]$ and $\text{Cu}(\text{NHC})[\text{Ge}_9\{\text{P}(\text{NH}_2)_2\}_3]$ and obtained a simple and chemically intuitive bonding pattern which can explain the variety of active sites and the existence of both D_{3h} and C_{4v} geometries for such clusters. Moreover, the $[\text{Ge}_9]^{4-}$ core is found to be a unique example of an inorganic Zintl cluster with multiple local σ -aromaticity.

3.1 Introduction

The concept of aromaticity has long gone beyond the classical Hückel organic structures.^{1,2} Today, the terms π - and σ -aromaticity are well used for a variety of compounds, including complex inorganic structures.³ In these cases, the delocalized bonding well describes the formation of highly symmetric stable compounds. Numerous planar boron clusters,⁴⁻⁷ metal clusters,^{3,7-13} and metallabenzenes¹⁴⁻¹⁸ fit well into the concept of aromaticity. Along with π - and σ -aromaticity, multiple local π aromaticity is found to be a useful tool to describe complex conjugate systems such as graphene.¹⁹⁻²¹ This concept has been accepted up to a point. In our work we showed that the concept of multiple

¹ Coauthored by Nikolay V. Tkachenko and Alexander I. Boldyrev. Reproduced from *Chem. Sci.*, **2019**, *10*, 5761-5765 with permission. Copyright © 2019, Royal Society of Chemistry.

local σ -aromaticity could be applied in chemistry. It should be noted that the analysis of completely delocalized canonical MOs cannot lead to a reliable picture of chemical bonding in such clusters,^{22,23} since there is a mixture of electron lone pairs (an element that does not participate in chemical bonding interactions) with bonding elements of the cluster. Thus, to analyze aromaticity, firstly we need to localize all classical elements (such as 1c–2e lone pairs and 2c–2e Lewis bonds). The adaptive natural density partitioning algorithm (AdNDP) can be very useful for this purpose.

Homoatomic clusters of type $[M_9]^{z-}$ ($M = \text{Si, Ge, Sn, and Pb}$) have been investigated both experimentally and theoretically.^{24,25} The structures of most such clusters confirm the predictions from Wade's rules.^{26,27} Interestingly, the expectation of the geometry of $[M_9]^{4-}$ species with $2n+4$ ($n = 9$) skeletal electrons leads us to a *nido* nine-vertex polyhedron (C_{4v} capped square antiprism).

An isolated $[\text{Ge}_9]^{4-}$ cluster has been experimentally obtained in the solid state in the form of alkali metal salts (K_4Ge_9 ,²⁸ Cs_4Ge_9 , and Rb_4Ge_9 (ref. 29)). The geometry of these clusters (except Rb_4Ge_9) was found by X-ray crystallography and it was slightly distorted from the ideal C_{4v} capped square antiprism, confirming Wade's rules.²⁴ However, various DFT calculations (Table 1) suggest that the global minimum structure for $[\text{Ge}_9]^{4-}$ is a tricapped trigonal prism (D_{3h} symmetry).^{23,30} In turn, the C_{4v} symmetric structure has one imaginary frequency. A similar picture could be found, for instance, in a biphenyl system (twisted geometry in the gaseous phase and completely planar in the solid state). D_{3h} and C_{4v} structures transform from one to another through the diamond square process (Fig. 3-1).^{31,32}

Although Wade's rules can give us a prediction of the cluster structure, we still do not have a comprehensive picture of the chemical bonding for such species. In this paper, we presented a new description of bonding in $[\text{Ge}_9]^{4-}$ clusters, based on the local σ -aromaticity concept. The obtained bonding pattern explains both the presence of active sites and the existence of C_{4v} and D_{3h} geometries for these compounds.

3.2 Computational methods

All structures were optimized at the PBE0/aug-cc-pvdz^{33,34} level of theory. Frequency calculations were performed using the harmonic approximation. To understand the chemical bonding pattern, matrix representation of the first order reduced density operator in the NAO basis set was analysed by the adaptive natural density partitioning (AdNDP) algorithm³⁵ as implemented in the AdNDP 2.0 code³⁶ at the PBE0/cc-pvdz level of theory. In the AdNDP method, we followed general ideas of the NBO analysis proposed by Weinhold.³⁷ It represents a chemical bonding structure in terms of $nc-2e$ bonds following the concept of electron pairs and $2c-2e$ classical bonds. To assess the aromaticity of each aromatic fragment, nucleus-independent chemical shift (NICS)^{38,39} calculations were performed at the PBE0/aug-cc-pvtz level. The ChemCraft 1.8 software was used to visualize chemical bonding patterns and geometries of the investigated compounds.

3.3 Results and discussion

To understand the stability of both D_{3h} and C_{4v} isomers, we conducted AdNDP analysis of the first order reduced NAO density matrix for C_{4v} and D_{3h} $[\text{Ge}_9]^{4-}$ clusters. We found that the C_{4v} structure has nine classical Lewis lone pairs on germanium atoms with occupation numbers (ONs) 1.91–1.90 |e|. The remaining electron density forms eleven delocalized σ -bonds with ON = 2.00–1.90 |e| (Fig. 3-2). These delocalized σ -type

fragments bind three areas of the germanium cluster. The first area is the cap of the square antiprism (Fig. 3-2b–d) and consists of three 5c–2e bonds with $ON = 2.00\text{--}1.95 |e|$. The shape of these elements as well as the number of electrons (6 electrons fit the $4n+2$ Hückel's rule) indicates σ -aromaticity in the Ge_5 cap fragment. Next three 8c–2e σ -bonds with $ON = 2.00 |e|$ bind the bottom square fragment (Fig. 3-2e–g). The contribution of this Ge_4 fragment into the 8c–2e bonds is $\sim 99.0\%$ for the bond shown in Fig. 3-2e and $\sim 81.9\%$ for bonds shown in Fig. 3-2f and g. The whole Ge_8 square antiprism fragment is bound by five 8c–2e σ -bonds with $ON = 2.00\text{--}1.90 |e|$. The shapes of 8c–2e and 5c–2e bonds (one bond without a nodal plane, two bonds with one nodal plane, *etc.*) and $4n+2$ electrons ($n = 1, 2$) on each area render these fragments σ -aromatic. Therefore, the stability of the C_{4v} structure can be explained by the existence of three σ -aromatic areas: the Ge_5 cap fragment, Ge_4 bottom square fragment and Ge_8 square antiprism fragment.

An equally interesting picture of chemical bonding was found for the D_{3h} $[\text{Ge}_9]^{4-}$ cluster (Fig. 3-3). According to AdNDP analysis, the 40 valence electrons in $[\text{Ge}_9]^{4-}$ can be localized into nine classical 1c–2e lone pairs on Ge atoms, two 3c–2e sigma bonds with $ON = 1.97 |e|$, and nine delocalized 5c–2e bonds. These nine 5c–2e bonds with $ON = 1.98\text{--}1.89 |e|$ are responsible for binding interactions inside each Ge_5 cap fragment (rectangular pyramids built on the sides of a trigonal prism). Three σ -bonds per cap constitute σ -aromaticity. It should be mentioned that the 3c–2e bonds could be also considered σ -aromatic since the number of electrons fits well in Hückel's rule ($n = 0$). Thus, the chemical bonding pattern for the D_{3h} $[\text{Ge}_9]^{4-}$ cluster includes nine lone pairs, two 3c–2e σ -aromatic bonds and three symmetric Ge_5 σ -aromatic areas with 5c–2e σ -bonds, which explains the stability and the variety of active sites for such a structure.

To assess local σ -aromaticity in D_{3h} and C_{4v} structures, we calculated NICS_{zz} and NICS_{iso} indices at different points of the clusters (Fig. 3-4). The coordinates of chosen points can be found in the Table 3-2. Significantly negative values of NICS indices at the centers of aromatic fragments (points 1, 3, and 4 for C_{4v} and points 1 and 4 for the D_{3h} structure) corroborate our local σ -aromatic description of the bonding pattern for such clusters (Table 3-3).

It should be noted that the described bonding pattern is not unique to germanium clusters and could be found in other isoelectronic species. To show that, we performed AdNDP analysis for $[\text{Si}_9]^{4-}$ and $[\text{Sn}_9]^{4-}$ clusters. The chemical bonding pattern was found to be similar to nonagermanide clusters (Fig. 3-5, Fig. 3-6, Fig. 3-7).

The described chemical bonding pattern also could be found in other synthesized germanium clusters. Various derivatized nonagermanide systems were reported,⁴⁰⁻⁵¹ including mono-, di- and tri-substituted species. Of all the series, threefold phosphine-functionalized nonagermanide clusters, synthesized in 2018 by Fässler and coworkers, are of particular interest due to their high reactivity and ease of synthesis.⁵¹ In these clusters, the geometry of the core Ge_9 fragment is found to be slightly distorted from that of the tricapped D_{3h} symmetric trigonal prism. In our model calculations of the $[\text{Ge}_9\{\text{P}(\text{N}^i\text{Pr}_2)_2\}_3]^-$ cluster, we attached three $\text{P}(\text{NH}_2)_2^+$ substituents to the three capping Ge atoms. The results are shown in Fig. 3-8. We found that the bonding pattern of the core Ge_9 fragment remains the same as that of the D_{3h} - $[\text{Ge}_9]^{4-}$ cluster. The main difference in bonding is that three peripheral 1c–2e lone pairs on capping Ge atoms participate in the formation of new two-center classical bonds with phosphorus ($\text{ON} = 1.97 |e|$). The occupancy of the nine 5c–2e bonds, which are responsible for the local σ -aromaticity,

remains almost the same (Fig. 5d–f). The $-\text{P}(\text{NH}_2)_2$ substituents exhibit a classical bonding pattern with 1c–2e lone pairs on P (ON = 1.94 |e|) and N atoms (ON = 1.91 |e|) and 2c–2e σ N–H (ON = 1.99 |e|) and σ N–P (ON = 1.99 |e|) bonds (Fig. S1†).

Previously, an intriguing reactivity was found for such threefold phosphine-functionalized nonagermanide clusters.⁵¹ The reaction of $[\text{Ge}_9\{\text{P}(\text{N}^i\text{Pr}_2)_2\}_3]^-$ and $\text{NHC}^{\text{Dipp}}\text{CuCl}$ leads to the formation of a $(\text{NHC}^{\text{Dipp}}\text{Cu})[\text{Ge}_9\{\text{P}(\text{N}^i\text{Pr}_2)_2\}_3]$ compound, containing the D_{3h} symmetric Ge_9 fragment. For understanding the bonding pattern within the copper containing structure, we started our analysis from the model molecule – $(\text{Cu})[\text{Ge}_9\{\text{P}(\text{NH}_2)_2\}_3]$. The results are shown in Fig. 3-9. We found that the Cu atom keeps five 1c–2e *d*-type lone pairs with an occupation number of 1.99–1.96 |e|. The bonding pattern of the $[\text{Ge}_9\{\text{P}(\text{NH}_2)_2\}_3]^-$ part remains almost the same, except one 3c–2e σ -aromatic fragment on the top of the trigonal prism that transforms into a 4c–2e Ge_3Cu σ -bond with ON = 1.97 |e|. The contribution of the Ge_3 triangle fragment into the 4c–2e bond is found to be ~83.7%. Even though this model molecule is a good object for studying bonding patterns, the optimized geometry noticeably differs from the experimentally obtained structure. For instance, the Ge–Ge distance in the upper triangle of the trigonal prism is 3.17 Å (experimental value is 2.87 Å). That is why we decided to include the NHC ligand attached to the Cu atom, which models the NHC^{Dipp} ligand.

The geometry of the optimized structure with the NHC ligand attached to the Cu atom corroborates with the experimental data. So, the Ge–Ge distance in the upper triangle and the distance between capped germanium and germanium in the upper triangle of the prism is 2.93 Å and 2.50 Å, respectively (experimental data are 2.87 Å and 2.50 Å, respectively). It should be mentioned that the attachment of the second $[\text{Ge}_9\{\text{P}(\text{NH}_2)_2\}_3]^-$ fragment to the

(Cu)[Ge₉{P(NH₂)₂}₃] molecule also leads to Ge–Ge distances similar to the experimental ones. By conducting AdNDP analysis we found that the bonding pattern of the core Ge₉ fragment remains the same (Fig. 3-10). It consists of six *s*-type 1c–2e lone pairs on Ge atoms, three local σ -aromatic Ge₅ fragments, one 3c–2e σ -aromatic bond at the bottom, and one 4c–2e CuGe₄ σ -bond at the top of the prism. The binding interactions of the Cu atom are illustrated in Fig. 3-11. The new 2c–2e σ Cu–C bond with ON = 1.95 |e| appears due to the attachment of the NHC ligand. The contribution of the carbon atom into the Cu–C bond is assessed to be ~85.3%, indicating the donor–acceptor type of the sigma bond.

3.3 Conclusions

In summary, we performed a chemical bonding analysis for five nonagermanide species. The stability of both *D*_{3h} and *C*_{4v} structures of the Ge₉⁴⁻ cluster could be well described *via* the concept of multiple local σ -aromaticity. We are not aware of such a chemical bonding in the literature. On the basis of AdNDP analysis we can separate the electron density in locally aromatic regions: the Ge₅ cap, Ge₈ antiprism, and Ge₄ square fragments for *C*_{4v} [Ge₉]⁴⁻, and then three Ge₅ caps, and two 3c–2e triangular fragments for *D*_{3h} [Ge₉]⁴⁻. We found a similar bonding pattern for the core Ge₉ fragment for previously synthesized trisubstituted [Ge₉{P(NR₂)₂}₃] clusters. The –P(NH₂)₂ groups are bound with the tricapped trigonal prism core *via* classical 2c–2e Ge–P σ -bonds.

A variety of active sites are well described with the obtained bonding picture. Thus, it was found that the copper atom in Cu[Ge₉{P(NH₂)₂}₃] and Cu(NHC)[Ge₉{P(NH₂)₂}₃] clusters interacts with the 3c–2e σ -bond of the Ge₉ core to form a 4c–2e bond. Therefore, the described picture is indeed in good agreement with the experimental reactivity of such compounds. The same chemical bonding was also found in isoelectronic [Si₉]⁴⁻ and [Sn₉]⁴⁻

clusters. We hope that the newly obtained bonding pattern with locally σ -aromatic fragments could be an important step to build a coherent bonding structure of Ge-family clusters and congener species. It will also help in the development and understanding of chemical bonding for complicated cases in inorganic chemistry.

References

- (1) E. Hückel *Z. Phys.*, 1931, **70**, 204.
- (2) E. Hückel *Z. Phys.*, 1932, **76**, 628.
- (3) C. Liu, I. A. Popov, Z. Chen, A. I. Boldyrev and Z. M. Sun, *Chem.–Eur. J.*, 2018, **24**, 14583.
- (4) A. P. Sergeeva, I. A. Popov, Z. A. Piazza, W. L. Li, C. Romanescu, L. S. Wang and A. I. Boldyrev, *Acc. Chem. Res.*, 2014, **47**, 1349.
- (5) A. N. Alexandrova, A. I. Boldyrev, H. J. Zhai and L. S. Wang, *Coord. Chem. Rev.*, 2006, **250**, 2811.
- (6) A. I. Boldyrev and L. S. Wang, *Phys. Chem. Chem. Phys.*, 2016, **18**, 11589.
- (7) J. M. Mercero, A. I. Boldyrev, G. Merino and J. M. Ugalde, *Chem. Soc. Rev.*, 2015, **44**, 6519.
- (8) A. I. Boldyrev and L. S. Wang, *Chem. Rev.*, 2005, **105**, 3716.
- (9) C. A. Tsipis *Coord. Chem. Rev.*, 2005, **249**, 2740.
- (10) D. Yu. Zubarev, B. B. Averkiev, H. J. Zhai, L. S. Wang and A. I. Boldyrev, *Phys. Chem. Chem. Phys.*, 2008, **10**, 257.
- (11) I. A. Popov, A. A. Starikova, D. V. Steglenko and A. I. Boldyrev, *Chem.–Eur. J.*, 2018, **24**, 292.

- (12) X. Huang, H. J. Zhai, B. Kiran and L. S. Wang, *Angew. Chem., Int. Ed.*, 2005, **44**, 7251.
- (13) A. N. Alexandrova and A. I. Boldyrev, *J. Phys. Chem.*, 2003, **107**, 554.
- (14) I. Fernandez, G. Frenking and G. Merino, *Chem. Soc. Rev.*, 2015, **44**, 6452.
- (15) J. R. Bleeker *Chem. Rev.*, 2001, **101**, 1205.
- (16) J. R. Bleeker, Y. F. Xie, W. J. Peng and M. Chiang, *J. Am. Chem. Soc.*, 1989, **111**, 4118.
- (17) J. R. Bleeker, R. Behm, Y. F. Xie, T. W. Clayton and K. D. Robinson, *J. Am. Chem. Soc.*, 1994, **116**, 4093.
- (18) J. R. Bleeker, R. Behm, Y. F. Xie, M. Y. Chiang, K. D. Robinson and A. M. Beatty, *Organometallics*, 1997, **16**, 606.
- (19) I. A. Popov, K. V. Bozhenko and A. I. Boldyrev, *Nano Res.*, 2012, **5**, 117.
- (20) I. A. Popov and A. I. Boldyrev, *Eur. J. Org. Chem.*, 2012, **2012**, 3485.
- (21) D. Y. Zubarev and A. I. Boldyrev, *J. Org. Chem.*, 2008, **73**, 9251.
- (22) T. B. Tai and M. T. Nguyen, *J. Chem. Theory Comput.*, 2011, **7**, 1119.
- (23) G. N. Reedy, P. Jena and S. Giri, *Chem. Phys. Lett.*, 2017, **686**, 195.
- (24) T. F. Fässler *Coord. Chem. Rev.*, 2001, **215**, 347.
- (25) S. Scharfe, F. Kraus, S. Stegmaier, A. Schier and T. F. Fässler, *Angew. Chem., Int. Ed.*, 2011, **50**, 3630.
- (26) K. Wade *Chem. Commun.*, 1971, **10**, 210.
- (27) K. Wade *Adv. Inorg. Chem. Radiochem.*, 1976, **16**, 1.
- (28) S. Ponou and T. F. Fässler, *Z. Anorg. Allg. Chem.*, 2007, **633**, 393.
- (29) V. Queneau and S. C. Sevov, *Angew. Chem., Int. Ed. Engl.*, 1997, **36**, 1754.

- (30) R. B. King and I. Silaghi-Dumitrescu, *Inorg. Chem.*, 2003, **42**, 6701.
- (31) W. N. Lipscomb *Science*, 1966, **153**, 373.
- (32) L. J. Guggenberger and E. L. Muetterties, *J. Am. Chem. Soc.*, 1976, **98**, 7221.
- (33) C. Adamo and V. Barone, *J. Chem. Phys.*, 1999, **110**, 6158.
- (34) T. H. Dunning *J. Chem. Phys.*, 1989, **90**, 1007
- (35) D. Y. Zubarev and A. I. Boldyrev, *Phys. Chem. Chem. Phys.*, 2008, **10**, 5207
- (36) N. V. Tkachenko and A. I. Boldyrev, *Phys. Chem. Chem. Phys.* **2019**, *21*, 9590.
- (37) F. Weinhold and C. R. Landis, *Valency and Bonding: A Natural Bond Orbital Donor–Acceptor Perspective*, Cambridge University Press, Cambridge, UK, 2005.
- (38) Z. Chen, C. S. Wannere, C. Corminboeuf, R. Puchta and P. v. R. Schleyer, *Chem. Rev.*, 2005, **105**, 3842.
- (39) A. Stanger *J. Org. Chem.*, 2006, **71**, 883.
- (40) O. Kysliak, T. Kunz and A. Schnepf, *Eur. J. Inorg. Chem.*, 2017, **2017**, 805.
- (41) O. Kysliak and A. Schnepf, *Z. Anorg. Allg. Chem.*, 2019, **645**, 335.
- (42) O. Kysliak and A. Schnepf, *Dalton Trans.*, 2016, **45**, 2404.
- (43) F. Li and S. C. Sevov, *Inorg. Chem.*, 2012, **51**, 2706.
- (44) A. Schnepf *Angew. Chem., Int. Ed.*, 2003, **42**, 2624.
- (45) F. S. Geitner, J. V. Dums and T. F. Fassler, *J. Am. Chem. Soc.*, 2017, **139**, 11933.
- (46) L. Xu and S. C. Sevov, *J. Am. Chem. Soc.*, 1999, **131**, 9245.
- (47) P. D. Pancharatna and R. Hoffmann, *Inorg. Chim. Acta*, 2006, **359**, 3776.
- (48) M. B. Boeddinghaus, S. D. Hoffmann and T. F. Fässler, *Z. Anorg. Allg. Chem.*, 2007, **633**, 2338.
- (49) K. Mayer, L. J. Schiegerl and T. F. Fässler, *Chem.–Eur. J.*, 2016, **22**, 18794.

- (50) J. M. Goicoechea and S. C. Sevov, *Angew. Chem., Int. Ed.*, 2005, **44**, 4026.
- (51) F. S. Geitner, W. Klein and T. F. Fässler, *Angew. Chem., Int. Ed.*, 2018, **57**, 1.

Tables and figures

Table 3-1. Relative energies with ZPE corrections (kcal mol⁻¹) of D_{3h} and C_{4v} [Ge₉]⁴⁻ structures at various levels of theory.

Structure	PBE0			B3LYP		
	LANL2DZ	Aug-cc-pvdz	Aug-cc-pvtz	LANL2DZ	Aug-cc-pvdz	Aug-cc-pvtz
D_{3h} [Ge ₉] ⁴⁻	0.0	0.0	0.0	0.0	0.0	0.0
C_{4v} [Ge ₉] ⁴⁻	0.0	1.6	10.2 ^a	0.0	0.4	9.1 ^a

^a Structure is a first order stationary point

Table 3-2. Cartesian coordinates of points for NICS calculation.

$D_{3h} - [Ge_9]^{4-}$	<p><i>Ge</i> 1.608480000 0.000000000 -1.410366000</p> <p><i>Ge</i> -0.804240000 -1.392985000 -1.410366000</p> <p><i>Ge</i> -0.804240000 1.392985000 -1.410366000</p> <p><i>Ge</i> 1.608480000 0.000000000 1.410366000</p> <p><i>Ge</i> -0.804240000 1.392985000 1.410366000</p> <p><i>Ge</i> -0.804240000 -1.392985000 1.410366000</p> <p><i>Ge</i> 1.250482000 2.165898000 0.000000000</p> <p><i>Ge</i> 1.250482000 -2.165898000 0.000000000</p> <p><i>Ge</i> -2.500963000 0.000000000 0.000000000</p> <p><i>Point 1</i> -1.652600000 0.000000000 0.000000000</p> <p><i>Point 2</i> -0.804240000 0.000000000 0.000000000</p> <p><i>Point 3</i> 0.000000000 0.000000000 0.000000000</p> <p><i>Point 4</i> 0.000000000 0.000000000 -1.410366000</p> <p><i>Point 5</i> 0.000000000 0.000000000 -2.410366000</p>
$C_{4v} - [Ge_9]^{4-}$	<p><i>Ge</i> 1.419021000 1.419021000 -0.793758000</p> <p><i>Ge</i> -1.419021000 1.419021000 -0.793758000</p> <p><i>Ge</i> 0.000000000 1.857957000 1.413427000</p> <p><i>Ge</i> 1.419021000 -1.419021000 -0.793758000</p> <p><i>Ge</i> 0.000000000 -1.857957000 1.413427000</p> <p><i>Ge</i> -1.419021000 -1.419021000 -0.793758000</p> <p><i>Ge</i> 1.857957000 0.000000000 1.413427000</p> <p><i>Ge</i> 0.000000000 0.000000000 -2.478676000</p> <p><i>Ge</i> -1.857957000 0.000000000 1.413427000</p> <p><i>Point 1</i> 0.000000000 0.000000000 -1.636218000</p> <p><i>Point 2</i> 0.000000000 0.000000000 -0.793758000</p> <p><i>Point 3</i> 0.000000000 0.000000000 0.309837000</p> <p><i>Point 4</i> 0.000002000 0.000000000 1.413427000</p> <p><i>Point 5</i> 0.000002000 0.000000000 2.413427000</p>

Table 3-3. NICS_{zz} and NICS_{iso} indices calculated at chosen points for D_{3h} and C_{4v} [Ge₉]⁴⁻ clusters.

Point	C_{4v} [Ge ₉] ⁴⁻		D_{3h} [Ge ₉] ⁴⁻	
	NICS _{zz}	NICS _{iso}	NICS _{zz}	NICS _{iso}
1	-152.42	-85.91	-62.91	-50.81
2	-102.32	-94.10	-90.53	-67.92
3	-99.76	-90.68	-90.47	-65.89
4	-97.46	-78.02	-87.71	-55.38
5	-55.43	-26.92	-68.37	-22.68

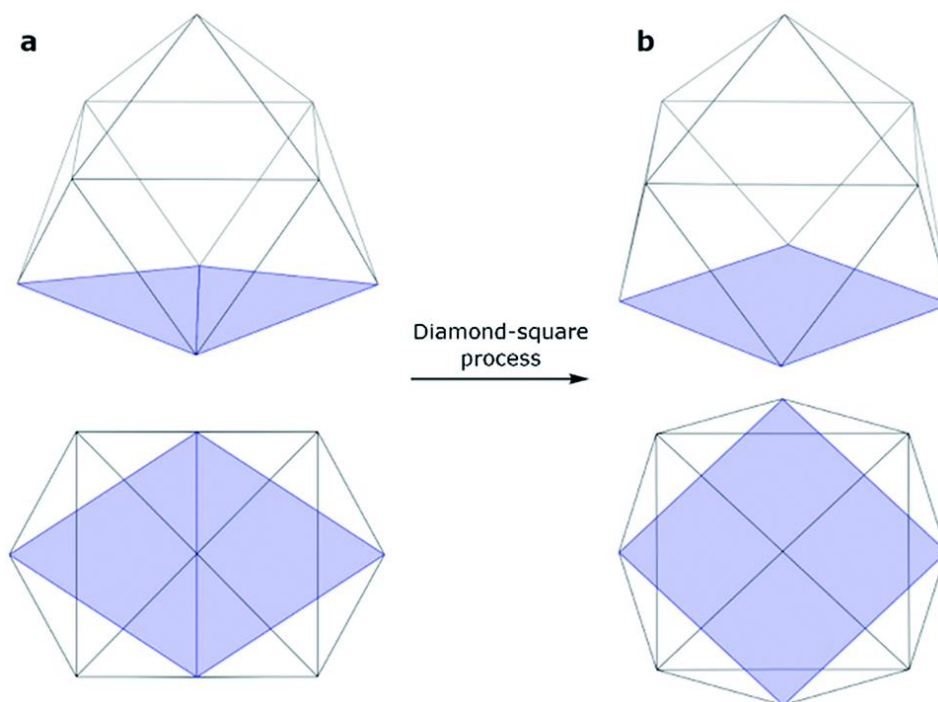


Figure 3-1. Side and top views of a (a) tricapped trigonal prism (D_{3h} symmetry) and (b) capped square antiprism (C_{4v} symmetry).

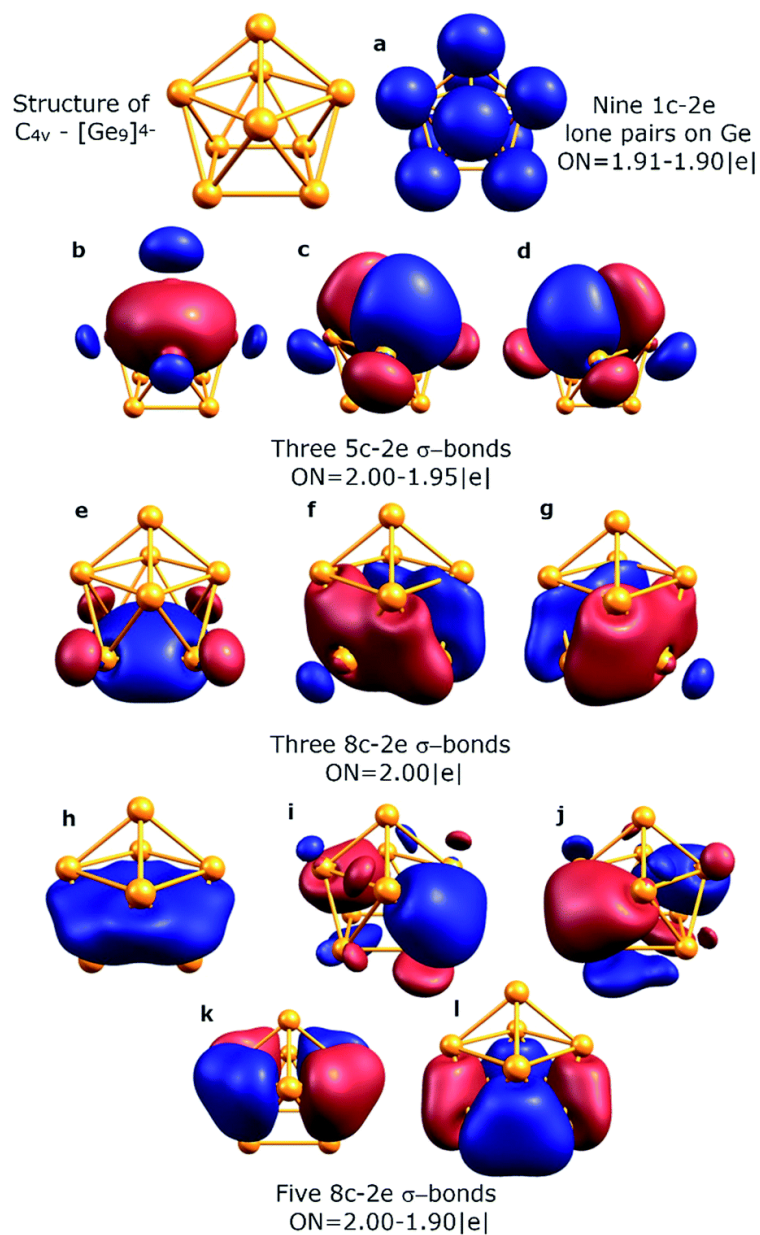


Figure 3-2. Overall chemical bonding picture obtained for the C_{4v} capped square antiprism $[\text{Ge}_9]^{4-}$ cluster. ON denotes the occupation number (equal to 2.00 |e| in an ideal case). Lines between atoms help in visualization and do not represent 2c-2e bonds here and elsewhere.

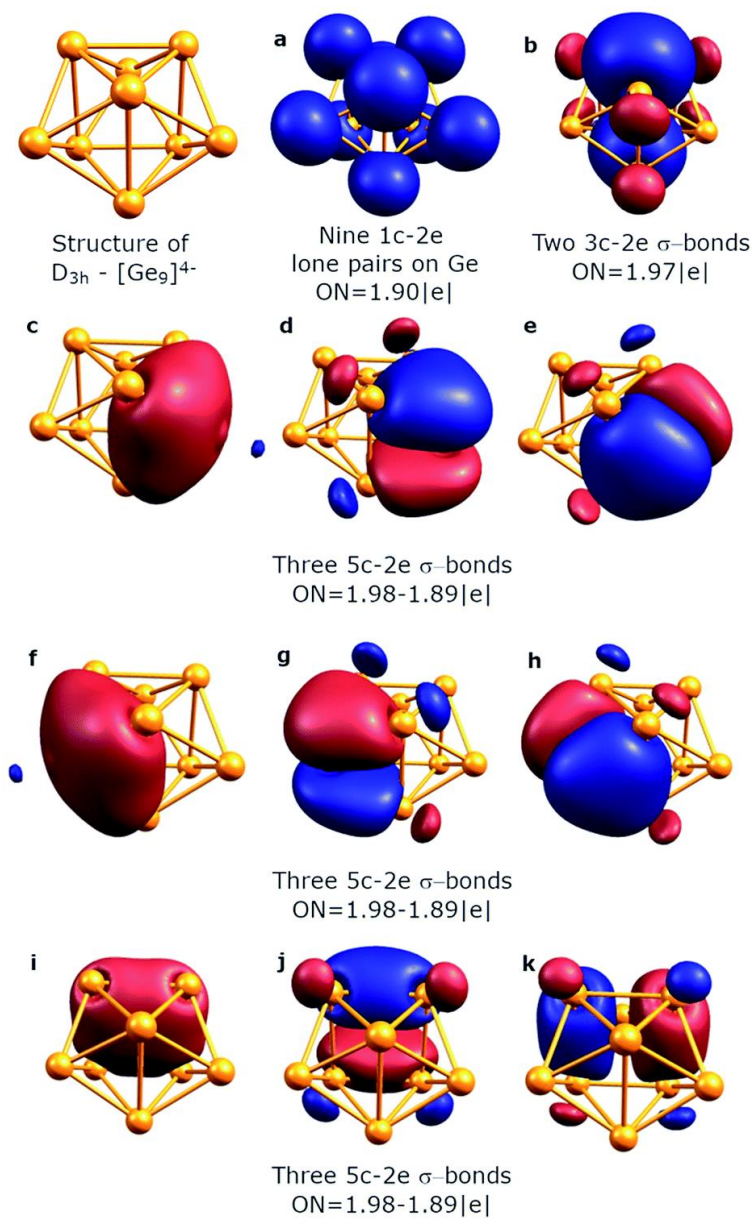


Figure 3-3. Overall chemical bonding picture obtained for the D_{3h} tricapped trigonal prism $[\text{Ge}_9]^{4-}$ cluster.

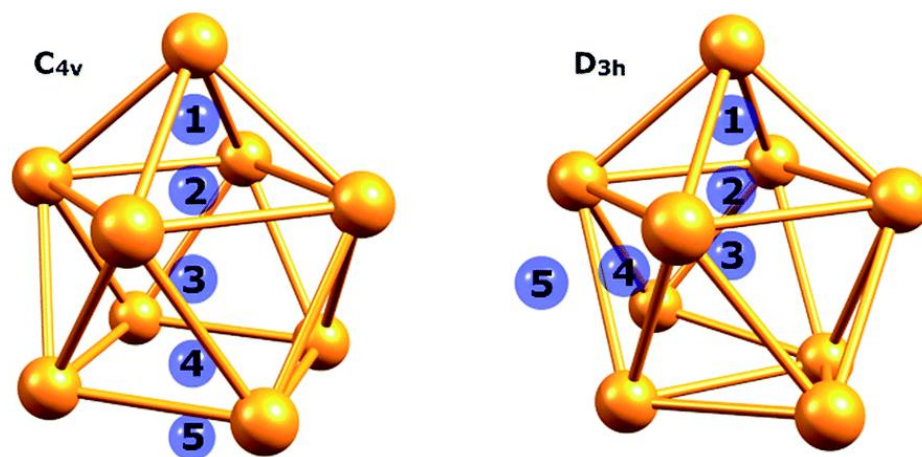


Figure 3-4. Points that were chosen for the NICS indices calculation.

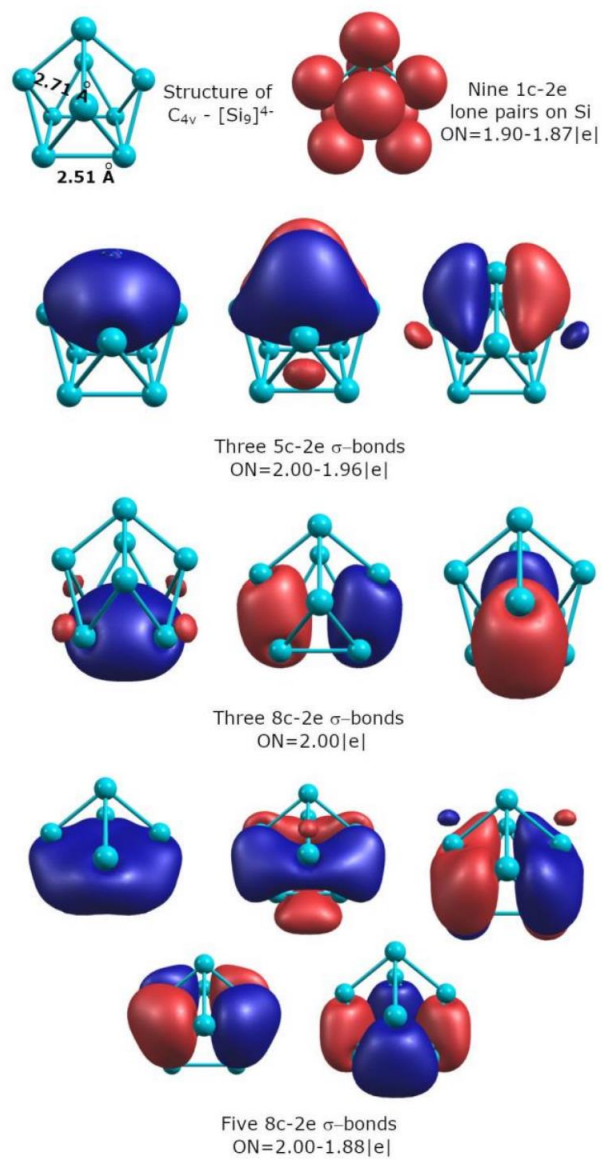


Figure 3-5. Chemical bonding picture of C_{4v} $[Si_9]^{4-}$ cluster.

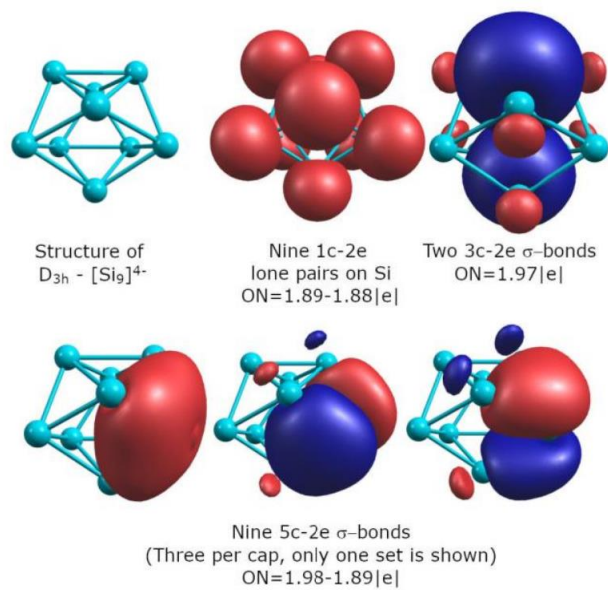


Figure 3-6. Chemical bonding picture of D_{3h} $[\text{Si}_9]^{4-}$ cluster.

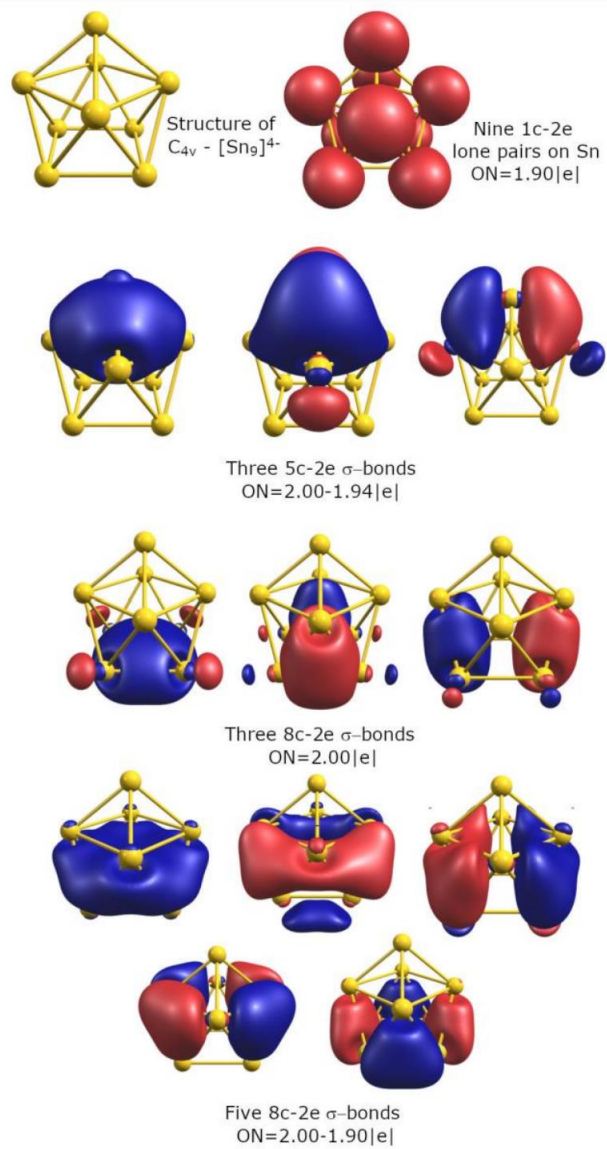


Figure 3-7. Chemical bonding picture of C_{4v} $[Sn_9]^{4-}$ cluster.

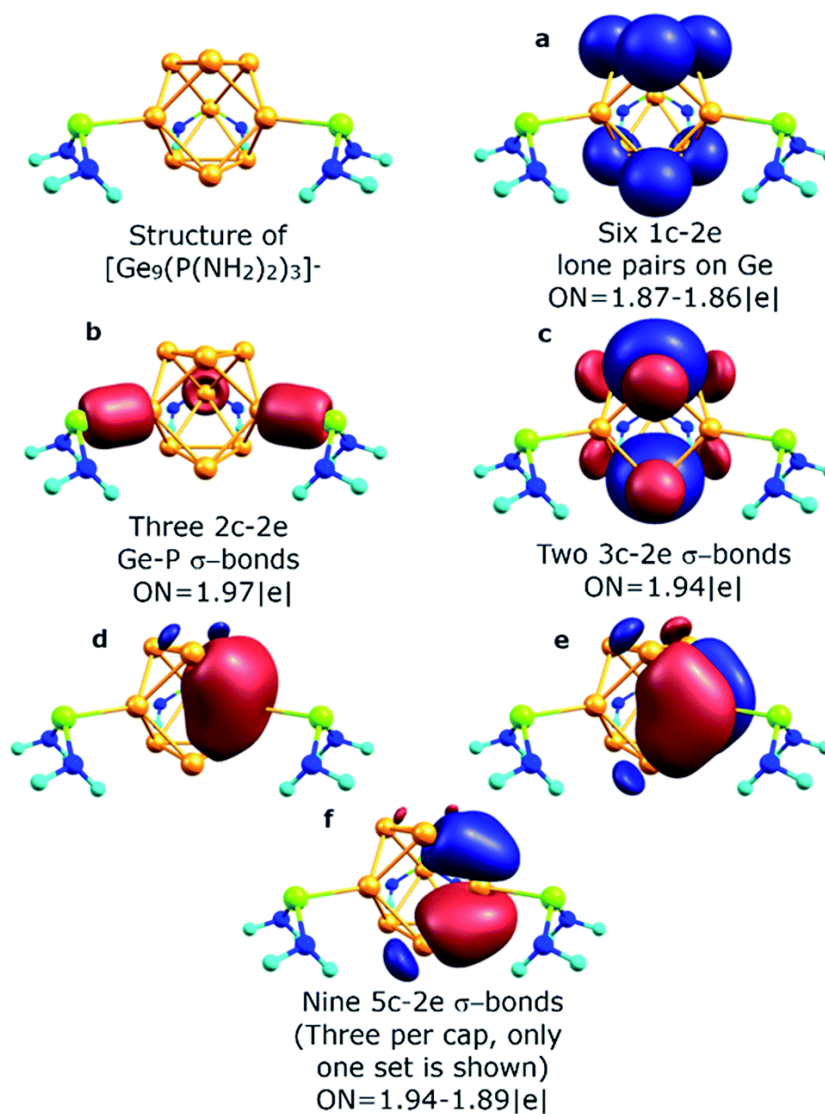


Figure 3-8. Chemical bonding picture of the core Ge_9 fragment obtained for the $[\text{Ge}_9\{\text{P}(\text{NH}_2)_2\}_3]^-$ cluster.

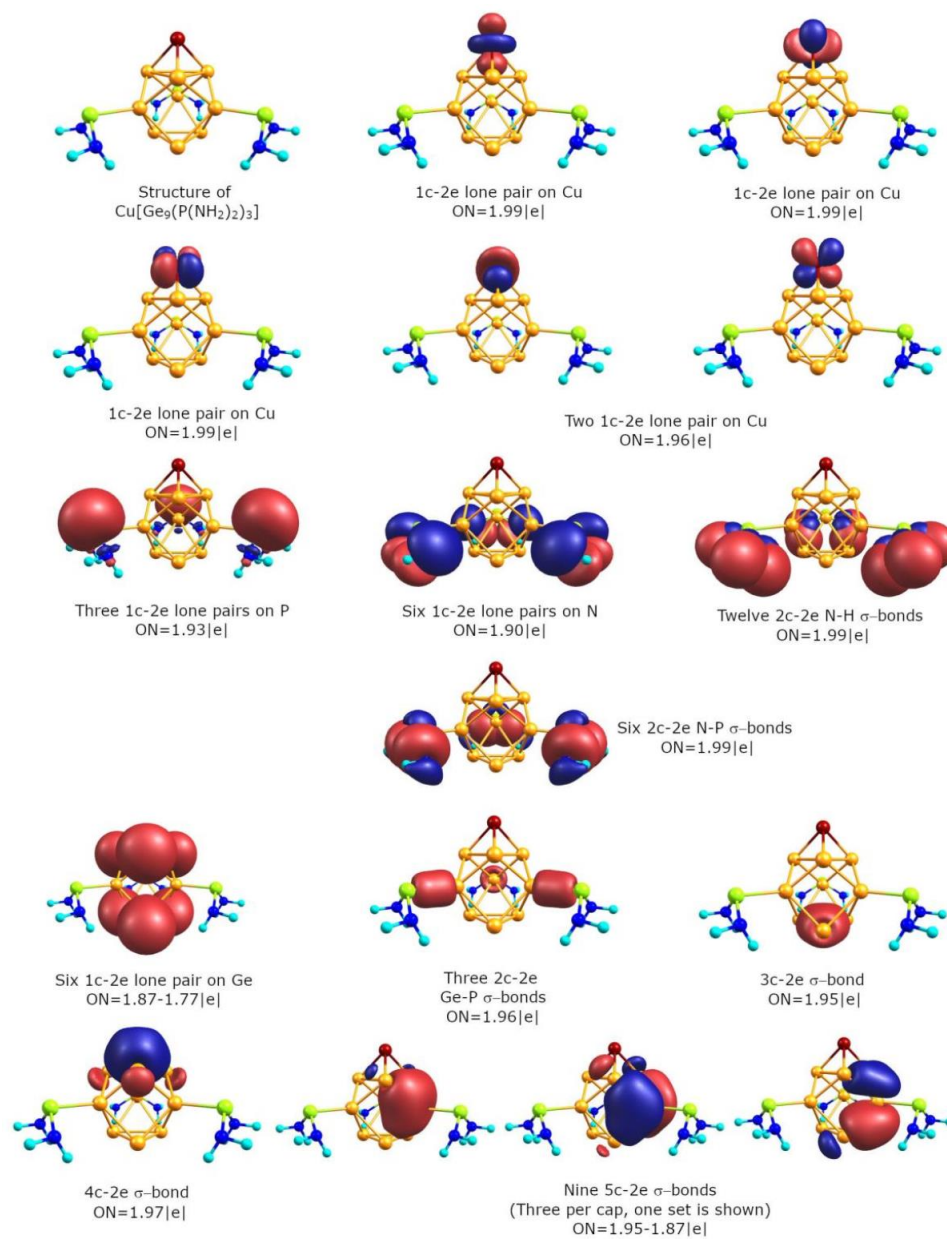


Figure 3-9. Chemical bonding picture of $\text{Cu}[\text{Ge}_9\{\text{P}(\text{NH}_2)_2\}_3]$ cluster.

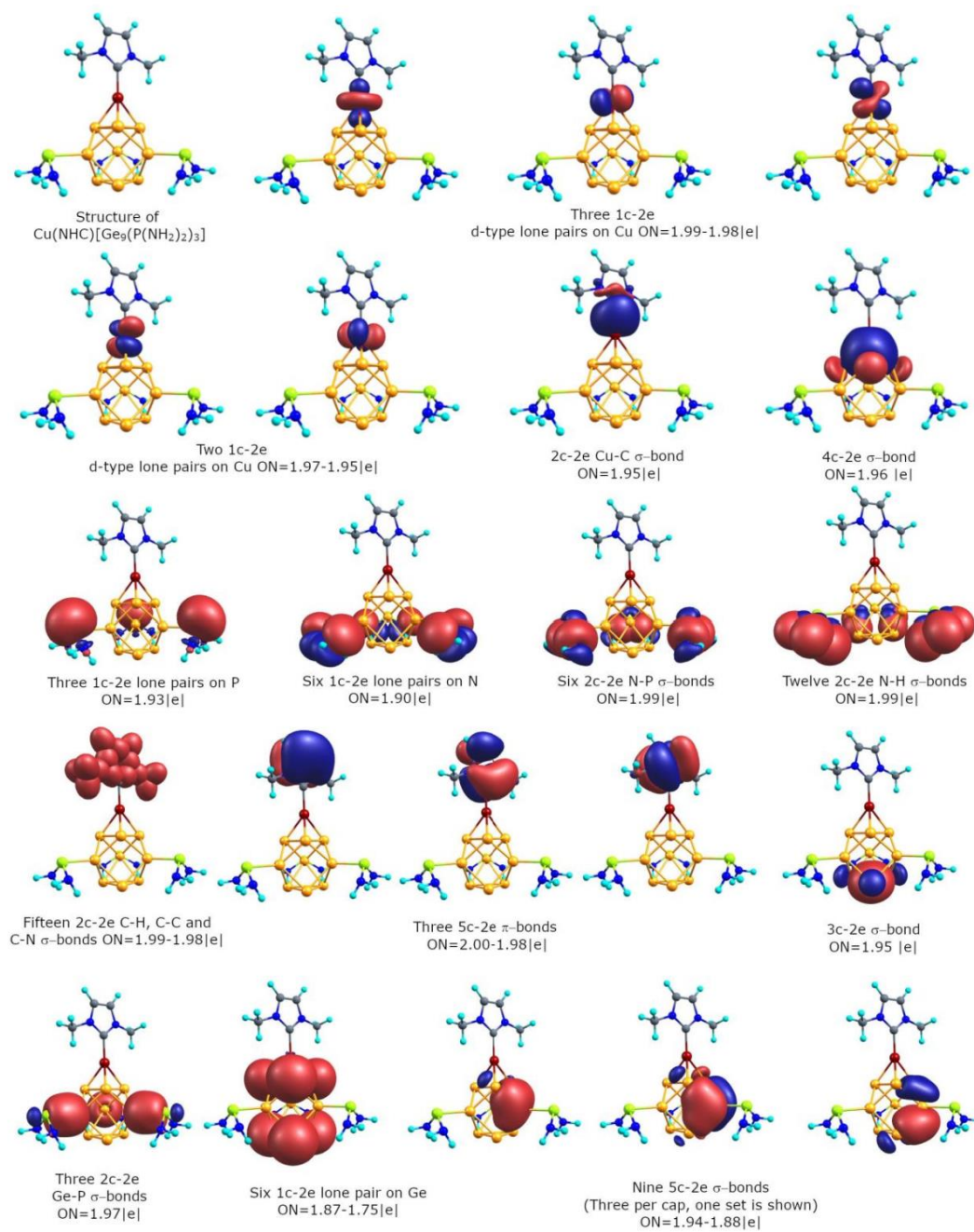


Figure 3-10. Chemical bonding picture of $\text{Cu}(\text{NHC})[\text{Ge}_9\{\text{P}(\text{NH}_2)_2\}_3]$ cluster.

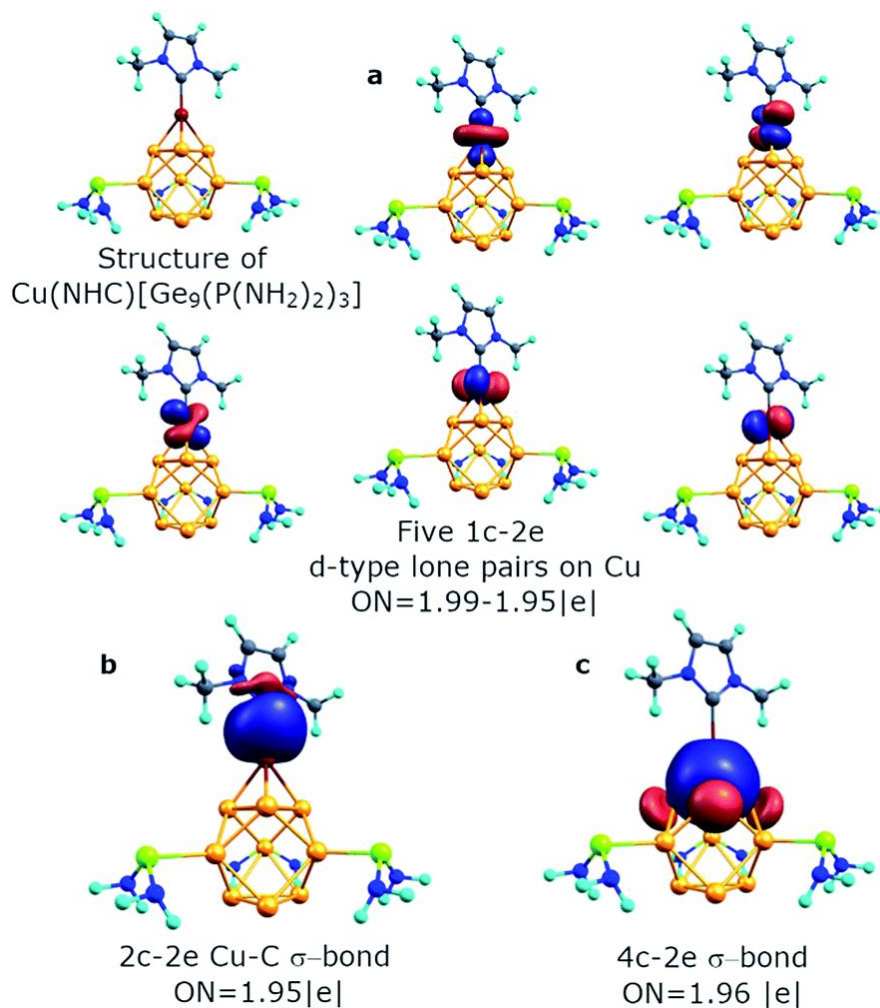


Figure 3-11. Chemical bonding of the Cu atom in the $\text{Cu}(\text{NHC})[\text{Ge}_9\{\text{P}(\text{NH}_2)_2\}_3]^-$ cluster.

CHAPTER 4
SYMMETRY COLLAPSE DUE TO THE PRESENCE OF MULTIPLE LOCAL
AROMATICITY IN Ge_{24}^{4-} ¹

Abstract

Understanding the structural changes taking place during the assembly of single atoms leading to the formation of atomic clusters and bulk materials remains challenging. The isolation and theoretical characterization of medium-sized clusters can shed light on the processes that occur during the transition to a solid-state structure. In this work, we synthesize and isolate a continuous 24-atom cluster Ge_{24}^{4-} , which is characterized by X-ray diffraction analysis and Energy-dispersive X-ray spectroscopy, showing an elongated structural characteristic. Theoretical analysis reveals that electron delocalization plays a vital role in the formation and stabilization of the prolate cluster. In contrast with carbon atoms, 4 s orbitals of Ge-atoms do not easily hybridize with 4p orbitals and s-type lone-pairs can be localized with high occupancy. Thus, there are not enough electrons to form a stable symmetrical fullerene-like structure such as C_{24} fullerene. Three aromatic units with two $[\text{Ge}_9]$ and one $[\text{Ge}_6]$ species, connected by classical 2c-2e Ge-Ge σ -bonds, are aligned together forming three independent shielding cones and eventually causing a collapse of the global symmetry of the Ge_{24}^{4-} cluster.

4.1 Introduction

Understanding how the addition of atoms one by one leads to the transition from a single atom to a diatomic molecule to atomic clusters and finally to the formation of bulk

¹ Coauthored by Hong-Lei Xu, Nikolay V. Tkachenko, Dariusz W. Szczepanik, Ivan A. Popov, Alvaro Muñoz-Castro, Alexander I. Boldyrev & Zhong-Ming Sun. Reproduced from *Nat. Commun.*, **2022**, *13*, 2149 with permission. Copyright © 2022 Springer Nature.

solid-state allotropes is a dream of many chemists. This understanding will help us to design tailorable materials with ever-unusual structures and other physical and chemical properties. Today we still do not understand how such evolution is happening. A striking example is carbon—one of the most investigated elements. Although it is known that the transition from diatomic C_2 to larger carbon clusters goes through the formation of linear chains,¹ cyclic structures,² and cage-like fullerenes,³ we still do not completely know how fullerenes will transform upon further addition of atoms and finally form bulk graphite or diamond. For other elements, our knowledge of this evolution is less clear. Even for the most similar isoelectronic elements of the IV group of the Periodic Table (Ge and Si), computational studies showed that atomic clusters' structures behave differently upon growth.^{4,5,6} Thus, the smallest fullerene-like structure for carbon atom occurs at 20 atoms⁷ and continues to evolve beyond. However, according to the computational results, Si and Ge tend to form prolate structures for medium-sized clusters rather than spherical-like fullerenes. The experimental evidence of such behavior so far was limited to ion mobility experiments⁸ and 2D electron microscopy experiments.⁹ Although theory can propose some trustworthy candidates for low energy structures, one of the most reliable pieces of experimental evidence—a solid state X-Ray characterization, is still lacking for large continuous Ge clusters. Hence the isolation of medium-sized pure germanium species as a key intermediate to understanding the structural transition is of the greatest importance. The isolated ligand-free germanium clusters with over 10 atoms known to date always exhibited a sole coupling model of small clusters,^{10,11,12} which should be better regarded as polymerization tendency. In addition, although the silyl-protected $Ge_{18}[Si(SiMe_3)_3]_6$ cluster cannot be seen as polymers like $[Ge_9-Ge_9]^{6-}$, the outer ligands may dramatically

affect the structures of cluster cores and thus it cannot represent the real structure of pure germanium cluster with 18 atoms.^{13,14}

Here, we show the successful isolation and structural characterization of a germanium cluster Ge_{24}^{4-} (**1a**) featuring an extended prolate structure with fused three-fold faces. Our theoretical calculations show that Ge_{24}^{4-} consists of three independent local sigma-aromatic fragments, which is the reason for the collapse of the symmetry and the formation of a prolate structure. This result helps us understand why carbon structures are so different from silicon and germanium ones. Such a model of Ge_{24}^{4-} reveals the structural features of medium-sized germanium clusters providing solid prospects for further rationalization of larger species.

4.2 Results

4.2.1 Preparation of the anionic Ge_{24}^{4-} cluster

The title complex $[\text{K}(2,2,2\text{-crypt})]_4\text{Ge}_{24}$ (**1**) was synthesized by mild oxidation of $\text{K}_{12}\text{Ge}_{17}$ using excess $\text{Co}(\text{dppe})\text{Cl}_2$ in ethylenediamine solution at 55 °C. After being layered with toluene for 5 weeks, black block-like crystals occurred on the wall of a reaction test tube in an approximate 25% yield based on $\text{K}_{12}\text{Ge}_{17}$. The structure of **1** was characterized by X-ray diffraction analysis, in which some restraints (SIMU, ISOR and/or DFIX for one K atom and related C, N, O atoms on 2,2,2-crypt) were used in the refined process for better building the model of corresponding $[\text{K}(2,2,2\text{-crypt})]^+$ fragment. The Co(II) complex of $\text{Co}(\text{dppe})\text{Cl}_2$ was used as a mild oxidizing agent here, which played a crucial role in the formation of a large title cluster. Similarly, the oxidation reactions of Zintl ions could be observed in the previous cluster formation, such as ten-vertex *closo*- E_{10}^{2-} (E = Ge/Pb)^{15,16} and $[\text{Ge}_{10}\text{Mn}(\text{CO})_4]^{3-}$,¹⁷ as well as larger $\text{Ge}_{18}[\text{Si}(\text{SiMe}_3)_3]_6$ ¹⁴ and

coupled $[\text{Ge}_9 = \text{Ge}_9 = \text{Ge}_9]^{6-}$ ¹¹ in which Fe(II) salt and organic reagent like PPh_3 serve as oxidizing agents, respectively. Furthermore, the redox chemistry involving $\text{Co}(\text{dppe})\text{Cl}_2$ was presented in the synthesis of silyl-protected $[\text{Co}(\text{dppe})_2][\text{Ge}_9\{\text{Si}(\text{SiMe}_3)_3\}_3]$ where the Co(II) reagent was reduced by excess $\text{K}[\text{Ge}_9\{\text{Si}(\text{SiMe}_3)_3\}_3]$ as one counter cation $[\text{Co}(\text{dppe})_2]^+$.¹⁸ Such behavior may be useful to understand the role of $\text{Co}(\text{dppe})\text{Cl}_2$ in the synthesis of Ge_{24}^{4-} cluster. Besides, several Co-centered cluster species have been also prepared by reactions with different Co complexes, such as $[\text{Co}@Ge_{10}]^{3-}$,¹⁹ $[\text{Co}_2@Ge_{16}]^{4-}$,^{20,21} $[\text{Co}@M_{12}]^{3-}$ ($M = \text{Ge}/\text{Pb}$),^{22,23} $[\text{Co}@Sn_6Sb_6]^{3-}$ and $[\text{Co}_2@Sn_5Sb_7]^{3-}$.²⁴ Interestingly, the $[\text{Co}_2@Ge_{16}]^{4-}$ anion contained two types of cluster units (α and β form) and could be obtained by using different Co reagents, $\text{Co}(\text{PPhEt}_2)_2(\text{mes})_2$ and $\{(\text{ArN})_2\text{C}t\text{Bu}\}\text{Co}(\eta^6\text{-toluene})$. Unlike the synthesis of $[\text{Co}(\text{dppe})_2][\text{Ge}_9\{\text{Si}(\text{SiMe}_3)_3\}_3]$ or $[\text{Co}@Ge_{10}]^{3-}$, the related reduced products containing Co element failed to be observed or isolated from the en/tol solution. The as-synthesized **1** could not be reproduced by using other cobalt reagents such as CoMe_2 or tuning down the reaction temperature, otherwise, only some small Ge clusters such as $[\text{K}(2,2,2\text{-crypt})]_2\text{Ge}_9$ and $[\text{K}(2,2,2\text{-crypt})]_2\text{Ge}_5$ were afforded.

4.2.2 Experimental characterization of Ge_{24}^{4-} cluster

Energy-dispersive X-ray spectroscopy (EDX, Supplementary Fig. 8 of the original manuscript) displayed the composition of **1**, including only two (semi)metal elements of K and Ge, which is in good agreement with the calculated values. Electrospray-ionization mass spectrometry by dissolving crystals of **1** in DMF solution indicated besides small fragment of $\{[\text{K}(2,2,2\text{-crypt})][\text{Ge}_{10}]\}^-$, only the corresponding weak signal of parent

cluster was observed at $m/z = 2989.7936$ for $\{[\text{K}(2,2,2\text{-crypt})]_3[\text{Ge}_{24}]\}^-$ due to the inevitable decomposition during the experiments.

As shown in Fig. 4-1a, the overall structure of Ge_{24}^{4-} is prolate with an aspect ratio of nearly 3:1 and can be divided into four different polyhedron sections, including a D_{3h} -symmetric Ge_9 cage (unit-1, Ge1–9), distorted prism (unit-2, Ge7–12), second peculiar Ge_9 cage (unit-3, Ge10–18) and the third distorted C_{4v} -symmetric Ge_9 cage (unit-4, Ge16–24). This prolate geometry is similar to the ligand-protected tin cluster $\text{Sn}_{20}(\text{Si}^t\text{Bu}_3)_{10}\text{Cl}_2$ with raspberry-like arrangement of smaller Sn_{10} units, which is formed by the disproportionation reaction of a Sn(I) halide.²⁵ In light of the structural feature, cluster **1a** exhibits a larger prolate structure compared with previous ten-vertex *closo*- E_{10}^{2-} ($\text{E} = \text{Ge}/\text{Pb}$)^{15,16} and $[\text{Ge}_{10}\text{Mn}(\text{CO})_4]^{3-}$ ¹⁷ which are formed by similar soft oxidation from basic E_9 ($\text{E} = \text{Ge}/\text{Pb}$) units. Such atomic arrangement in **1a** is different from the oxidative coupling forms of $(\text{Ge}_9)_n$.¹⁰⁻¹³ In this sense, Ge_{24}^{4-} may undergo a more complex growth pattern. The attempt using the K_4Ge_9 as a precursor failed to obtain the title compound under parallel experimental conditions. In contrast to smaller Ge_{10} species, the formation of the title cluster **1a** may require a downsizing and further combination of additional Ge_9 units. The effect of Ge_4 units from $\text{K}_{12}\text{Ge}_{17}$ is still unclear in the formation of cluster Ge_{24}^{4-} . Compared with the binary $[\text{Au}_3\text{Ge}_{45}]^{9-}$,²⁶ the Ge_{24}^{4-} cluster represents a medium-sized Ge cluster without doped transition metals. Furthermore, except for the similar structural characteristic from one Ge_9 of unit-4 and central Ge_6 fragment, the Ge_{24}^{4-} cluster exhibits another type of coordinated Ge_9 unit to the central Ge_6 fragment, which is different from the $[\text{Au}_3\text{Ge}_{45}]^{9-}$ due to the effect of Au atoms.

From another perspective, the Ge_{24}^{4-} cluster could also be described as two-terminal Ge_9 -units bridged via a Ge_6 central fragment along exo-bonds to triangular faces. In this sense, the central bowl-shaped Ge_6 fragment plays a crucial role in the formation of **1a**, and it is suggested as a growth-trigger in the evolution toward larger species. Furthermore, it is also likely to affect the shapes of two terminal Ge_9 -cages by the different coordination fashions. The whole structure can be also viewed as three connected Ge_9 -units involving a terminal cage and fused nine-membered cages sharing three atoms, providing many flavors of the Ge Zintl-ion chemistry in a single molecular structure, able to coincide under similar experimental conditions. Apart from the K_4Ge_9 , the $\text{K}_{12}\text{Ge}_{17}$ was also used as the source of Ge_9 unit and related examples have been reported, such as $[\text{Ge}_9\text{-Ge}_9]^{6-}$ (with ZnCp^*_2 , $\text{Cp}^* =$ pentamethylcyclopentadienyl),²⁷ $(\text{NHC}^{\text{DippM}})_2\{\eta^3\text{-Ge}_9(\text{Si}(\text{TMS})_3)_2\}$ ($\text{M} = \text{Cu}/\text{Ag}/\text{Au}$),²⁸ $[\text{Ph}_2\text{Bi}-(\text{Ge}_9)\text{-BiPh}_2]^{2-}$.²⁹

The bowl-shaped Ge_6 fragment (Fig. 4-1b) is reminiscent of similar organic molecules corannulene ($\text{C}_{20}\text{H}_{10}$)³⁰ or sumanene ($\text{C}_{21}\text{H}_{12}$),³¹ a fullerene fragment, with a curved molecular surface. In contrast, the bowl depth of the Ge_6 fragment is 0.93 Å, which is close to corannulene (~0.88 Å).³² As shown in Fig. 4-1c, the central triangle (dotted lines) in the Ge_6 fragment has elongated Ge-Ge distances of av. 2.813 Å like in $[\text{Au}_3\text{Ge}_4]^{9-}$,²⁶ which is remarkably longer than other Ge-Ge bonds with an average length of 2.487 Å. Furthermore, the Ge_6 bowl combines with a neighboring Ge_3 face from unit-4 by three Ge-Ge bonds (2.471–2.495 Å) to form an interesting nine-atom cage (Fig. 4-1d) in which two staggered Ge_3 faces lead to three almost identical edge-sharing pentagons. In unit-1, the Ge-Ge distances (2.5304(16)-2.6739(16) Å) are in the expected range³³ and lengths of the prisms (Ge1–Ge7, 2–8, 3–9: 2.8084(16)–2.8744(16) Å) are elongated compared with those

(2.71–2.73 Å) in bare D_{3h} -[Ge₉]²⁻ cluster.³⁴ Additionally, the extended bottom face of the central Ge₆ fragment coordinates to the triangle face of unit-1 through three *exo* Ge-Ge bonds (av. 2.581 Å) forming a distorted triangular prism (Fig. 4-1e). In contrast to D_{3h} -unit-1, unit-4 exhibits a largely distorted C_{4v} -structure with a broader range of Ge-Ge contacts (2.4960(14)-2.8598(15) Å).

4.2.3 Computational Studies

To understand the reason for the stability and geometrical features of the Ge₂₄⁴⁻ cluster we performed density functional theory (DFT) calculations.^{35,36} The details of theoretical calculations are given in the methods section of this chapter. The optimized geometry resembles all structural features that were found in the X-Ray experiment. The average Ge-Ge distance of the optimized structure is ~0.07 Å longer than the experimental one, which is a common deviation for the calculation of highly charged Zintl ions with DFT methods. A high HOMO-LUMO gap (2.67 eV) was found for the optimized cluster indicating its remarkably high stability, while shapes of three lowest-lying valence molecular orbitals show certain lack of global aromaticity as the extent of electron delocalization is restricted to three disjoint fragments, D_{3h} -Ge₉ (HOMO-49), C_{4v} -Ge₉ (HOMO-48), and Ge₆ (HOMO-47) (Fig. 4-2a). To evaluate whether and to what extent these characteristic delocalization patterns survive the interference with all the remaining valence molecular orbitals, we performed the Electron Density of Delocalized Bonds (EDDB) analysis.³⁷ The EDDB is a part of the state-of-the-art theoretical method combining different quantum-chemistry and information-theory techniques to decompose the valence-electron density of a molecule into density layers representing chemical entities such as lone pairs, localized (Lewis-type) bonds, and delocalized (‘resonating’) bonds.³⁸ The results of the EDDB analysis clearly

show that 28.5% of the valence-shell electrons do not participate in chemical bonding giving rise to fifteen (4s-type) lone-pairs, about 39.2% of the valence-shell electrons is involved in the Lewis-type Ge-Ge σ -bonding, while the remaining electrons are delocalized in full accordance with topology of HOMO-49, HOMO-48, and HOMO-47, thus marking three independent locally aromatic units: two 3D-aromatic Ge₉ cages and a single σ -aromatic Ge₆ fragment (Fig. 4-2b). We note that the presented case is different from cylindrical aromaticity,³⁹ or organic cages with antiaromatic circuits stacked to each other⁴⁰ since three independent aromatic fragments are aligned together, preserving their individual aromatic properties. The average contribution of each germanium atom in the Ge₂₄⁴⁻ cluster to the electron delocalization is 1.43 |e|, 1.42 |e|, and 1.10 |e| in units D_{3h}-Ge₉, C_{4v}-Ge₉, and Ge₆, respectively, which is even higher than in the archetypical aromatic system - benzene, where each of the sp²-hybridized carbon atoms contributes to the aromatic ring 0.89 |e| and 0.10 |e| through π - and σ -channel, respectively.³⁷ All this may account for crucial role of the composite aromatic stabilization in the Ge₂₄⁴⁻ cluster, and the lack of effective *s-p* atomic-orbital hybridization, especially in the Ge₉ 3D-cages, seems to significantly increase the ability to charge delocalization.

For a more in-depth and systematic study of the chemical bonding in the synthesized cluster, we performed the Adaptive Natural Density Partitioning (AdNDP) analysis.^{41,42} The AdNDP is an electron-localization technique that partitions the natural density of the system and reproduces the most occupied localized bonding elements. The results of the analysis are shown in Fig. 4-3. Considering one-center two-electron (1c-2e) elements, AdNDP found fifteen *s*-type lone-pairs with high occupation number values (ON = 1.90–1.87 |e|) on Ge atoms. Chemical bonding of the middle part of the cluster majorly consists

of classical 2c-2e Ge-Ge σ -bonds with $ON = 1.95\text{--}1.91 |e|$ and describes a bonding between Ge_6 and two Ge_9 fragments. Highly occupied delocalized 3c-2e σ -bond ($ON = 1.96 |e|$) governs the bonding within the Ge_6 fragment and stabilizes the bowl-like Ge_6 structure. Chemical bonding of the D_{3h} - Ge_9 fragment consists of two 3c-2e σ -bonds with $ON = 1.97 |e|$ and nine 5c-2e σ -bonds (three bonds per each Ge_5 cap) with $ON = 1.91\text{--}1.79 |e|$. The collection of such delocalized bonding elements possesses spherical-like shielding cones as was shown in our previous studies.^{43,44} Analogically, the chemical bonding of the C_{4v} - Ge_9 fragment consists of three delocalized bonding regions resulting in three 5c-2e bonding elements within the Ge_5 cap ($ON = 1.98\text{--}1.93 |e|$), three 4c-2e bonding elements within the Ge_4 square ($ON = 1.95\text{--}1.62 |e|$), and five 8c-2e bonding elements within the Ge_8 antiprism ($1.99\text{--}1.87 |e|$). We note that the low occupation number of 4c-2e bonding element could be increased up to $1.94 |e|$ with the inclusion of all atoms of Ge_8 antiprism (Fig. 4-4). A similar situation was earlier described for the isolated C_{4v} - Ge_9^{4-} cluster.⁴⁵ That assignment does not change the overall chemical bonding picture. Shapes of the found bonds and numbers of electrons on the fragments that agree with the Hückel's $(4n + 2)$ electron counting rule render two Ge_9 fragments locally σ -aromatic.⁴⁵ From the chemical bonding analysis described above, we can expect the presence of three independent aromatic regions from the C_{4v} - Ge_9 , Ge_6 , and D_{3h} - Ge_9 fragments, in full agreement with theoretical results obtained by the EDDB method.

In order to further explore the aromatic characteristics of **1a**, the magnetic criteria of aromaticity was employed (Fig. 4-5a).^{46,47,48} The isotropic term, given by NICS_{iso} three-dimensional grids, similar to isochemical shielding surface (ICSS) maps, shows a continuous shielding region along with the entire structure. Significantly, under different

orientations of the applied field, the shielding cone characteristics were found. In contrast to planar aromatic species for which shielding cones are enabled only when the field is oriented perpendicular to the ring,⁴⁹ we found the presence of three cones merged together for any direction of the applied field.^{48,50} With the field-oriented along the axis containing all the three cluster fragments (*i.e.* external field oriented along with the z -axis, $\mathbf{B}_z^{\text{ind}}$), a formation of three-overlapped shielding cones centered at each Ge-fragment is observed. For perpendicular orientations (*i.e.* y - and x -axis, $\mathbf{B}_y^{\text{ind}}$ and $\mathbf{B}_x^{\text{ind}}$ respectively), the three shielding cones are aligned similarly to the anthracene molecule, which features three fused aromatic rings as depicted in previous works.^{51,52} Such features are retained under arbitrary orientations of the applied field, denoting how the three adjacent shielding cones evolve under rotation (Fig. 4-6).

Next, we explore the characteristics of each aromatic unit. To represent Ge_6 bowl-like structure, a Ge_9 cluster with a shared triangular face of C_{4v} - Ge_9 was chosen. Interestingly, despite of fragments' different shapes, each isolated fragment exhibits similar characteristics to spherical aromatic species with a continuous shielding region from NICS_{iso} , and shielding cone characteristics under different orientations of the field (Fig. 4-5b).⁴⁹ Noteworthy, the overlap between the aromatic characteristics of the three isolated Ge_9^{4-} clusters largely resembles the behavior of the overall Ge_{24}^{4-} cluster supporting that after aggregation involving both exo-bonds and face-fusion schemes, each Ge_9 unit meets the electronic distribution requirements to behave as spherical aromatics. Hence, Ge_{24}^{4-} can be viewed as a linear trimer built-up by related aromatic clusters, exhibiting different shapes and aggregation schemes.

4.3 Conclusions

The synthesis and characterization of Ge_{24}^{4-} cluster in a solid-state is a missing chain link between small germanium clusters and bulk solid-state germanium. It confirms the prolate structure that was predicted computationally in a gas phase for neutral germanium species,^{4,5,6} providing an explicit structural characteristic of a medium-sized Ge cluster. High symmetry collapse in Ge_{24}^{4-} occurs due to the presence of multiple local aromaticity and lack of *s-p* hybridization in Ge. The formation of three independent aromatic units shed light on the reason for the formation of low-symmetric prolate structure. We expect that this kind of aromatic units' aggregation will be found in many cluster chemical compounds made in the future. We believe that further investigation of the transition from atomic clusters to bulk materials will bring an understanding and a significant advancement for materials design with a target physical property.

4.4 Methods

4.4.1 Materials

All manipulations and reactions were performed under a dry nitrogen atmosphere in glove box. Ethylenediamine (Aldrich, 99%) and DMF (Aldrich, 99.8%) used in experiments were freshly distilled by CaH_2 prior to use. Toluene (Aldrich, 99.8%) was distilled from sodium/benzophenone under nitrogen and stored under nitrogen. 2,2,2-crypt (4,7,13,16,21,24-Hexaoxa-1,10-diazabicyclo (8.8.8) hexacosane, purchased from Sigma-Aldrich, 98%) and $\text{Co}(\text{dppe})\text{Cl}_2$ (purchased from Alfa Aesar, $\geq 97\%$) were dried in vacuum for 12 h prior to use. According to reported literature,⁵³ the precursor $\text{K}_{12}\text{Ge}_{17}$ was synthesized by heating a stoichiometric mixture of the elements (K: 551 mg, Ge: 1.45 g; K: + 99%, Ge: 99.999%, all from Strem) at a rate of 150 °C per hour to 900 °C and keeping

it for 3 days in sealed niobium containers closed in evacuated quartz ampules. The furnace was slowly cooled to room temperature at a rate of 100 °C per hour.

4.4.2 Synthesis of $[K(2,2,2\text{-crypt})]_4Ge_{24}$ (**1**)

$K_{12}Ge_{17}$ (170 mg, 0.100 mmol) and 2,2,2-crypt (160 mg, 0.424 mmol) were dissolved in 3 mL en in a reaction vial and stirred for 10 min. $Co(dppe)Cl_2$ (63.4 mg, 0.120 mmol) was added and stirred for 6 h at 55 °C. The resulting brown-red solution was filtered with standard glass frit and layered with 4 mL toluene. About 35 days later, black block-like crystals **1** were observed in the test tube (25% yield based on $K_{12}Ge_{17}$).

4.4.3 X-ray diffraction

Suitable crystal from **1** was selected for X-ray diffraction analysis. Crystallographic data was collected on Rigaku XtalAB Pro MM007 DW diffractometer with graphite monochromated Mo $K\alpha$ radiation ($\lambda = 0.71073 \text{ \AA}$). The structure of crystal **1** was solved using direct methods and then refined using SHELXL-2014 and Olex2.^{54,55,56} All the non-hydrogen atoms were refined anisotropically. All hydrogen atoms of organic groups were rationally placed by geometrical considerations. We used the PLATON SQUEEZE procedure to remove the solvent molecules which could not be modeled properly.⁵⁷ We refined the structure by using the rational restraints of anisotropy (SIMU, ISOR, DFIX for K-crypt fragments) and omitted the most disagreeable reflections.

4.4.4 Electrospray ionization mass spectrometry (ESI-MS)

Negative ion mode ESI-MS of the DMF solution of crystals of **1** was measured on an LTQ linear ion trap spectrometer by Agilent Technologies ESI-TOF-MS (6230). The spray voltage was 5.48 kV and the capillary temperature was kept at 300 °C. The capillary voltage was 30 V. The samples were prepared inside a glovebox and very rapidly

transferred to the spectrometer in an airtight syringe by direct infusion with a Harvard syringe pump at 0.2 mL/min.

4.4.5 Energy dispersive X-ray (EDX)

EDX analysis on the title cluster 1 was performed using a scanning electron microscope (FE-SEM, JEOL JSM-7800F, Japan). Data acquisition was performed with an acceleration voltage of 20 kV and an accumulation time of 60 s.

4.4.6 Powder X-ray diffraction

Powder X-ray diffraction (PXRD) data were collected on a Rigaku diffractometer using Cu K α radiation ($\lambda = 1.5418 \text{ \AA}$). The sealed samples were scanned for every 0.01° increment over the Bragg angle range of $10 - 80^\circ$.

4.4.7 Magnetic response analysis

Geometry optimizations and subsequent calculations were performed using scalar relativistic DFT methods employing the ADF code with the all-electron triple- ζ Slater basis set plus the double-polarization (STO-TZ2P) basis set in conjunction with the PBE0 functional.^{36,58,59} In order to evaluate the induced field (\mathbf{B}^{ind}) upon an external magnetic field (\mathbf{B}^{ext}) at the molecular surroundings, according to $\mathbf{B}_i^{\text{ind}} = -\sigma_{ij}\mathbf{B}_j^{\text{ext}}$,^{46,60,61,62,63} the nucleus-independent shielding tensors (σ_{ij})^{46,63,64} were calculated within the GIAO formalism, employing the OPBE^{59,65,66} functional and the all-electron triple- ζ Slater basis set plus the double-polarization (STO-TZ2P), placed in a three-dimensional grid. Relativistic effects were considered through the ZORA Hamiltonian,⁶⁷ ensuring an equal footing treatment of different clusters. For convenience, the i and j suffixes are related to the x-, y- and z-axes of the molecule-fixed Cartesian system ($i, j = x, y, z$). The values of \mathbf{B}^{ind} are given in ppm in relation to \mathbf{B}^{ext} .

4.4.8 Chemical bonding analysis

Geometry optimization and frequency calculations were performed using Gaussian 16 software at the PBE0/Def2-QZVP level of theory.^{36,59,68} To analyze the extent of electron delocalization in the investigated species, we performed the electron density of delocalized bonds (EDDB) calculations,^{37,38} to identify and characterize the chemical bonding, we carried out adaptive natural density partitioning (AdNDP) analysis as implemented in the AdNDP 2.0 code.^{41,42} The EDDB and AdNDP analyses were performed at PBE0/Def2-TZVP level of theory; previously, the results by both methods have been shown to be insensitive to the size of the basis set used.^{38,69}

References

- (1) Orden, A. V. & Saykally, R. J. Small carbon clusters: spectroscopy, structure, and energetics. *Chem. Rev.* **98**, 2313–2358 (1998).
- (2) Kaiser, K. et al. An sp-hybridized molecular carbon allotrope, cyclo[18]carbon. *Science* **365**, 1299–1301 (2019).
- (3) Kroto, H. W. et al. C₆₀: Buckminsterfullerene. *Nature* **318**, 162–163 (1985).
- (4) Yoo, S. & Zeng, X. C. Search for global-minimum geometries of medium-sized germanium clusters. II. Motif-based low-lying clusters Ge₂₁–Ge₂₉. *J. Chem. Phys.* **124**, 184309 (2006).
- (5) Lu, W.-C. et al. Appearance of bulk-like motifs in Si, Ge, and Al clusters. *Phys. Chem. Chem. Phys.* **12**, 8551–8556 (2010).
- (6) Zhao, L.-Z. et al. Fragmentation behavior of Ge_n clusters (2 ≤ n ≤ 33). *Chem. Phys. Lett.* **455**, 225–231 (2008).

- (7) Prinzbach, H. et al. Gas-phase production and photoelectron spectroscopy of the smallest fullerene, C₂₀. *Nature* **407**, 60–63 (2000).
- (8) Hunter, J. M. et al. Structural transitions in size-selected germanium cluster ions. *Phys. Rev. Lett.* **73**, 2063–2066 (1994).
- (9) Bals, S. et al. Atomic scale dynamics of ultrasmall germanium clusters. *Nat. Commun.* **3**, 897 (2012).
- (10) Ugrinov, A. & Sevov, S. C. [Ge₉Ge₉Ge₉Ge₉]⁸⁻: a linear tetramer of nine-atom germanium clusters, a nanorod. *Inorg. Chem.* **42**, 5789–5791 (2003).
- (11) Ugrinov, A. & Sevov, S. C. [Ge₉Ge₉Ge₉]⁶⁻: a linear trimer of 27 germanium atoms. *J. Am. Chem. Soc.* **124**, 10990–10991 (2002).
- (12) Downie, C., Tang, Z.-J. & Guloy, A. M. An unprecedented $_{1\infty}$ [Ge₉]²⁻ polymer: a link between molecular zintl clusters and solid-state phases. *Angew. Chem. Int. Ed.* **39**, 337–340 (2000).
- (13) Xu, L. & Sevov, S. C. Oxidative coupling of deltahedral [Ge₉]⁴⁻ zintl ions. *J. Am. Chem. Soc.* **121**, 9245–9246 (1999).
- (14) Kysliak, O., Schrenk, C. & Schnepf, A. The Largest Metalloid Group 14 Cluster, Ge₁₈[Si(SiMe₃)₃]₆: An Intermediate on the Way to Elemental Germanium. *Angew. Chem. Int. Ed.* **55**, 3216–3219 (2016).
- (15) Bentlohner, M. M., Fischer, C. & Fässler, T. F. Synthesis and characterization of pristine *closo*-[Ge₁₀]²⁻. *Chem. Commun.* **52**, 9841–9843 (2016).
- (16) Spiekermann, A., Hoffmann, S. D. & Fässler, T. F. The Zintl Ion [Pb₁₀]²⁻: a rare example of a homoatomic *closo* Cluster. *Angew. Chem., Int. Ed.* **45**, 3459–3462 (2006).

- (17) Rios, D. & Sevov, S. C. The elusive *closo*-Ge₁₀²⁻ zintl ion: finally “captured” as a ligand in the complex [Ge₁₀Mn(CO)₄]³⁻. *Inorg. Chem.* **49**, 6396–6398 (2010).
- (18) Kysliak, O., Schrenk, C. & Schnepf, A. Reactivity of [Ge₉{Si(SiMe₃)₃]₃]⁻ towards transition-metal M²⁺ cations: coordination and redox chemistry. *Chem. Eur. J.* **22**, 18787–18793 (2016).
- (19) Wang, J.-Q., Stegmaier, S. & Fässler, T. F. [Co@Ge₁₀]³⁻: an intermetalloid cluster with Archimedean pentagonal prismatic structure. *Angew. Chem., Int. Ed.* **48**, 1998–2002 (2009).
- (20) Jin, X. et al. Structure and bonding in a bimetallic endohedral cage, [Co₂@Ge₁₆]²⁻. *J. Organomet. Chem.* **792**, 149–153 (2015).
- (21) Liu, C. et al. [Co₂@Ge₁₆]⁴⁻: localized versus delocalized bonding in two isomeric intermetalloid clusters. *Chem. Eur. J.* **24**, 699–705 (2018).
- (22) Liu, C. et al. Symmetry reduction upon size mismatch: the non-icosahedral intermetalloid cluster [Co@Ge₁₂]³⁻. *Chin. J. Chem.* **36**, 1165–1168 (2018).
- (23) Li, A.-M. et al. Endohedral plumbaspherenes of the group 9 metals: synthesis, structure and properties of the [M@Pb₁₂]³⁻ (M=Co, Rh, Ir) Ions. *Chem. Eur. J.* **26**, 5824–5833 (2020).
- (24) Wilson, R. J. et al. [Co@Sn₆Sb₆]³⁻: an off-center endohedral 12-vertex cluster. *Angew. Chem. Int. Ed.* **57**, 15359–15363 (2018).
- (25) Binder, M., Schrenk, C. & Schnepf, A. Sn₂₀(Si^tBu₃)₁₀Cl₂ – the largest metalloid group 14 cluster shows a raspberry-like arrangement of smaller units. *Chem. Commun.* **55**, 12148–12151 (2019).

- (26) Spiekermann, A. et al. $[\text{Au}_3\text{Ge}_{45}]^{9-}$ —A Binary Anion Containing a $\{\text{Ge}_{45}\}$ Cluster. *Angew. Chem. Int. Ed.* **46**, 5310–5313 (2007).
- (27) Mayer, K. et al. Redetermination of the crystal structure of di-(4,7,13,16,21,24-hexaoxa-1,10-diazabicyclo[8.8.8]hexacosane- $\kappa^8\text{N}_2, \text{O}_6$) potassium – tetrapotassium octadecagermanide – ethylenediamine (1:1:7), $\text{C}_{25}\text{H}_{64}\text{Ge}_9\text{K}_3\text{N}_9\text{O}_6$. *Z. für Kristallographie - N. Cryst. Struct.* **230**, 286–288 (2015).
- (28) Geitner, F. S. et al. N-heterocyclic carbene coinage metal complexes of the germanium-rich metalloid clusters $[\text{Ge}_9\text{R}_3]^-$ and $[\text{Ge}_9\text{R}^1_2]^{2-}$ with $\text{R} = \text{Si}(\text{iPr})_3$ and $\text{R}^1 = \text{Si}(\text{TMS})_3$. *Molecules* **22**, 1204 (2017).
- (29) Ugrinov, A. & Sevov, S. C. $[\text{Ph}_2\text{Bi}-(\text{Ge}_9)-\text{BiPh}_2]^{2-}$: a deltahedral zintl ion functionalized by exo-bonded ligands. *J. Am. Chem. Soc.* **124**, 2442–2443 (2002).
- (30) Barth, W. E. & Lawton, R. G. Dibenzo[ghi,mno]fluoranthene. *J. Am. Chem. Soc.* **88**, 380–381 (1966).
- (31) Sakurai, H., Daiko, T. & Hirao, T. A synthesis of sumanene, a fullerene fragment. *Science* **301**, 1878 (2003).
- (32) Zabula, A. V. et al. A main group metal sandwich: five lithium cations jammed between two corannulene tetraanion decks. *Science* **333**, 1008–1011 (2011).
- (33) Wilson, R. J. et al. Intermetalloid and heterometallic clusters combining p-block (Semi)metals with d- or f-block metals. *Chem. Rev.* **119**, 8506–8554 (2019).
- (34) Åkerstedt, J. et al. Structural Investigation of a Fully Ordered *closo*- Ge_9^{2-} Cluster in the Compound $[\text{K}^+(2,2,2\text{-crypt})]_2\text{Ge}_9^{2-}$. *Eur. J. Inorg. Chem.* **2011**, 3999–4005 (2011).

- (35) Adamo, C. & Barone, V. Toward reliable density functional methods without adjustable parameters: The PBE0 model. *J. Chem. Phys.* **110**, 6158–6169 (1999).
- (36) Weigend, F. & Ahlrichs, R. Balanced basis sets of split valence, triple zeta valence and quadruple zeta valence quality for H to Rn: Design and assessment of accuracy. *Phys. Chem. Chem. Phys.* **7**, 3297–3305 (2005).
- (37) Szczepanik, D. W., Solà, M. “The electron density of delocalized bonds (EDDBs) as a measure of local and global aromaticity” in *Aromaticity: Modern Computational Methods and Applications*, <https://doi.org/10.1016/B978-0-12-822723-7.00008-X>.
- (38) Szczepanik, D. W. A new perspective on quantifying electron localization and delocalization in molecular systems. *Comput. Theor. Chem.* **1080**, 33–37 (2016).
- (39) Sundholm, D., Fliegl, H. & Berger, R. J. Calculations of magnetically induced current densities: theory and applications. *WIREs Comput. Mol. Sci.* **6**, 639–678 (2016).
- (40) Corminboeuf, C., von Schleyer, P. R. & Warner, P. Are antiaromatic rings stacked face-to-face aromatic? *Org. Lett.* **9**, 3263–3266 (2007).
- (41) Zubarev, D. Y. & Boldyrev, A. I. Developing paradigms of chemical bonding: adaptive natural density partitioning. *Phys. Chem. Chem. Phys.* **10**, 5207–5217 (2008).
- (42) Tkachenko, N. V. & Boldyrev, A. I. Chemical bonding analysis of excited states using the adaptive natural density partitioning method. *Phys. Chem. Chem. Phys.* **21**, 9590–9596 (2019).

- (43) Xu, H.-L. et al. A sandwich-type cluster containing Ge@Pd₃ planar fragment flanked by aromatic nonagermanide caps. *Nat. Commun.* **11**, 5286 (2020).
- (44) Xu, H.-L. et al. [Sn₈]⁶⁻-bridged mixed-valence Zn^I/Zn^{II} in {[K₂ZnSn₈(ZnMes)]₂}⁴⁺ inverse sandwich-type cluster supported by a Zn^I-Zn^I bond. *Angew. Chem. Int. Ed.* **60**, 9990–9995 (2021).
- (45) Tkachenko, N. V. & Boldyrev, A. I. Multiple local σ -aromaticity of nonagermanide clusters. *Chem. Sci.* **10**, 5761–5765 (2019).
- (46) Islas, R., Heine, T. & Merino, G. The Induced Magnetic Field. *Acc. Chem. Res.* **45**, 215–228 (2012).
- (47) Benassi, R., Lazzeretti, P. & Taddei, F. Magnetic criteria for aromaticity. *J. Phys. Chem.* **79**, 848–851 (1975).
- (48) von Schleyer, P. R. & Jiao, H. What is aromaticity? *Pure Appl. Chem.* **68**, 209–218 (1996).
- (49) Muñoz-Castro, A. The shielding cone in spherical aromatic structures: insights from models for spherical 2(N+1)² aromatic fullerenes. *Phys. Chem. Chem. Phys.* **19**, 12633–12636 (2017).
- (50) Pople, J. A. & Untch, K. G. Induced paramagnetic ring currents. *J. Am. Chem. Soc.* **88**, 4811–4815 (1966).
- (51) Charistos, N. D., Muñoz-Castro, A. & Sigalas, M. P. The pseudo- π model of the induced magnetic field: fast and accurate visualization of shielding and deshielding cones in planar conjugated hydrocarbons and spherical fullerenes. *Phys. Chem. Chem. Phys.* **21**, 6150–6159 (2019).

- (52) Kaipio, M. et al. Effect of fluorine substitution on the aromaticity of polycyclic hydrocarbons. *J. Phys. Chem. A* **116**, 10257–10268 (2012).
- (53) Von Schnering, H. G. et al. Binary alkali metal compounds with the zintl anions $[\text{Ge}_9]^{4-}$ and $[\text{Sn}_9]^{4-}$. *Z. Anorg. Allg. Chem.* **623**, 1037–1039 (1997).
- (54) Sheldrick, G. M. SHELXT – Integrated space-group and crystal-structure determination. *Acta Cryst. A* **71**, 3–8 (2015).
- (55) Dolomanov, O. V. et al. OLEX2: a complete structure solution, refinement and analysis program. *J. Appl. Crystallogr.* **42**, 339–341 (2009).
- (56) Spek, A. L. Structure validation in chemical crystallography. *Acta Cryst. D* **65**, 148–155 (2009).
- (57) Spek, A. L. PLATON SQUEEZE: a tool for the calculation of the disordered solvent contribution to the calculated structure factors. *Acta Crystallogr. Sect. C. Cryst. Struct. Commun.* **71**, 9–18 (2015).
- (58) Amsterdam Density Functional (ADF 2019) Code, Vrije Universiteit: Amsterdam, The Netherlands. Available at: <http://www.scm.com>
- (59) Perdew, J. P., Burke, K. & Ernzerhof, M. Generalized gradient approximation made simple. *Phys. Rev. Lett.* **77**, 3865–3868 (1996).
- (60) Baranac-Stojanović, M. New insight into the anisotropic effects in solution-state NMR spectroscopy. *RSC Adv.* **4**, 308–321 (2014).
- (61) Klod, S. & Kleinpeter, E. Ab initio calculation of the anisotropy effect of multiple bonds and the ring current effect of arenes—application in conformational and configurational analysis. *J. Chem. Soc. Perkin Trans.* **2**, 1893–1898 (2001).

- (62) Charistos, N. D., Papadopoulos, A. G. & Sigalas, M. P. Interpretation of electron delocalization in benzene, cyclobutadiene, and borazine based on visualization of individual molecular orbital contributions to the induced magnetic field. *J. Phys. Chem. A* **118**, 1113–1122 (2014).
- (63) Heine, T., Corminboeuf, C. & Seifert, G. The magnetic shielding function of molecules and Pi-electron delocalization. *Chem. Rev.* **105**, 3889–3910 (2005).
- (64) Merino, G., Heine, T. & Seifert, G. The Induced Magnetic Field in Cyclic Molecules. *Chem. Eur. J.* **10**, 4367–4371 (2004).
- (65) Perdew, J. P., Burke, K. & Wang, Y. Generalized gradient approximation for the exchange-correlation hole of a many-electron system. *Phys. Rev. B* **54**, 16533–16539 (1996).
- (66) Handy, N. C. & Cohen, A. J. Left-right correlation energy. *Mol. Phys.* **99**, 403–412 (2001).
- (67) van Lenthe, E., Baerends, E. J. & Snijders, J. G. Relativistic total energy using regular approximations. *J. Chem. Phys.* **101**, 9783–9792 (1994).
- (68) M. J. Frisch, et al. Gaussian 16, Revision B.01, Gaussian, Inc., Wallingford (2016).
- (69) Sergeeva, A. P. & Boldyrev, A. I. The chemical bonding of Re_3Cl_9 and $\text{Re}_3\text{Cl}_9^{2-}$ revealed by the adaptive natural density partitioning analyses. *Comm. Inorg. Chem.* **31**, 2–12 (2010).

Tables and figures

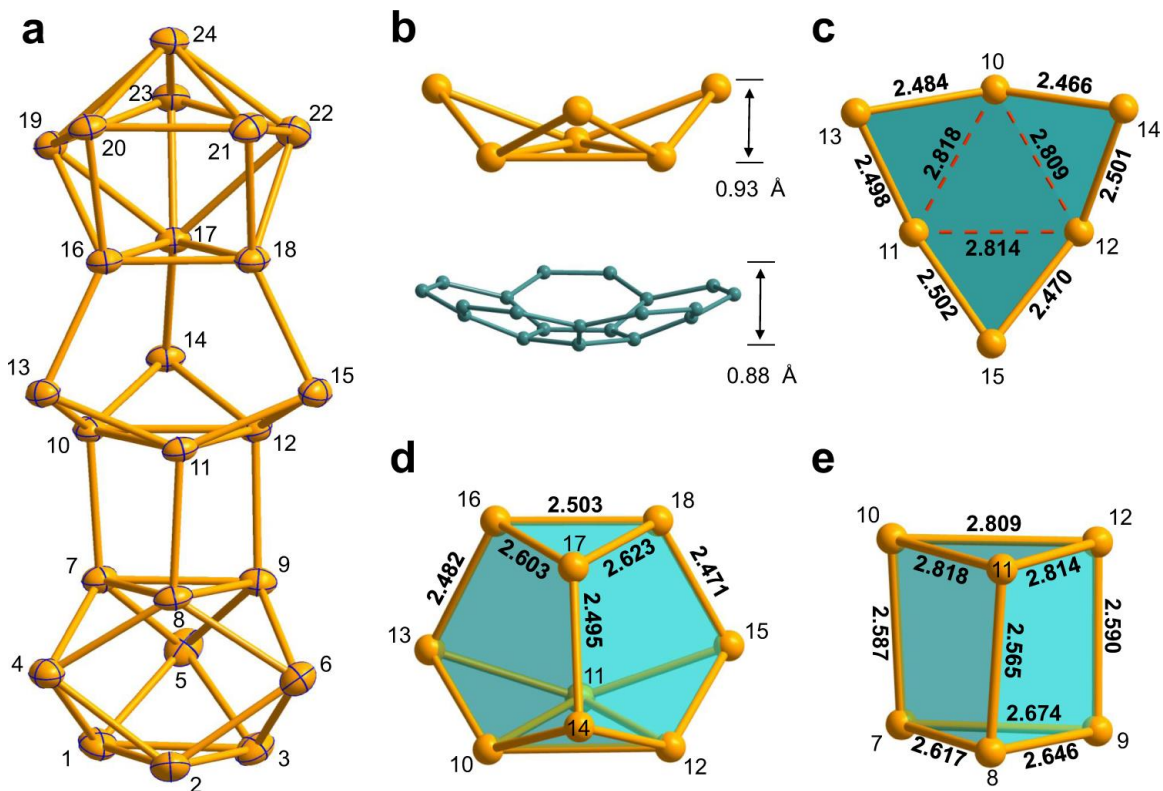


Figure 4-1. Structures of the Ge_{24}^{4-} cluster and its selected fragments. (a) Ge_{24}^{4-} cluster (1a) (thermal ellipsoids are drawn at 50% probability). (b) The contrast of bowl-shaped Ge_6 fragment (top, Ge10-Ge15) with bowl depth of 0.93 Å and corannulene $\text{C}_{20}\text{H}_{10}$ (bottom) with ~ 0.88 Å. (c) The bowl-shaped Ge_6 fragment shown from a vertical view. (d) View of Ge_9 cage (Ge10-Ge18). (e) The distorted prism Ge_6 fragment consisting of a triangle of Ge7-9 and an extended triangle of Ge10-12. All selected bond lengths are given in Å. The Ge and C atoms are drawn in yellow and blue, respectively.

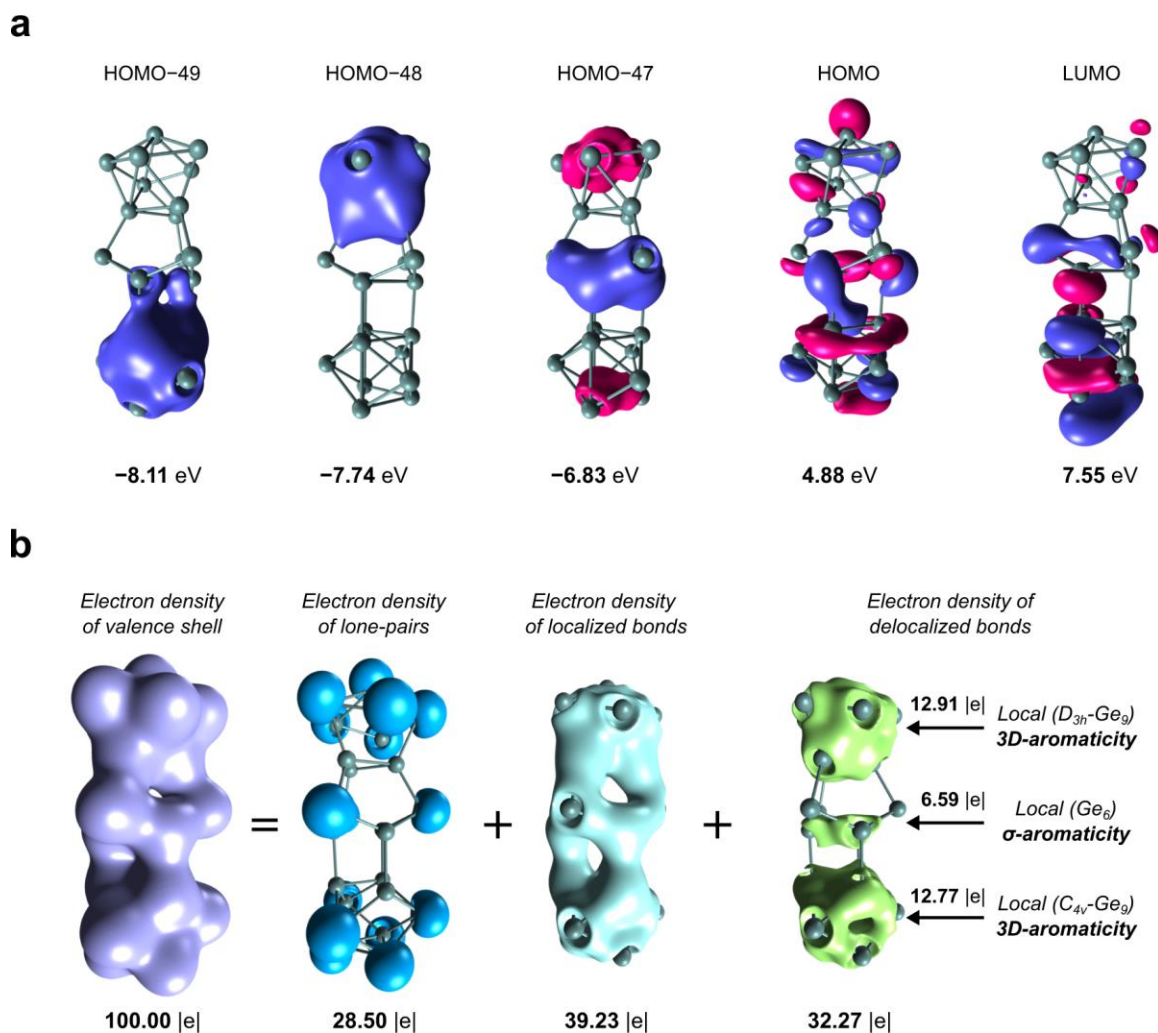


Figure 4-2. The selected valence molecular orbitals and chemical components of the electron density of Ge_{24}^{4-} . **(a)** Selected lowest-lying and frontier valence molecular orbitals in the Ge_{24}^{4-} cluster. Different phases of molecular orbitals are represented with different colors. Positive: magenta; negative: purple. **(b)** The chemical components of the valence-electron density of Ge_{24}^{4-} with the corresponding electron populations from the EDDB method. Isosurface value is set at ± 0.015 |e|.

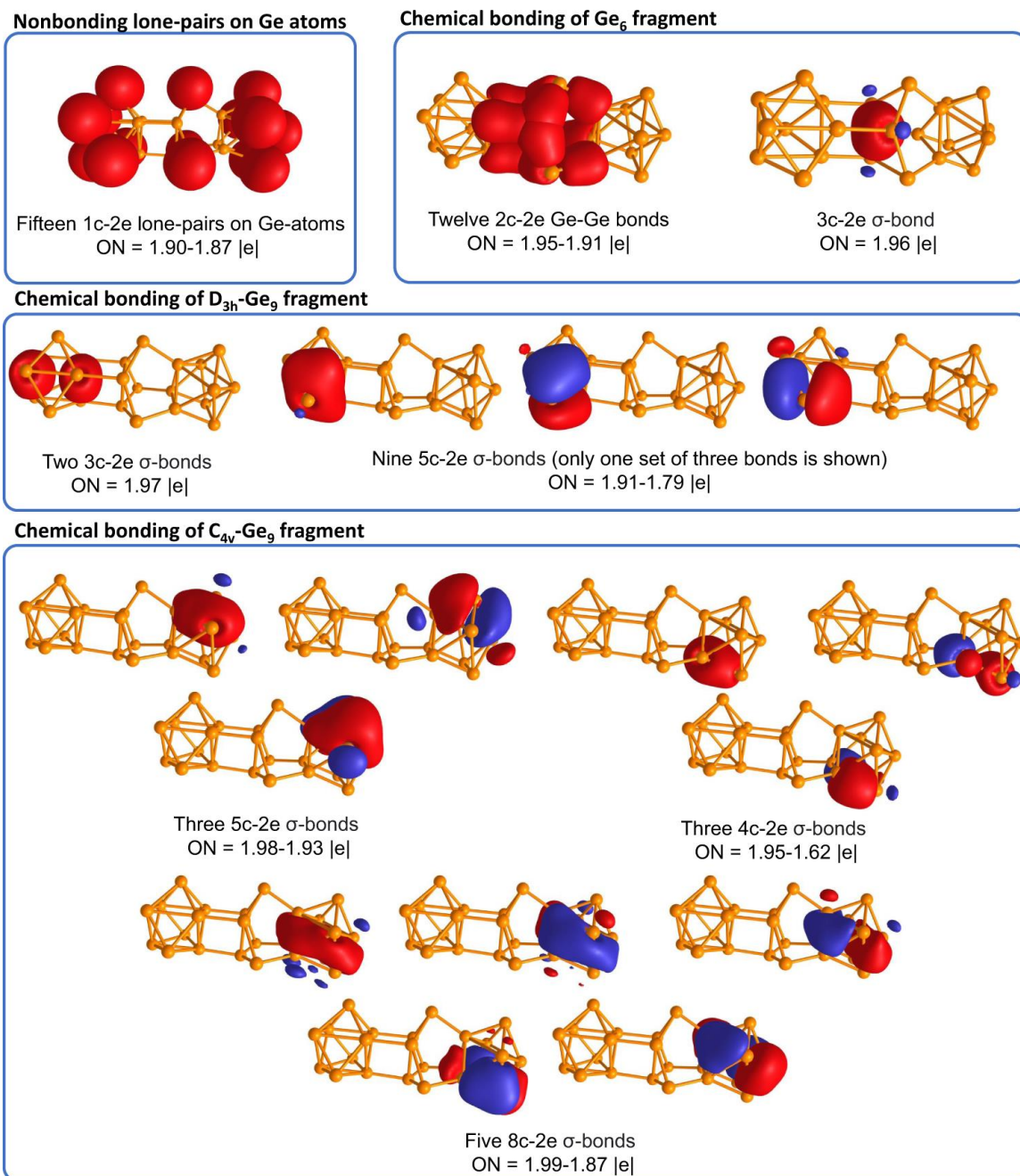


Figure 4-3. Chemical bonding pattern of the Ge₂₄⁴⁻ cluster. Different phases of bonding elements are represented with different colors. Positive: red; negative: blue.

Chemical bonding of Ge_8 square antiprism fragment

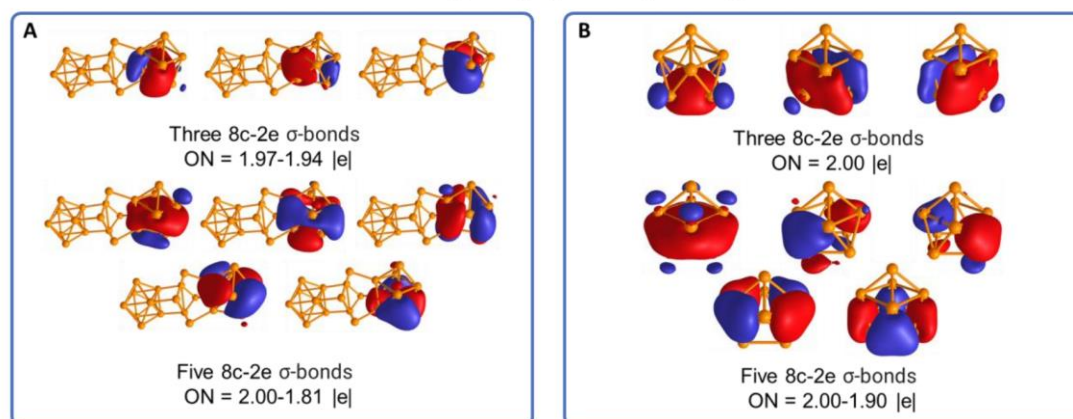


Figure 4-4. AdNDP analysis of Ge_8 antiprism fragment of Ge_{24}^{4-} (a) and $C_{4v}\text{-Ge}_9^{4-}$ (b) clusters.

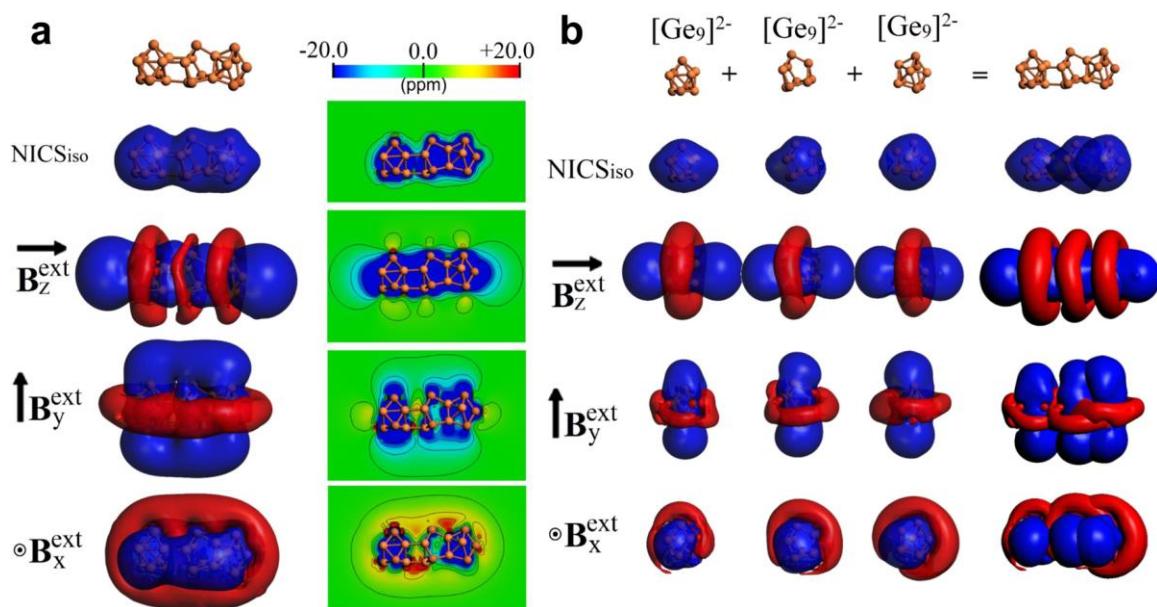


Figure 4-5. Contour plots and isosurfaces of magnetic response of the Ge₂₄⁴⁻ cluster and various Ge₉⁴⁻ units. (a) Isosurface and contour plot representation for NICS_{iso} and certain orientations of the external field for Ge₂₄⁴⁻. Isosurface value is set at ± 3.0 ppm. (b) Isosurface representation for NICS_{iso} and certain orientations of the external field for the three isolated Ge₉⁴⁻ units, as found in Ge₂₄⁴⁻. Isosurface value is set at ± 3.0 ppm. Blue surface: shielding; Red surface: deshielding.

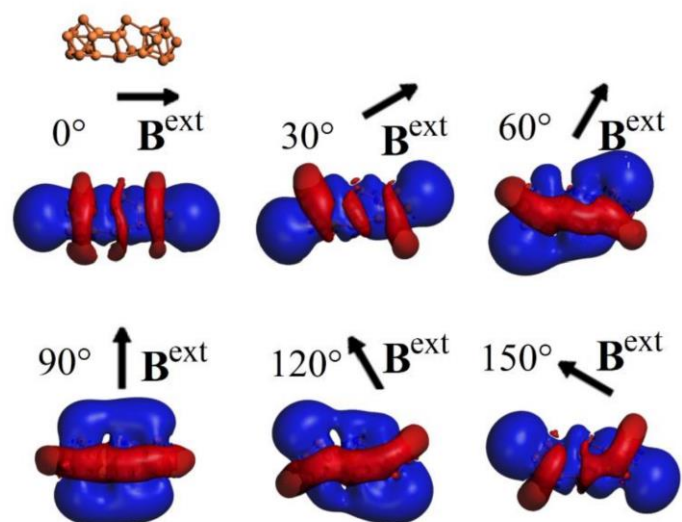


Figure 4-6. Isosurface representation for the induced magnetic field for [Ge₂₄]⁴⁻ under different orientations of the external field, noted by arrows. Isosurface value set at ± 3.0 ppm.

CHAPTER 5

 $[\text{Sn}_8]^{6-}$ -BRIDGED MIXED-VALENCE $\text{Zn}^{\text{I}}/\text{Zn}^{\text{II}}$ IN $\{[\text{K}_2\text{ZnSn}_8(\text{ZnMes})]_2\}^{4-}$ INVERSE SANDWICH-TYPE CLUSTER SUPPORTED BY A $\text{Zn}^{\text{I}}-\text{Zn}^{\text{I}}$ BOND¹**Abstract**

Since $[\text{Sn}_8]^{6-}$ was discovered from the solid-state phase in 2000, its solution chemistry has been elusive due to the high charges and chemical activity. Herein, we report the synthesis and characterization of an inverse sandwich-type cluster dimer $\{[\text{K}_2\text{ZnSn}_8(\text{ZnMes})]_2\}^{4-}$ (**1 a**), in which the highly charged $[\text{Sn}_8]^{6-}$ is captured by mixed-valence $\text{Zn}^{\text{I}}/\text{Zn}^{\text{II}}$ to form the dimer $\{closo-[\text{Zn}_2\text{Sn}_8]\}_2$ moieties bridged by a Zn-Zn bond. Such Zn-Sn cluster not only exhibits a novel example of mixed-valence $\text{Zn}^{\text{I}}/\text{Zn}^{\text{II}}$ for stabilizing highly active anion species, but also indicates the $[\text{Sn}_8]^{6-}$ cluster can act as a novel bridging ligand, like arene, with a $\eta^4:\eta^4$ -fashion. Theoretical calculations indicate that a significant delocalization of electrons over Zn atoms plays a vital role in the stabilization of the $[\text{Sn}_8]^{6-}$ species. The AdNDP and magnetic response analyses clearly showed the presence of local σ -aromaticity in three cluster fragments: two ZnSn_4 caps and Sn_8 square antiprism.

5.1 Introduction

Polyhedral boranes have been attracting great interest due to their extraordinary performances in all branches of chemistry.¹ Fascinating structures brought the pathbreaking bonding patterns. The situation induced the development of Wade rules, which helped us figure out the relationship between geometric structures of borane clusters

¹ Coauthored by Hong-Lei Xu, Nikolay V. Tkachenko, Alvaro Muñoz-Castro, Alexander I. Boldyrev, and Zhong-Ming Sun. Reproduced from *Angew. Chem. Int. Ed.*, **2021**, *60*, 9990-9995 with permission. Copyright © 2021, John Wiley & Sons.

and their electronic structures.² For example, deltahedral *closo*-boranes $[B_nH_n]^{2-}$ obey the electron counting rules of borane structures, that they should possess $n+1$ electron pairs where n is the number of vertices. As in the case of a polyhedron with missing vertices, namely *nido* or *arachno*, the number of skeletal electron pairs needs to satisfy $n+1+p$ (p is the number of missing vertices) for the stability of skeletons. As the isoelectronic relationship between fragments $\{BH\}$ and E atoms (E=Si–Pb), these rules have been long borrowed to illustrate and predict the related structures from group 14.³ Expectedly, the *closo*- $[E_5]^{2-}$ (E=Si, Ge, Sn, Pb) and $[E_{10}]^{2-}$ (E=Ge, Pb) as an isostructural and isoelectronic species with corresponding boranes $[B_5H_5]^{2-}$ and $[B_{10}H_{10}]^{2-}$ have been isolated from solutions,⁴ whereas the very stable *closo*-structures limit their reactivity in solutions.⁵ In contrast, the *nido*-clusters of $[E_9]^{4-}$ (E=Si, Ge, Sn, Pb) and $[E_4]^{4-}$ (E=Si, Ge, Sn) have exhibited good reactivity and accounted for a number of new derivatives,⁶ such as oxidative coupling,⁷ functionalization with main-group/transition-metal fragments,^{8,9,10,11} cluster fusion and assembly.¹² Hence, it is foreseeable that the solution chemistry of $[E_8]^{6-}$ clusters of missing two vertices from the $[E_{10}]^{2-}$ will be fascinating. The observation of $[Sn_8]^{6-}$ in solid-state Zintl phases $A_4Li_2Sn_8$ (A=K, Rb) and $Ba_{16}Na_{204}Sn_{310}$ ¹³ shows the existence of such species as predicted by Wade's rules. However, it still remains challenging to bring the cluster into solution¹⁴ and thus related derivative has been elusive so far. Herein, we report a new cluster anion $\{[K_2ZnSn_8(ZnMes)]_2\}^{4-}$ (**1a**) as a $[K(2,2,2-crypt)]^+$ salt (**1**) containing two individual Sn_8 units stabilized by two groups of capped Zn atoms and combined with a Zn-Zn bond. The successful preparation of **1** not only represents a rare example of the mixed-valence Zn^I/Zn^{II} together for capturing highly charged anion species,

but might open the way to solution chemistry of multiple vertex deficient main-group metal clusters.

5.2 Results and Discussions

The title compound, $[\text{K}(2,2,2\text{-crypt})]_4\{[\text{K}_2\text{ZnSn}_8(\text{ZnMes})]_2\}$ (**1**), was synthesized by solution reaction of “ K_4ZnSn_4 ” and ZnMes_2 in the presence of 2,2,2-crypt. After 20 days, dark-red plate crystals were observed in the test tube (21 % yield based on loaded starting material ZnMes_2). The X-ray diffraction analysis (XRD) reveals that the compound crystallizes in the monoclinic space group $P2_1/n$ and there is one cluster anion $\{[\text{K}_2\text{ZnSn}_8(\text{ZnMes})]_2\}^{4-}$ (**1 a**) with four $[\text{K}(2,2,2\text{-crypt})]^+$ counter cations in the molecular structure. Additional characterization of energy-dispersive X-ray spectroscopy (EDS) showed the composition of **1** including K, Zn, and Sn elements. Electrospray-ionization mass spectrometry (ESI-MS) and ^{119}Sn NMR spectroscopy were also attempted, but the related characterizations suffered from failure due to inevitable fast decomposition of **1** in DMF solutions.

At first glance, the cluster anion **1a** exhibits a specific dimeric structure containing two identical subunits of $[\text{ZnSn}_8(\text{ZnMes})]$ which are surrounded by four non-cryptated K-cations (Figures 5-1a, 5-1b). The four free K-cations around the neck of the whole cluster construct a square plane with K-K distances ranging from 4.762 to 4.878 Å. Although the long distances between four surrounding K-cations and Sn atoms (K-Sn: 3.775(3)–3.837(4) Å) indicate weak interactions, the K-cations play a vital role in the formation and stabilization of the unusual highly charged dimeric product based on the fact that crystals of **1** cannot be isolated by adding the excess of 2,2,2-crypt under parallel experiments. The K-cations act as an attractive force to pull the two anions together by screening their

charges and thus allowing them to dimerize. Such situation is also observed in $[\text{Ge}_9\text{-Ge}_9]^{6-}$ and $[\text{Ge}_9\text{Zn-ZnGe}_9]^{6-}$.^{7a,15} Additionally, **1a** can also be viewed as a sandwich-type structure where a dinuclear $[\text{Zn-Zn}]^{2+}$ unit is flanked by two heteroatomic cluster anions of $[\text{Sn}_8\text{ZnMes}]^{5-}$. However, it should be better described as a multilayer inverse-sandwich dimer in which both $[\text{Sn}_8]^{6-}$ units are respectively jammed by $[\text{Zn}^{\text{II}}\text{Mes}]$ and Zn^{I} and then combined with a Zn-Zn bond, thus the structure is supported by four surrounding K-cations. According to Wade-Mingos rules,² the cluster bonding electrons would be 22 for a ten-vertex *closo*-species. In this sense, the $[\text{Sn}_8]^{6-}$ capped by two Zn atoms forms a heteroatomic *closo*-cluster of $[\text{Sn}_8\text{Zn}_2]$ ($6 e^- + 8 \times (2 e^-) = 22 e^-$), with $6 e^-$ from the charges, $2 e^-$ from each Sn atom and none from the Zn atoms. Hence, on top of the Zn atom is functionalized with -Mes to result in $[\text{ZnSn}_8(\text{ZnMes})]$ with $4 e^-$, which is dimerized to form $\{[\text{K}_2\text{ZnSn}_8(\text{ZnMes})]_2\}^{4-}$.

Zn atoms cap the open square faces of Sn_8 , resulting in the retention of an intact “*arachno*” structure. Hence, the Sn_8 units in **1a** possess a nearly perfect square antiprism structure (D_{4d}) with two almost parallel bases (Figure 5-1c). The dihedral angle between the two bases is only 0.33° , similar to that in $[\text{Li}_2\text{Sn}_8]^{4-}$ (0.27° and 0.48°).^{13a} The Sn-Sn bond lengths in the waist (2.9263(12)–2.9507(12) Å) are slightly shorter than those in the bases (3.1039(10)–3.1615(11) Å) and all values (2.9263(12)–3.1615(11) Å) are in the normal range, comparable to those in $[\text{Li}_2\text{Sn}_8]^{4-}$ from $\text{Rb}_4\text{Li}_2\text{Sn}_8$ (2.947(3)–3.037(2) Å), $[\text{Sn}_8\text{TiCp}]^{3-}$ (2.859(2)–3.108(2) Å)¹⁶ and other Sn clusters, such as $[\text{Sn}_9]^{4-}$ and its derivatives.^{8c,9a,9c,12b,17} The distances from the bases of Sn_8 units to their capped Zn atoms are in a very narrow range of 2.7768(18)–2.8014(18) Å, comparing well with those of 2.7397(4)–2.7867(4) Å in $[\text{Sn}_9\text{ZnPh}]^{3-}$,^{9c} and this indicates different valences of Zn almost

have no effect on the corresponding Zn-Sn bond lengths in **1a**. The Zn-Zn bond acts as a linker between the two $[\text{Sn}_8\text{ZnMes}]$ moieties. Despite the rather high electrostatic repulsion within the highly charged anion $\{[\text{ZnSn}_8(\text{ZnMes})]_2\}^{8-}$, the Zn-Zn bond length (2.449(3) Å) is only slightly longer than those in $[\text{Ge}_9\text{Zn-ZnGe}_9]^{6-}$ (2.420(1) Å)¹⁵ and other monovalent organozinc species (2.305(3)–2.430(1) Å),¹⁸ but shorter than the Zn-Zn distances (2.544(3)–2.831(5) Å) in $[\text{K}_2\text{Zn}_{20}\text{Bi}_{16}]^{6-}$.¹⁹

To understand the chemical bonding and electronic structure of the investigated cluster, we performed density functional theory (DFT) calculations. All DFT calculations were performed using Gaussian 16 software²⁰ at PBE0/def2TZVP level of theory.²¹ A detailed description of quantum chemical calculations could be found in the Quantum Chemical methods section of this chapter. The isolated $\{[\text{K}_2\text{ZnSn}_8(\text{ZnMes})]_2\}^{4-}$ cluster was proved to be a local minimum exhibiting no imaginary frequencies. The optimized structure resembles all essential geometrical features that were found in the experimental X-ray data. The calculated Zn-Zn bond distance is slightly overestimated by 0.1 Å, while the average of Sn-Sn distances is larger by only 0.04 Å. We note that this is a common deviation in calculations of highly charged Zintl anions with DFT methods. The high HOMO–LUMO gap was found for the investigated structure 1.99 eV which is larger than that of $[\text{Sn}_8]^{6-}$ by 0.45 eV, indicating the higher stability of the Zn-containing cluster.

While the role of K-atoms is quite clear in the stabilization of the structure: they provide extra electrons and stabilize the high negative charge of the cluster; the role of Zn atoms is not so obvious. The analysis of molecular orbitals of the $\{[\text{K}_2\text{ZnSn}_8(\text{ZnMes})]_2\}^{4-}$ shows that Zn participates in the delocalization of electrons via the interaction of vacant 4*p* orbitals of Zn with the linear combinations of Sn 5*s*/5*p*-orbitals. Thus, the delocalization

of electrons over $4p$ Zn-orbitals present in nearly degenerate HOMO, HOMO-1 (Figure 5-2), and other lower-lying molecular orbitals indicating a significant contribution of Zn in the stabilization of the structure.

Analysis of molecular orbitals provides us a general idea of the role of Zn-atom in cluster stabilization, while electron localization techniques deliver a more illustrative and explicit picture of chemical bonding. To get insight on the localized chemical bonding pattern of $\{[\text{K}_2\text{ZnSn}_8(\text{ZnMes})]_2\}^{4-}$, we performed an adaptive natural partitioning (AdNDP) analysis of electron density as implemented in AdNDP 2.0 code.²² We started the localization procedure from one-center two-electron (1c-2e) elements (lone pairs). We found that electrons are localized into twenty d -type lone pairs on Zn-atom (5 lone pairs per each Zn atom) with occupation numbers (ON) 2.00–1.99 |e| (Figure 5-3a) and sixteen s -type lone pairs on Sn-atom with ON=1.82–1.79 |e| (Figure 5-3e). The chemical bonding in organic ligand consists of forty 2c-2e C–C and C–H σ -bonds with ON=1.99–1.97 |e|. The aromaticity of benzene rings is manifested via six 6c-2e π -bonds with ON=1.99–1.97 |e| (Figure 5-3c). The binding between an organic ligand and metal cluster occurs via 2c-2e Zn–C bond with high ON=1.93 |e|. Two metal clusters are held together by one 2c-2e Zn–Zn σ -bond with ON=1.85 |e| (Figure 5-3f). We want to note that although the Zn–Zn distance is quite elongated (presumably due to the electrostatic repulsion), it is a two-center two-electron covalent interaction.

The chemical bonding inside each Zn_2Sn_8 cage can be separated into three structural fragments with delocalized bonding elements: two ZnSn_4 caps and Sn_8 square antiprism (Figure 5-3g-i). We found three 5c-2e σ -bonds per each ZnSn_4 cap with ON=1.98–1.76 |e|. Predictably, we observed a significant contribution of Zn-atoms into those delocalized

elements (29–14 %). The high contribution of Zn-atom confirms that this delocalization plays a crucial role in the stabilization of the investigated cluster. The remaining 20 electrons can be localized into ten 8c-2e σ -bonds (5 bonds per Sn₈ cage) with high ONs=2.00–1.88 |e|. We note that such delocalization is common in various Zintl clusters.²³ Remarkably, the presented chemical bonding pattern of the Zn₂Sn₈ cage resembles the chemical bonding in [Sn₈]⁶⁻ cluster (Figure 5-4), indicating that Zinc atoms act as a stabilizing factor without significantly changing the chemical bonding pattern in the [Sn₈]⁶⁻ fragment. It has been discussed before, that the PBE0 functional could overestimate electron delocalization and aromaticity.²⁴ To make sure that the obtained results are not a consequence of the choice of the functional, we performed the same calculations using CAM-B3LYP functional²⁵ that does not suffer from delocalization error. The obtained results reproduce results obtained with PBE0 functional.

We note that such delocalization inside each Zn₂Sn₈ cage is usually accompanied by unique magnetic properties, which resembles the behavior of aromatic species.^{12m} The magnetic criteria of aromaticity²⁶ are evaluated to confirm the aromatic behavior of the investigated cluster. The induced magnetic field (B^{ind}), which was evaluated globally along the molecular backbone, contributes to the characterization of aromatic species based on the potential ability to sustain a long-range shielding cone. This behavior is a distinctive feature of both planar and spherically aromatic compounds.²⁷ The B^{ind} is related to the applied field (B^{ext}), in terms of the shielding tensor (σ_{ii}) according to the relation $B_i^{\text{ind}} = -\sigma_{ii} B_j^{\text{ext}}$. Different representative orientations of the B^{ext} are considered via different i and j suffixes which represent x -, y - and z -axes. The orientationally-averaged term ($B_{\text{iso}}^{\text{ind}} = -(1/3)(\sigma_{xx} + \sigma_{yy} + \sigma_{zz}) B_j^{\text{ext}}$) accounts for the in-solution molecular tumbling.

For orientationally-averaged term, we found a shielding surface originated from each aromatic motif given by mesityl and Zn_2Sn_8 cage fragments, as observed from the contour-plot representation (Figure 5-5). Under specific orientation of the applied field, the inherent characteristics of the B^{ind} along the series can be depicted. Under z -axis orientation, B^{ind} results in a long-range shielding response, with a complementary perpendicular deshielding region. From the contour-plot, it is observed that the overall shielding cone is enabled by the four independent shielding cones from each aromatic motif, where both Zn_2Sn_8 cages share shielding regions of ≈ -8.0 ppm, and mesityl- Zn_2Sn_8 of ≈ -3 ppm. These results suggest that each aromatic circuit is independent, as denoted by the bonding analysis provided by the AdNDP analysis. Under a field along the x -axis (B_x^{ext}), only Zn_2Sn_8 shielding cones are enabled, denoting the spherical-like aromatic behavior of the ten-membered cage.²⁸ Moreover, for a field along the y -axis (B_y^{ext}), two overlapped shielding cones are observed, originated from the spherical-like aromatic characteristic of the bridged Zn_2Sn_8 cages, resulting in an extended shielding region complemented with two deshielding contours centered at each cage.

As a result, we can conclude that the shape of delocalized bonding elements (one bond without a nodal plane, two bonds with one nodal plane, etc.), number of electrons that agrees with Hückel's rule ($6|e|$ for ZnSn_4 and $10|e|$ for Sn_8), and peculiar magnetic properties render the described fragments as σ -aromatic. Thus, the chemical bonding inside each Zn_2Sn_8 cage can be described as three locally σ -aromatic fragments: two ZnSn_4 caps and Sn_8 square antiprism.

The analysis of electron localization function (ELF)²⁹ confirms the results obtained via AdNDP analysis: we observe the established 2c-2e Zn-Zn bond and a significant

delocalization within Zn_2Sn_8 cages (Figure 5-6a). We also can confirm that there are no K-K or K-Zn covalent interactions (Figure 5-6b). Thus, K atoms provide the lacking electrons and compensate the overall negative charge of the cluster to stabilize the structure, which also can be confirmed by the highly positive Natural charge of K-atoms (+0.85 a.u.). In turn, the natural charges of Zn atoms are also positive. Moreover, we can see a clear difference between Zn atoms connected with mesityl ligand and Zn atoms in the Zn_2 fragment. For the former, the calculated natural charge is +1.23 a.u., while for the latter it is +0.60 a.u. The quantum theory of atoms in molecules³⁰ and CM5³¹ atomic charge analyses produce qualitatively the same results (Supplementary Table S3 of the original manuscript) confirming the formal $\text{Zn}^{\text{I}}/\text{Zn}^{\text{II}}$ oxidation state assignment.

5.3 Quantum Chemical Methods

Quantum chemical calculations (geometry optimization and frequency calculations) were performed using Gaussian 16 software package at the PBE0/Def2-TZVP level of theory. To account possible delocalization error of PBE0 functional, additional calculations were performed using CAM-B3LYP functional. To identify the chemical bonding of investigated species, we carried out adaptive natural density partitioning (AdNDP) analysis as implemented in the AdNDP 2.0 code. The ELF analysis and QTAIM atomic charge analysis were performed via MultiWFN software. In addition, the isosurface and cut-plane representation of the induced magnetic field (Bind) was obtained within the GIAO formalism at the relativistic ZORA-PBE0/TZ2P level of theory by using the ADF suite unraveling the long-range characteristics of the magnetic response. To analyze natural atomic charge distribution NBO7 software was used.

5.3 Conclusions

In summary, we have realized the synthesis and isolation of an inverse sandwich-type cluster dimer $\{[K_2ZnSn_8(ZnMes)]_2\}^{4-}$ involving $[Sn_8]^{6-}$ and mixed-valence Zn^I/Zn^{II} . Such Zn-Sn cluster species indicates the $[Sn_8]^{6-}$ cluster can act as a potential bridging ligand due to its unusual structure and thus might provide an ideal building unit for constructing new types of one-dimensional materials. In turn, the Zn-Zn bonded cluster anion shows a novel example of mixed-valence Zn^I/Zn^{II} together for capturing anion species, which opens the opportunity for new zinc chemistry.

References

- (1) E. D. Jemmis, M. M. Balakrishnarajan, P. D. Pancharatna, *J. Am. Chem. Soc.* 2001, **123**, 4313–4323.
- (2a) K. Wade, *J. Chem. Soc. D* 1971, **0**, 792–793;
- (2b) D. M. P. Mingos, *Acc. Chem. Res.* 1984, **17**, 311–319;
- (2c) R. E. Williams, *Adv. Inorg. Chem. Radiochem.* 1976, **18**, 67–142;
- (2d) K. Wade, *Adv. Inorg. Chem. Radiochem.* 1976, **18**, 1–66.
- (3) R. J. Wilson, F. Weigend, S. Dehnen, *Angew. Chem. Int. Ed.* 2020, **59**, 14251–14255;
- (4a) P. A. Edwards, J. D. Corbett, *Inorg. Chem.* 1977, **16**, 903–907;
- (4b) J. Campbell, G. J. Schrobilgen, *Inorg. Chem.* 1997, **36**, 4078–4081;
- (4c) M. Somer, W. Carrillo-Cabrera, E. M. Peters, K. Peters, M. Kaupp, H. G. von Schnering, *Z. Anorg. Allg. Chem.* 1999, **625**, 37–42;
- (4d) C. Suchentrunk, N. Korber, *New J. Chem.* 2006, **30**, 1737–1739;
- (4e) J. M. Goicoechea, S. C. Sevov, *J. Am. Chem. Soc.* 2004, **126**, 6860–6861;

- (4f) M. M. Bentlohner, C. Fischer, T. F. Fässler, *Chem. Commun.* 2016, **52**, 9841–9843;
- (4g) A. Spiekermann, S. D. Hoffmann, T. F. Fässler, *Angew. Chem. Int. Ed.* 2006, **45**, 3459–3462;
- (5a) C. Liu, L. J. Li, Q. J. Pan, Z. M. Sun, *Chem. Commun.* 2017, **53**, 6315–6318;
- (5b) D. Rios, S. C. Sevov, *Inorg. Chem.* 2010, **49**, 6396–6398.
- (6a) J. M. Goicoechea, S. C. Sevov, *Organometallics* 2006, **25**, 5678–5692;
- (6b) R. J. Wilson, N. Lichtenberger, B. Weinert, S. Dehnen, *Chem. Rev.* 2019, **119**, 8506–8554;
- (6c) S. Scharfe, F. Kraus, S. Stegmaier, A. Schier, T. F. Fässler, *Angew. Chem. Int. Ed.* 2011, **50**, 3630–3670;
- Angew. Chem.* 2011, **123**, 3712–3754.
- (7a) L. Xu, S. C. Sevov, *J. Am. Chem. Soc.* 1999, **121**, 9245–9246;
- (7b) A. Ugrinov, S. C. Sevov, *J. Am. Chem. Soc.* 2002, **124**, 10990–10991;
- (7c) A. Ugrinov, S. C. Sevov, *Inorg. Chem.* 2003, **42**, 5789–5791;
- (7d) R. Hauptmann, T. F. Fässler, *Z. Anorg. Allg. Chem.* 2003, **629**, 2266–2273;
- (7e) R. Hauptmann, T. F. Fässler, *Z. Anorg. Allg. Chem.* 2004, **630**, 1977–1981;
- (7f) L. Yong, S. D. Hoffmann, T. F. Fässler, *Z. Anorg. Allg. Chem.* 2005, **631**, 1149–1153.
- (8a) A. Ugrinov, S. C. Sevov, *J. Am. Chem. Soc.* 2003, **125**, 14059–14064;
- (8b) M. W. Hull, S. C. Sevov, *Angew. Chem. Int. Ed.* 2007, **46**, 6695–6698;
- (8c) D. J. Chapman, S. C. Sevov, *Inorg. Chem.* 2008, **47**, 6009–6013;
- (8d) M. W. Hull, S. C. Sevov, *J. Am. Chem. Soc.* 2009, **131**, 9026–9037;
- (8e) F. Li, S. C. Sevov, *Inorg. Chem.* 2012, **51**, 2706–2708;

- (8f) F. Li, A. Muñoz-Castro, S. C. Sevov, *Angew. Chem. Int. Ed.* 2012, **51**, 8581–8584;
- (8g) M. M. v. Bentlohner, W. Klein, Z. H. Fard, L. A. Jantke, T. F. Fässler, *Angew. Chem. Int. Ed.* 2015, **54**, 3748–3753;
- (8h) F. S. Geitner, W. Klein, T. F. Fässler, *Angew. Chem. Int. Ed.* 2018, **57**, 14509–14513;
- (8i) F. S. Geitner, J. V. Dums, T. F. Fässler, *J. Am. Chem. Soc.* 2017, **139**, 11933–11940;
- (8j) C. Wallach, F. S. Geitner, A. J. Karttunen, T. F. Fässler, *Angew. Chem. Int. Ed.* 2021, **60**, 2648–2653;
- (8k) A. Ugrinov, S. C. Sevov, *J. Am. Chem. Soc.* 2002, **124**, 2442–2443;
- (8l) F. Li, A. Muñoz-Castro, S. C. Sevov, *Angew. Chem. Int. Ed.* 2016, **55**, 8630–8633;
- (8m) F. Li, S. C. Sevov, *Inorg. Chem.* 2015, **54**, 8121–8125.
- (9a) B. W. Eichhorn, R. C. Haushalter, *J. Am. Chem. Soc.* 1988, **110**, 8704–8706;
- (9b) A. M. Li, Y. Wang, P. Y. Zavalij, F. Chen, A. Muñoz-Castro, B. W. Eichhorn, *Chem. Commun.* 2020, **56**, 10859–10862;
- (9c) J. M. Goicoechea, S. C. Sevov, *Organometallics* 2006, **25**, 4530–4536;
- (9d) E. N. Esenturk, J. Fettinger, Y. F. Lam, B. W. Eichhorn, *Angew. Chem. Int. Ed.* 2004, **43**, 2132–2134;
- (9e) L. Yong, S. D. Hoffmann, T. F. Fässler, *Eur. J. Inorg. Chem.* 2005, 3663–3669;
- (9f) B. Zhou, M. S. Denning, C. Jones, J. M. Goicoechea, *Dalton Trans.* 2009, 1571–1578;
- (9g) S. Scharfe, T. F. Fässler, *Eur. J. Inorg. Chem.* 2010, 1207–1213;
- (9h) Y. Wang, Q. Qin, J. Y. Wang, R. L. Sang, L. Xu, *Chem. Commun.* 2014, **50**, 4181;

- (9i) F. S. Geitner, T. F. Fässler, *Chem. Commun.* 2017, **53**, 12974–12977.
- (10a) J. M. Goicoechea, S. C. Sevov, *J. Am. Chem. Soc.* 2006, **128**, 4155–4161;
- (10b) J. Q. Wang, S. Stegmaier, B. Wahl, T. F. Fässler, *Chem. Eur. J.* 2010, **16**, 1793–1798;
- (10c) J. Q. Wang, S. Stegmaier, T. F. Fässler, *Angew. Chem. Int. Ed.* 2009, **48**, 1998–2002;
- (10d) B. B. Zhou, M. S. Denning, D. L. Kays, J. M. Goicoechea, *J. Am. Chem. Soc.* 2009, **131**, 2802–2803;
- (10e) B. Kesanli, J. Fettinger, D. R. Gardner, B. Eichhorn, *J. Am. Chem. Soc.* 2002, **124**, 4779–4786.
- (11a) S. Stegmaier, M. Waibel, A. Henze, L. A. Jantke, A. J. Karttunen, T. F. Fässler, *J. Am. Chem. Soc.* 2012, **134**, 14450–14460;
- (11b) M. Waibel, F. Kraus, S. Scharfe, B. Wahl, T. F. Fässler, *Angew. Chem. Int. Ed.* 2010, **49**, 6611–6615;
- (11c) C. B. Benda, M. Waibel, T. Kçchner, T. F. Fässler, *Chem. Eur. J.* 2014, **20**, 16738–16746;
- (11d) F. Fendt, C. Koch, S. Gartner, N. Korber, *Dalton Trans.* 2013, **42**, 15548–15550;
- (11e) T. Henneberger, W. Klein, J. V. Dums, T. F. Fässler, *Chem. Commun.* 2018, **54**, 12381–12384;
- (11f) C. Wallach, K. Mayer, T. Henneberger, W. Klein, T. F. Fässler, *Dalton Trans.* 2020, **49**, 6191–6198;
- (11g) M. Waibel, T. Henneberger, L. A. Jantke, T. F. Fässler, *Chem. Commun.* 2012, **48**, 8676–8678.

- (12a) B. Kesanli, J. E. Halsig, P. Zavalij, J. C. Fettinger, Y. F. Lam, B. W. Eichhorn, *J. Am. Chem. Soc.* 2007, **129**, 4567–4574;
- (12b) F. S. Geitner, W. Kleinb, T. F. Fässler, *Dalton Trans.* 2017, **46**, 5796–5800;
- (12c) Z. M. Sun, H. Xiao, J. Li, L. S. Wang, *J. Am. Chem. Soc.* 2007, **129**, 9560–9561;
- (12d) J. M. Goicoechea, S. C. Sevov, *J. Am. Chem. Soc.* 2005, **127**, 7676–7677;
- (12e) J. M. Goicoechea, S. C. Sevov, *Angew. Chem. Int. Ed.* 2005, **44**, 4026–4028;
Angew. Chem. 2005, **117**, 4094–4096;
- (12f) L. G. Perla, S. C. Sevov, *Angew. Chem. Int. Ed.* 2016, **55**, 6721–6724;
- (12g) B. Zhou, M. S. Denning, T. A. D. Chapman, J. E. McGrady, J. M. Goicoechea, *Chem. Commun.* 2009, 7221–7223;
- (12h) C. Liu, X. Jin, L. J. Li, J. Xu, J. E. McGrady, Z. M. Sun, *Chem. Sci.* 2019, **10**, 4394–4401;
- (12i) L. G. Perla, S. C. Sevov, *J. Am. Chem. Soc.* 2016, **138**, 9795–9798;
- (12j) O. Kysliak, C. Schrenk, A. Schnepf, *Angew. Chem. Int. Ed.* 2016, **55**, 3216–3219;
Angew. Chem. 2016, **128**, 3270–3274;
- (12k) E. N. Esenturk, J. C. Fettinger, B. W. Eichhorn, *J. Am. Chem. Soc.* 2006, **128**, 12–13;
- (12l) A. Spiekermann, S. D. Hoffmann, F. Kraus, T. F. Fässler, *Angew. Chem. Int. Ed.* 2007, **46**, 1638–1640;
- (12m) H.-L. Xu, I. A. Popov, N. V. Tkachenko, Z.-C. Wang, A. Muñoz-Castro, A. I. Boldyrev, Z.-M. Sun, *Angew. Chem. Int. Ed.* 2020, **59**, 17286–17290;
- (12n) L. G. Perla, A. Muñoz-Castro, S. C. Sevov, *J. Am. Chem. Soc.* 2017, **139**, 15176–15181.

- (13a) S. Bobev, S. C. Sevov, *Angew. Chem. Int. Ed.* 2000, **39**, 4108–4110;
- (13b) S. Bobev, S. C. Sevov, *J. Am. Chem. Soc.* 2002, **124**, 3359–3365.
- (14) A. Ugrinov, S. C. Sevov, *Appl. Organomet. Chem.* 2003, **17**, 373–376.
- (15) K. Mayer, L. A. Jantke, S. Schulz, T. F. Fässler, *Angew. Chem. Int. Ed.* 2017, **56**, 2350–2355;
- (16) C. B. Benda, M. Waibel, T. F. Fässler, *Angew. Chem. Int. Ed.* 2015, **54**, 522–526;
- (17) J. D. Corbett, P. Edwards, *J. Chem. Soc. Chem. Commun.* 1975, 984–985.
- (18a) I. Resa, E. Carmona, E. Gutierrez-Puebla, A. Monge, *Science* 2004, **305**, 1136–1138;
- (18b) T. Li, S. Schulz, P. W. Roesky, *Chem. Soc. Rev.* 2012, **41**, 3759–3771;
- (18c) K. Freitag, C. Gemel, P. Jerabek, I. M. Oppel, R. W. Seidel, G. Frenking, H. Banh, K. Dilchert, R. A. Fischer, *Angew. Chem. Int. Ed.* 2015, **54**, 4370–4374;
- (18d) J. Hicks, E. J. Underhill, C. E. Kefalidis, L. Maron, C. Jones, *Angew. Chem. Int. Ed.* 2015, **54**, 10000–10004;
- (19) A. R. Eulenstein, Y. J. Franzke, P. Bügel, W. Massa, F. Weigend, S. Dehnen, *Nat. Commun.* 2020, **11**, 5122.
- (20) Gaussian 16, Revision B.01, M. J. Frisch, et al., Gaussian, Inc., Wallingford, **2016**.
- (21a) A. Schäfer, C. Huber, R. Ahlrichs, *J. Chem. Phys.* 1994, **100**, 5829–5835;
- (21b) C. Adamo, V. Barone, *J. Chem. Phys.* 1999, **110**, 6158–6170.
- (22a) D. Y. Zubarev, A. I. Boldyrev, *Phys. Chem. Chem. Phys.* 2008, **10**, 5207–5217;
- (22b) N. V. Tkachenko, A. I. Boldyrev, *Phys. Chem. Chem. Phys.* 2019, **21**, 9590–9596.
- (23a) N. V. Tkachenko, A. I. Boldyrev, *Chem. Sci.* 2019, **10**, 5761–5765;

- (23b) Z.-C. Wang, N. V. Tkachenko, L. Qiao, E. Matito, M. Muñoz-Castro, A. I. Boldyrev, Z.-M. Sun, *Chem. Commun.* 2020, **56**, 6583–6586;
- (23c) H.-L. Xu, N. V. Tkachenko, Z.-C. Wang, W.-X. Chen, L. Qiao, A. Muñoz-Castro, A. I. Boldyrev, Z.-M. Sun, *Nat. Commun.* 2020, **11**, 5286.
- (24) C.-R. Irene, R.-C. Eloy, T.-S. Miquel, M. Eduard, *Molecules* 2020, **25**, 711.
- (25) T. Yanai, D. P. Tew, N. C. Handy, *Chem. Phys. Lett.* 2004, **393**, 51–57.
- (26a) R. Benassi, P. Lazzeretti, F. Taddei, *J. Phys. Chem.* 1975, **79**, 848–851;
- (26b) R. Gershoni-Porannea, A. Stanger, *Chem. Soc. Rev.* 2015, **44**, 6597–6615.
- (27a) R. Islas, T. Heine, G. Merino, *Acc. Chem. Res.* 2012, **45**, 215–228;
- (27b) G. Merino, T. Heine, G. Seifert, *Chem. Eur. J.* 2004, **10**, 4367–4371;
- (27c) A. Muñoz-Castro, *Phys. Chem. Chem. Phys.* 2017, **19**, 12633–12636.
- (28) A. Muñoz-Castro, *ChemPhysChem* 2020, **21**, 1384–1387.
- (29a) B. Silvi, A. Savin, *Nature* 1994, **371**, 683–686;
- (29b) T. Lu, F. Chen, *J. Comput. Chem.* 2012, **33**, 580–592.
- (30) R. F. W. Bader, *Atoms in Molecules: A Quantum Theory*, Clarendon, Oxford, 1990.
- (31) A. V. Marenich, S. V. Jerome, C. J. Cramer, D. G. Truhlar, *J. Chem. Theory Comput.* 2012, **8**, 527–541.

Tables and figures

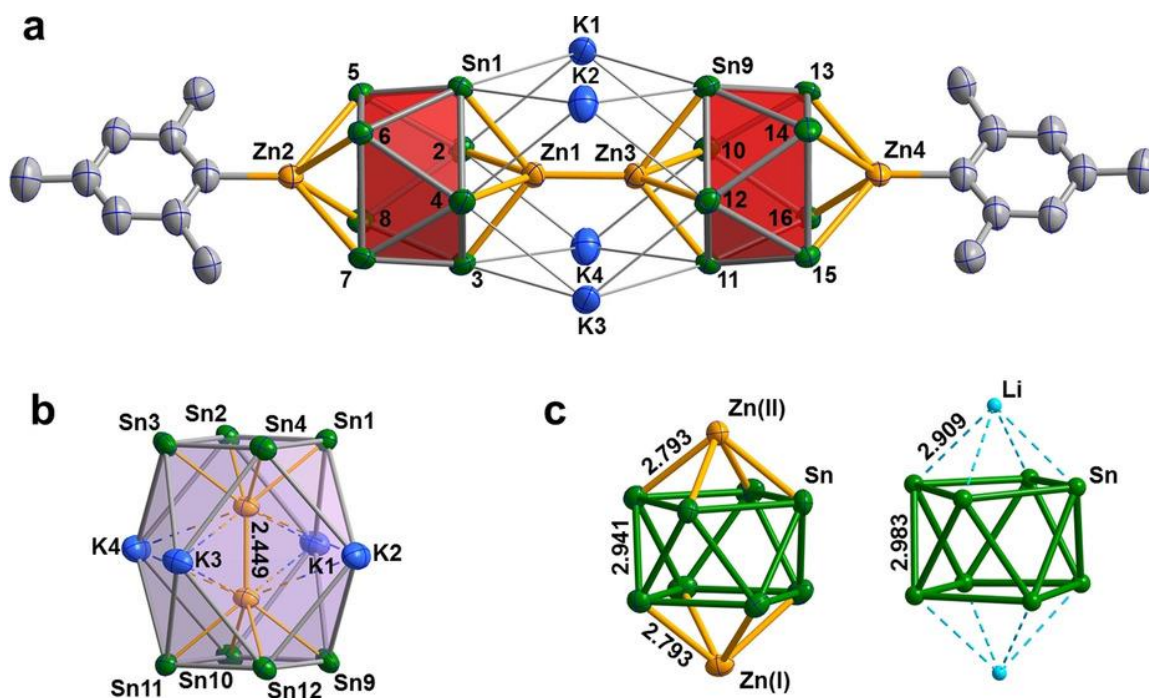


Figure 5-1. a) The cluster anion $\{[K_2ZnSn_8(ZnMes)_2]\}^{4-}$ (thermal ellipsoids are drawn at 50 % probability). b) The structure of fragment $[K_4Zn_2Sn_8]$ is shown by a rotation of 90 degrees. The $Zn-Zn$ bond length is given in Å. c) The contrast of $closo-[Zn_2Sn_8]$ moiety in anion **1a** and $closo-[Li_2Sn_8]^{4-}$ in the Zintl phase $K_4Li_2Sn_8$. The average bond lengths are given in Å.

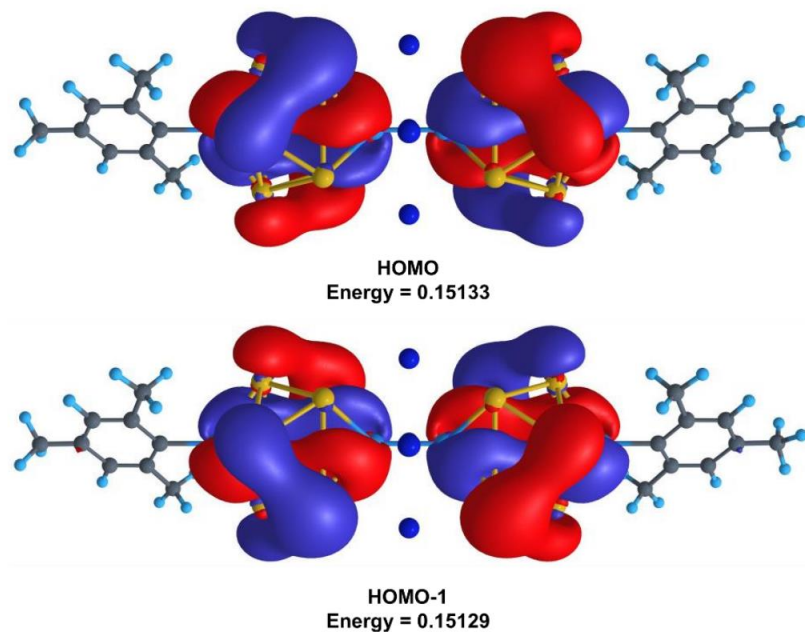


Figure 5-2. Plots of HOMO/HOMO-1 molecular orbitals and their energy (Hartree) for $\{[K_2ZnSn_8(ZnMes)_2]_2\}^{4-}$ cluster.

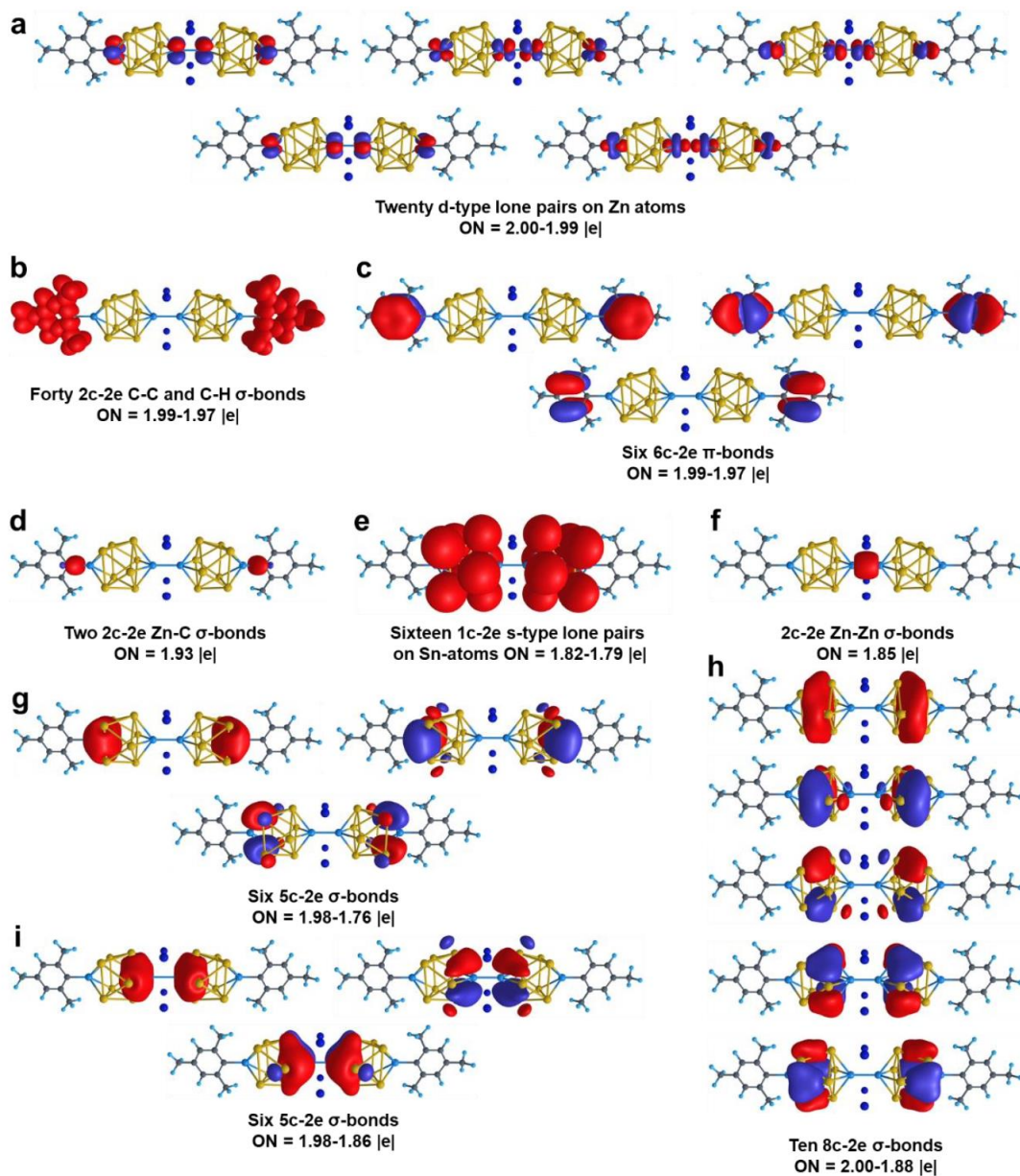


Figure 5-3. The results of AdNDP analysis for $\{[K_2ZnSn_8(ZnMes)_2]^{4-}\}$ cluster. Bonding elements are plotted at an iso-value of 0.03 a.u. Different phases of a wave function represented with different colors. Positive: red; negative: blue. For figure compactness, two multicentered bonds are plotted for each structure.

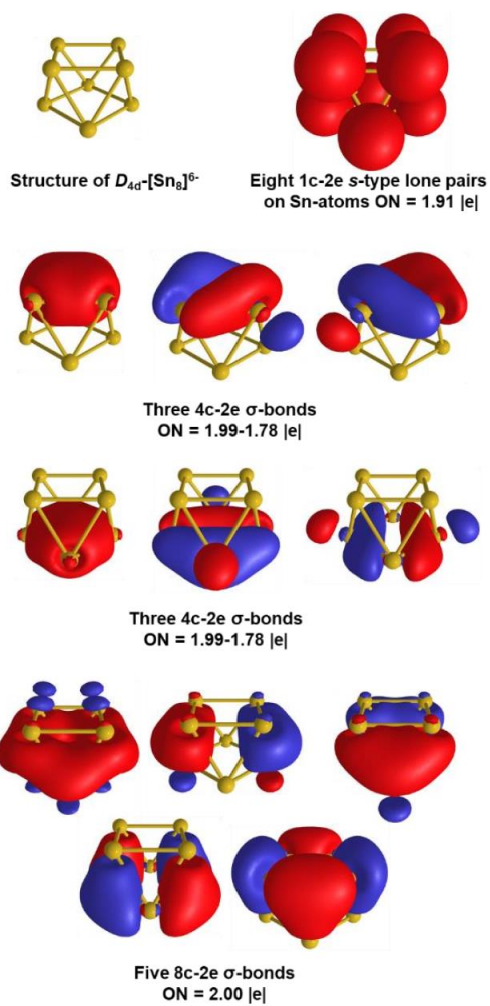


Figure 5-4. The complete chemical bonding pattern of [Sn₈]⁶⁻ cluster.

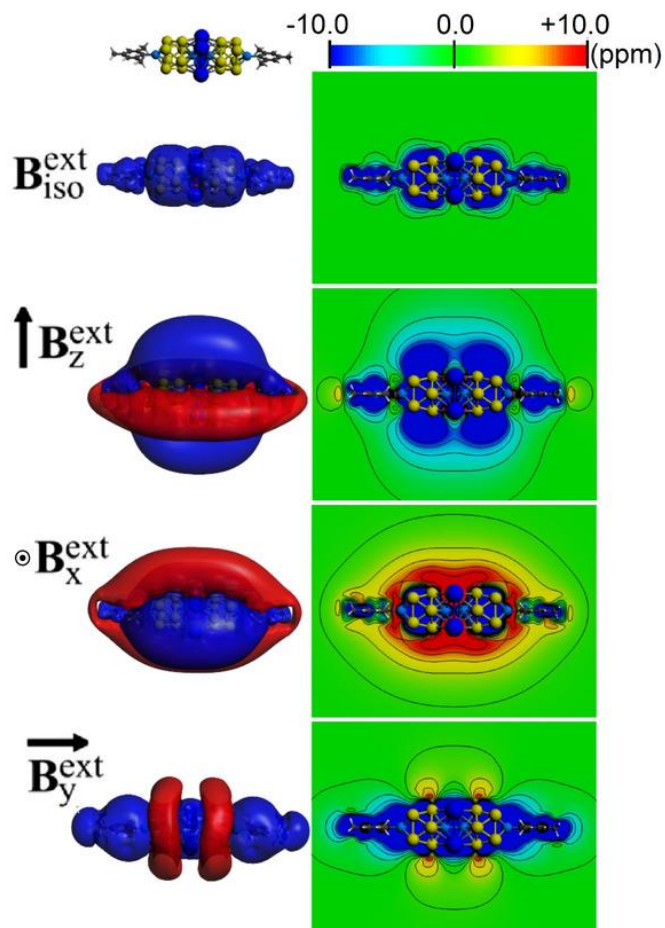


Figure 5-5. Three-dimensional (left) and contour-plot (right) representation of the magnetic response B^{ind} for $\{[\text{K}_2\text{ZnSn}_8(\text{ZnMes})]_2\}^{4-}$. Isosurface values are set at ± 2.0 ppm. Blue: shielding, red, deshielding regions.

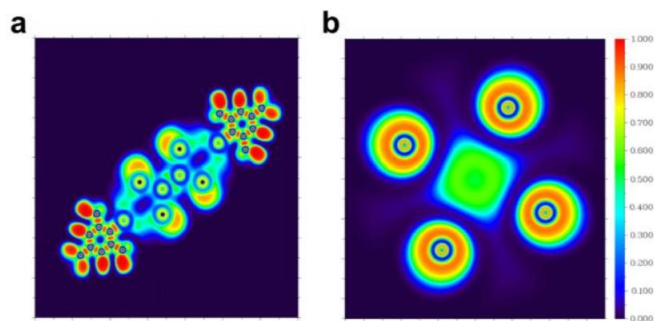


Figure 5-6. ELF plots of $\{[K_2ZnSn_8(ZnMes)]_2\}^{4-}$ cluster. A) plot is built in the plane of C_6 rings; B) plot is built in the plane of K_4 square.

CHAPTER 6

 σ -AROMATICITY-INDUCED STABILIZATION OF HETEROMETALLIC
SUPERTETRAHEDRAL CLUSTERS $[\text{Zn}_6\text{Ge}_{16}]^{4-}$ AND $[\text{Cd}_6\text{Ge}_{16}]^{4-}$ ¹**Abstract**

In this work, the largest heterometallic supertetrahedral clusters, $[\text{Zn}_6\text{Ge}_{16}]^{4-}$ and $[\text{Cd}_6\text{Ge}_{16}]^{4-}$, were directly self-assembled through highly-charged $[\text{Ge}_4]^{4-}$ units and transition metal cations, in which 3-center–2-electron σ bonding in Ge_2Zn or Ge_2Cd triangles plays a vital role in the stabilization of the whole structure. The cluster structures have an open framework with a large central cavity of diameter 4.6 Å for Zn and 5.0 Å for Cd, respectively. Time-dependent HRESI-MS spectra show that the larger clusters grow from smaller components with a single $[\text{Ge}_4]^{4-}$ and ZnMes_2 units. Calculations performed at the DFT level indicate a very large HOMO–LUMO energy gap in $[\text{M}_6\text{Ge}_{16}]^{4-}$ (2.22 eV), suggesting high kinetic stability that may offer opportunities in materials science. These observations offer a new strategy for the assembly of heterometallic clusters with high symmetry.

6.1 Introduction

Supertetrahedral clusters, which are made from the small tetrahedral building blocks arranged in a tetrahedral fashion, have an intrinsic appeal due to their high symmetry. They have found applications in a wide range of areas, from photolysis to fast-ion conductivity.¹ The flexibility of choice in sub-units has led to a diverse range of structures, many of which involve transition metals in combination with tetrelide or chalcogenide ions. Perhaps, the

¹ Coauthored by Hong-Lei Xu, Ivan A. Popov, Nikolay V. Tkachenko, Zi-Chuan Wang, Alvaro Muñoz-Castro, Alexander I. Boldyrev, and Zhong-Ming Sun. Reproduced from *Angew. Chem. Int. Ed.*, **2020**, 59, 17286-17290 with permission. Copyright © 2020, John Wiley & Sons.

most high-profile supertetrahedra are the gold clusters Au_{20} and Au_{40} which have been studied extensively in the gas phase and have shed light on the nature of metal-metal bonding.² As yet, however, no analogues have been stabilized in the solid state, and it remains a substantial challenge to synthetic chemistry to achieve this goal. One of the most important design tools available to the synthetic chemist is “self-assembly”, which allows simple building blocks to be used to construct complex and highly symmetric nanostructures. In the majority of cases, it remains the case that the architecture of the self-assembled product depends on a judicious choice of organic ligand and careful control of reaction conditions as well as chemical bond manipulation such as hydrogen bonds, van der Waals forces, and aurophilic interactions.³ It is anticipated that small metal clusters are very good candidates for the assembly of large heterometallic clusters. However, to the best of our knowledge, such kind of self-assemblies is very rare and still remains a challenging task. Herein, we report the successful self-assembly of two unprecedented heterometallic supertetrahedral clusters using highly charged $[\text{Ge}_4]^{4-}$ as building blocks and transition metals, Zn or Cd, as connection nodes.

6.2 Results and Discussions

The anionic clusters $[\text{M}_6\text{Ge}_{16}]^{4-}$ ($\text{M}=\text{Zn}$ (**1a**); Cd (**2a**)) were obtained from the reaction of $\text{K}_{12}\text{Ge}_{17}$ with $\text{ZnMes}_2/\text{CdMes}_2$ ($\text{Mes}=\text{2, 4, 6-Me}_3\text{C}_6\text{H}_2$) together with 2,2,2-crypt in solutions of N,N-dimethylformamide (DMF)/ethylenediamine (en), Figure 6-1A. Overall, the 22 atoms of the cluster define a highly symmetric concave polyhedron containing 24 Ge_3 and Ge_2M triangles and 4 chair-like concave M_3Ge_3 hexagons (for example: Zn1-Ge3-Zn3-Ge7-Zn5-Ge11). Rather long Zn-Zn and Cd-Cd distances (3.30–3.39 Å and 3.50–3.66 Å, respectively) suggest that direct interactions between the transition metal ions are not a

major stabilizing factor. Alternatively, the clusters can be viewed as containing four discrete $[\text{Ge}_4]^{4-}$ units at the vertices of the tetrahedron, with a transition metal ion ($\text{Zn}^{2+}/\text{Cd}^{2+}$) bridging each edge. The assembly of four Ge_4 units and the associated bridging metal ions creates a large cavity at the center of the clusters with the dimension of 4.6 Å (**1a**) or 5.0 Å (**2a**) (as measured by the distance from one metal to the opposite Ge). The coordination about each Zn/Cd is rather unusual in that it is approximately planar, with the four bonded Ge atoms in a single plane. There is precedent for such geometries in metal ions with a d^{10} configuration, such as $[\eta^2:\eta^2-(\text{Sb}_2\text{Sn}_2)\text{Au}^{\text{I}}(\text{Sb}_2\text{Sn}_2)]^{3-}$,⁴ but approximately tetrahedral coordination is a norm for d^{10} ions, as for example in $[\eta^2:\eta^2-\text{Sn}_4\text{Au}^{\text{I}}\text{Sn}_4]^{7-}$ and other analogues.⁵ The three Ge-Ge bonds of the coordinated edges of the Ge_4 units (2.709–2.717 Å in **1a**, 2.721–2.752 Å in **2a**) are elongated substantially compared to those in the isolated $[\text{Ge}_4]^{4-}$ anion (2.574–2.587 Å),⁶ while the three non-coordinated Ge-Ge bonds in each Ge_4 unit are, conversely, slightly shorter than those in $[\text{Ge}_4]^{4-}$ and other Zn/Ge clusters.^{5d,6b,7} The structure of **1a** can usefully be compared to the $[(\text{Ge}_4)\text{Zn}(\text{Ge}_4)]^{6-}$ anion, which is found in two distinct isomeric forms in Cs_6ZnGe_8 and $\text{K}_{14}\text{ZnGe}_{16}$, where the two Ge_4 units are coordinated $\eta^3:\eta^3$ and $\eta^3:\eta^2$, respectively.⁸ The Zn-Ge bond lengths in **1a** lie in a narrow range between 2.547 and 2.589 Å (average 2.569 Å, Figure 6-1C), slightly shorter than those in both of the above cases. The most direct comparison for **2a** is with $[\text{Cd}_3(\text{Ge}_3\text{P})_3]^{3-}$ which contains both η^3 and η^2 coordinated Ge_3P units,⁹ where the Cd-Ge bond lengths are ≈ 2.819 Å, similar to those in **2a** (average 2.736 Å).

The assembly of $[\text{Zn}_6\text{Ge}_{16}]^{4-}$ was followed by time-dependent ESI-MS (Figure S6). After 5 minutes, the reaction mixture is dominated by ions containing a single Ge_4 unit, $\{[\text{K}(2,2,2\text{-crypt})][\text{Ge}_4\text{Zn}_2\text{Mes}_2]\}^-$ and $\{[\text{K}(2,2,2\text{-crypt})][\text{Ge}_4\text{Zn}_2\text{Mes}_4]\}^-$, at $m/z=1074.94$

and 1313.11, respectively. After 30 minutes the peaks due to $\text{Ge}_4\text{Zn}_2\text{Mes}_x$ ($x=2, 4$) have disappeared, and were replaced by four new peaks due to $\{[\text{K}(2,2,2\text{-crypt})][\text{Zn}_6\text{Ge}_{16}]\}^-$, $\{[\text{K}(2,2,2\text{-crypt})]_3[\text{Zn}_6\text{Ge}_{16}]\}^-$ and two intermediate species $\{[\text{K}_3(2,2,2\text{-crypt})][\text{ZnGe}_8]\}^-$ and $\{[\text{K}(2,2,2\text{-crypt})][\text{Zn}_3\text{Ge}_8\text{Mes}_4]\}^-$. The fact that the peak of the ZnGe_8 fragment in the ESI-MS is very prominent confirms that it is stable in solution. After 90 minutes, the signals due to $\{[\text{K}_3(2,2,2\text{-crypt})][\text{ZnGe}_8]\}^-$ and $\{[\text{K}(2,2,2\text{-crypt})][\text{Zn}_3\text{Ge}_8\text{Mes}_4]\}^-$ are relatively reduced in intensity relative to the targeted products. At no point do we find evidence for intermediate $\text{Zn}_x(\text{Ge}_4)_y$ fragments containing more Zn or Ge_4 units, suggesting that the initial Zn-Ge bond formation event is followed by rapid assembly into the final $[\text{Zn}_6\text{Ge}_{16}]^{4-}$ cluster. Based on the above analysis, a possible assembly mechanism of $[\text{Zn}_6\text{Ge}_{16}]^{4-}$ is proposed in Figure 6-2. It is noted that ZnGe_8 may be the key intermediate in the formation of **1a**, two ZnGe_8 units together with two ZnMes_2 species can be directly assembled into ultimate supertetrahedral structure.

To explore the origins of high stability of the $[\text{M}_6\text{Ge}_{16}]^{4-}$ clusters, we have carried out a series of density functional theory (DFT) calculations using a large polarized quadruple-zeta basis with DFT hybrid functional (PBE0/Def2-QZVP level of theory)^{10,11} as implemented in the Gaussian 16 software package¹² (see the Supporting Information for computational details). The highest occupied molecular orbital (HOMO) is triply degenerate (t_1) and is made up of linear combinations of the Ge bonding orbitals (94 %) with a very small contribution from Zn (6 %) (Figure S20). In contrast, the lowest unoccupied molecular orbital (LUMO) has a significant character of Zn orbitals (54 %), along with some residual Ge-Ge bonding character (46 %). The large HOMO–LUMO gap of 2.22 eV found in both $[\text{Zn}_6\text{Ge}_{16}]^{4-}$ and $[\text{Cd}_6\text{Ge}_{16}]^{4-}$, preclude any second-order Jahn–

Teller instabilities, consistent with the rigorous T_d symmetry. It should be noted that the absolute values of the HOMO–LUMO gaps depend on the amount the Hartree–Fock exchange, and, hence, should be treated with caution. Typically, large HOMO–LUMO gaps suggest high kinetic stability and usually relate to aromatic compounds, which also exhibit high-symmetry structures.¹³ To better understand the reasons of the stability of these clusters, a more thorough chemical bonding analysis was developed. Because of the complexity of the canonical molecular orbitals (CMOs), which are intrinsically difficult to interpret in terms of chemical bonds due to delocalization, Adaptive Natural Density Partitioning (AdNDP)¹⁴ analysis was performed as implemented in AdNDP 2.0 code.¹⁵ The AdNDP algorithm has previously been used with great success to analyze chemical bonding patterns in a wide range of inorganic Zintl anions.¹⁶ The $[M_6Ge_{16}]^{4-}$ clusters have 140 valence electrons in total (12|e| from each M-atom, 4|e| from each Ge-atom and 4|e| from the 4– overall charge), giving rise to 70 two-electron AdNDP bonding elements. According to AdNDP, there are five *d*-type lone pairs on each M atom, and one *s*-type lone pair on each Ge atom, thus accounting for 46 electron pairs (Figure S21, S22). The remaining 24 pairs (48 electrons) form twelve 3c-2e Ge-Ge-Ge σ bonds (three per Ge_4) (Figure 6-3A) and twelve 3c-2e M-Ge-Ge σ bonds (three per Ge_4) (Figure 6-3B). Alternatively, twelve 3c-2e Ge-Ge-Ge σ bonds could also be viewed as twelve more localized 2c-2e Ge-Ge σ bonds located over the Ge_4 edges with lower occupation numbers (Figure 6-4). To complement the AdNDP localization, we have also explored the topology of the Electron Localization Function (ELF), $\eta(r)$,¹⁷ 2D plots of which are plotted for selected planes in Figure 6-3C. In agreement with the 3c-2e M-Ge-Ge σ bonds, there is a clear localization in the M-Ge-Ge region (in the plane of Ge_4M fragment, Figure 6-3C

(left)), with the major contribution coming from the two Ge atoms. In contrast, the ELF is close to zero in the cavity at the center of the cluster (Figure 6-3C (right)), supporting the absence of the M-M interactions in the M_6 octahedron.

The major contribution to the 3c-2e M-Ge-Ge σ bonds comes from two Ge atoms (84 % in $[Zn_6Ge_{16}]^{4-}$ and 86 % in $[Cd_6Ge_{16}]^{4-}$). However, the substantial delocalization over the M center drives the elongation of the coordinated Ge-Ge bonds, which are significantly longer than the sum of the Ge covalent radii for a single Ge-Ge bond, that is, 2.42 Å.¹⁸ In fact, the M contribution in each 3c-2e σ bond is significant, that is, 0.30|e|. Hence, the stability of the $[M_6Ge_{16}]^{4-}$ clusters may not be ascribed to pure ionic interactions of M^{2+} cations stabilizing the $[Ge_4]^{4-}$ anionic tetrahedra. The appreciable covalent character arises due to the delocalization over the M atom which is, in total, 0.60|e| per two 3c-2e bonds formed by one M atom. In this sense, the oxidation state of the transition metal ions is intermediate between 1+ and 2+. It is worth noting that the Au^{1+} and Ag^{1+} compounds have previously been shown to adopt similar planar tetracoordinate configurations of these coinage metals with tetrahedral sub-units composed out of Sn, Sb, or As atoms.^{4,19} As evident from the natural electron configuration of Zn in $[Zn_6Ge_{16}]^{4-}$ ($4s^{0.84}4p^{0.88}3d^{9.98}$), there is a considerable covalency that leads to a build-up of the electron density in Zn 4s and 4p, leading to the *sp*-hybridization.

Based on the most employed criterion of aromaticity, that is, the magnetic criterion that assumes that an aromatic fragment sustains ring current because of its delocalized electrons, we further calculated magnetic response properties of the $[M_6Ge_{16}]^{4-}$ clusters (E=Zn or Cd), which involves four spherical aromatic $[Ge_4]^{4-}$ fragments, as shown earlier by Hirsch and co-workers (a detailed discussion on why $[Ge_4]^{4-}$ is regarded as spherically

aromatic can be found in the Supporting Information).²⁰ In order to obtain a global view of the aromatic character, we computed the induced magnetic field ($B^{\text{ind.}_{iso}}$) in terms of isotropic ($B^{\text{ind.}_{iso}} = -(1/3)(\sigma_{xx} + \sigma_{yy} + \sigma_{zz})B^{\text{ext}}$) (orientational average) and for particular orientations of the external field (Figure 6-5). In general, for spherical aromatic clusters, such as $[\text{Ge}_4]^{4-}$, $B^{\text{ind.}_{iso}}$ exhibits a spherical-like shielding region. For $[\text{M}_6\text{Ge}_{16}]^{4-}$ clusters, $B^{\text{ind.}_{iso}}$ shows four spherical-like shielding regions connected via Zn^{2+} or Cd^{2+} , denoting four spherical aromatic Ge_4 fragments, indicating that in the self-assembly of $[\text{Ge}_4]^{4-}$ building blocks in the ionic limit, their aromatic character is retained. This suggests that a convenient strategy for designing controlled aggregates can be based on aromatic building blocks prone to be connected by d^{10} ions nodes. Indeed, under specific orientations of the field, the characteristic shielding cone is enabled with a complementary perpendicular deshielding, resembling the characteristics of planar Hückel aromatics. In the case of $[\text{M}_6\text{Ge}_{16}]^{4-}$ clusters, the different long-range shielding regions are overlapped resulting in a global induced magnetic field, unraveled as a characteristic of the tetrahedral cluster aggregates. Overall, these results reveal the aromatic character of 3c-2e Ge-Ge-Ge σ bonds, where 3c-2e M-Ge-Ge σ bonds are also involved in the spherical aromatic character of connected $[\text{Ge}_4]^{4-}$ blocks. Thus, the global aromatic character of $[\text{M}_6\text{Ge}_{16}]^{4-}$ species is determined by the addition of the individual spherical aromatic behavior of each Ge_4 fragment. The aromatic ring currents from the Ge_4 fragments generate the obtained shielding regions, which are superimposed. Hence, a superimposed ring current is expected to occur in the $[\text{M}_6\text{Ge}_{16}]^{4-}$ clusters in the magnetic field.

6.3 Conclusions

In summary, the supertetrahedral frameworks in the anionic components of **1a** and **2a**, are formed from the assembly of smaller $Zn_x(Ge_4)_y$ fragments, driven by the strong Zn-Ge-Ge interactions via three delocalized 3c-2e σ bonds per Ge_4 . Self-assembly processes of this type may open the door to new ligand-free metal-framework-based materials. Therefore, it represents a potential strategy for constructing many new heterometallic nanoclusters using other lower charged transition metal cations and tetrahedral cluster precursors as subunits, such as $[E_2Pn_2]^{2-}$ or $[E_3Pn]^{3-}$ (E=Ge, Sn, Pb; Pn=P, As, Sb, Bi), where spherical aromatic clusters are suggested as stable building blocks. Detailed AdNDP and ELF analyses confirmed that the stability of the $[M_6Ge_{16}]^{4-}$ clusters may not be ascribed to pure ionic interactions of M^{2+} cations stabilizing the $[Ge_4]^{4-}$ anionic tetrahedra. The appreciable covalent character arises due to the delocalization over the M atom by forming 3c-2e M-Ge-Ge σ bonds. Due to the substantial contribution of M atoms in these delocalized bonds, the oxidation state of the M atoms may be considered as intermediate between 1+ and 2+. The calculations of the magnetic response properties reveal the aromatic character of 3c-2e Ge-Ge-Ge σ bonds, where 3c-2e M-Ge-Ge σ bonds are also involved in the spherical aromatic character of connected tetrahedral blocks, thus explaining the stability of the $[M_6Ge_{16}]^{4-}$ clusters. Based on the chemical bonding analyses of $[M_6Ge_{16}]^{4-}$, it is expected to see that similar supertetrahedral clusters with planar tetracoordinate monovalent metal ions (e.g. Au^{1+} , Ag^{1+}) coordinating to the tetrahedral {Ge, Sn, Sn, Sb, or As}-based fragments may also be viable.

References

- (1a) N. F. Zheng, X. H. Bu, P. Y. Feng, *Nature* 2003, **426**, 428–432;

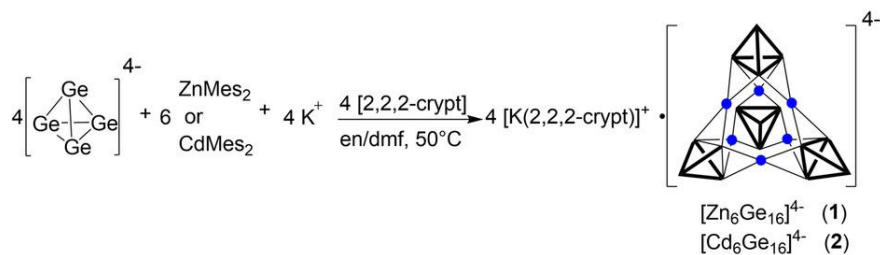
- (1b) M. Duchardt, U. Ruschewitz, S. Adams, S. Dehnen, B. Roling, *Angew. Chem. Int. Ed.* 2018, **57**, 1351–1355;
- (2a) J. Li, X. Li, H.-J. Zhai, L.-S. Wang, *Science* 2003, **299**, 864–867;
- (2b) E. S. Kryachko, F. Remacle, *Int. J. Quantum Chem.* 2007, **107**, 2922–2934;
- (2c) D.-E. Jiang, M. Walter, *Phys. Rev. B Condens. Matter* 2011, **84**, 193402.
- (3a) Z. Wu, Y. Du, J. Liu, Q. Yao, T. Chen, Y. Cao, H. Zhang, J. Xie, *Angew. Chem. Int. Ed.* 2019, **58**, 8139–8144;
- (3b) S. Kenzler, F. Fetzer, C. Schrenk, N. Pollard, A. R. Frojd, A. Z. Clayborne, A. Schnepf, *Angew. Chem. Int. Ed.* 2019, **58**, 5902–5905;
- (4) F. X. Pan, L. J. Li, Z. M. Sun, *Chin. J. Struct. Chem.* 2016, **35**, 1099–1106.
- (5a) C. B. Benda, M. Waibel, T. Kochner, T. F. Fässler, *Chem. Eur. J.* 2014, **20**, 16738–16746;
- (5b) R. J. Wilson, N. Lichtenberger, B. Weinert, S. Dehnen, *Chem. Rev.* 2019, **119**, 8506–8554;
- (5c) “Binary and Ternary Intermetalloid Clusters. Clusters—Contemporary Insight in Structure and Bonding”: B. Weinert, S. Dehnen in *Structure and Bonding, Vol. 174* (Eds.:), Springer, Cham, 2017, pp. 99–134;
- (5d) C. Wallach, K. Mayer, T. Henneberger, W. Klein, T. F. Fässler, *Dalton Trans.* 2020, **49**, 6191–6198.
- (6a) H. G. von Schnering, J. Llanos, J.-H. Chang, K. Peters, E.-M. Peters, R. Nesper, *Z. Kristallogr. New Cryst. Struct.* 2005, **220**, 324;
- (6b) T. Henneberger, W. Klein, J. V. Dums, T. F. Fässler, *Chem. Commun.* 2018, **54**, 12381–12384.

- (7a) K. Mayer, L. J. Schiegerl, T. F. Fässler, *Chem. Eur. J.* 2016, **22**, 18794–18800;
- (7b) K. Mayer, L. A. Jantke, S. Schulz, T. F. Fässler, *Angew. Chem. Int. Ed.* 2017, **56**, 2350–2355;
Angew. Chem. 2017, **129**, 2390–2395;
- (7c) J. M. Goicoechea, S. C. Sevov, *Organometallics* 2006, **25**, 4530–4536;
- (7d) F. Henke, C. Schenk, A. Schnepf, *Dalton Trans.* 2009, 9141–9145;
- (7e) S. Stegmaier, T. F. Fässler, *Inorg. Chem.* 2013, **52**, 2809–2816;
- (7f) M. Waibel, T. Henneberger, L. A. Jantke, T. F. Fässler, *Chem. Commun.* 2012, **48**, 8676–8678;
- (7g) C. B. Benda, R. Schäper, S. Schulz, T. F. Fässler, *Eur. J. Inorg. Chem.* 2013, 5964–5968.
- (8a) S. Stegmaier, M. Waibel, A. Henze, L.-A. Jantke, A. J. Karttunen, T. F. Fässler, *J. Am. Chem. Soc.* 2012, **134**, 14450–14460;
- (8b) V. Queneau, S. C. Sevov, *J. Am. Chem. Soc.* 1997, **119**, 8109–8110.
- (9) S. Mitzinger, J. Bandemehr, K. Reiter, J. S. McIndoe, X. Xie, F. Weigend, J. F. Corrigan, S. Dehnen, *Chem. Commun.* 2018, **54**, 1421–1424.
- (10) C. Adamo, V. Barone, *J. Chem. Phys.* 1999, **110**, 6158–6169.
- (11) F. Weigend, R. Ahlrichs, *Phys. Chem. Chem. Phys.* 2005, **7**, 3297–3305.
- (12) Gaussian 16, Revision B.01, M. J. Frisch, G. W. Trucks, H. B. Schlegel, et al., Gaussian, Inc., Wallingford CT, **2016**.
- (13) J. M. Mercero, A. I. Boldyrev, G. Merino, J. M. Ugalde, *Chem. Soc. Rev.* 2015, **44**, 6519–6534.
- (14) D. Y. Zubarev, A. I. Boldyrev, *Phys. Chem. Chem. Phys.* 2008, **10**, 5207–5217.

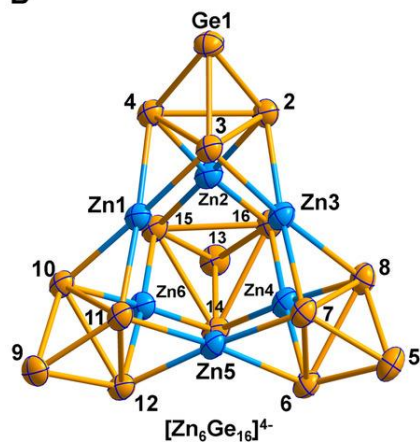
- (15) N. V. Tkachenko, A. I. Boldyrev, *Phys. Chem. Chem. Phys.* 2019, **21**, 9590–9596.
- (16a) I. A. Popov, F.-X. Pan, X.-R. You, L.-J. Li, E. Matito, C. Liu, H.-J. Zhai, Z.-M. Sun, A. I. Boldyrev, *Angew. Chem. Int. Ed.* 2016, **55**, 15344–15346;
- (16b) I. A. Popov, A. A. Starikova, D. V. Steglenko, A. I. Boldyrev, *Chem. Eur. J.* 2018, **24**, 292–305;
- (16c) N. V. Tkachenko, A. I. Boldyrev, *Chem. Sci.* 2019, **10**, 5761–5765;
- (16d) C. Liu, N. V. Tkachenko, I. A. Popov, N. Fedik, X. Min, C.-Q. Xu, J. Li, J. E. McGrady, A. I. Boldyrev, Z.-M. Sun, *Angew. Chem. Int. Ed.* 2019, **58**, 8367–8371;
- (17a) B. Silvi, A. Savin, *Nature* 1994, **371**, 683–686;
- (17b) T. Lu, F. Chen, *J. Comput. Chem.* 2012, **33**, 580–592.
- (18) P. Pyykkö, *J. Phys. Chem. A* 2015, **119**, 2326–2337.
- (19) C. Schwarzmaier, M. Sierka, M. Scheer, *Angew. Chem. Int. Ed.* 2013, **52**, 858–861;
- (20) A. Hirsch, Z. Chen, H. Jiao, *Angew. Chem. Int. Ed.* 2001, **40**, 2834–2837;

Tables and figures

A



B



C

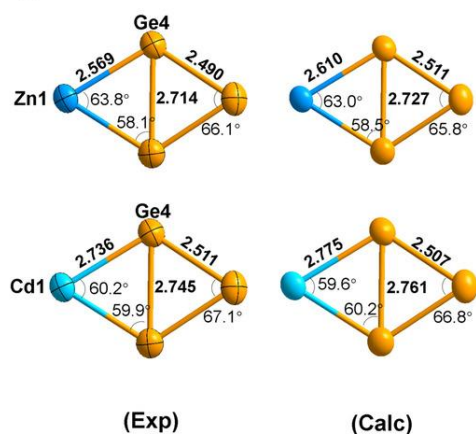


Figure 6-1. A) Formation scheme of $[\text{M}_6\text{Ge}_{16}]^{4-}$ ($\text{M}=\text{Zn}$ or Cd); B) Ellipsoid plot (50 % level) of the crystal structure of $[\text{Zn}_6\text{Ge}_{16}]^{4-}$ (the same structure for $[\text{Cd}_6\text{Ge}_{16}]^{4-}$); C) The experimental and computed geometries of the $\text{Ge}-\text{Ge}_2-\text{M}$ unit in $[\text{M}_6\text{Ge}_{16}]^{4-}$ and the average distances of $\text{Ge}-\text{M}$ and $\text{Ge}-\text{Ge}$ are given in Å.

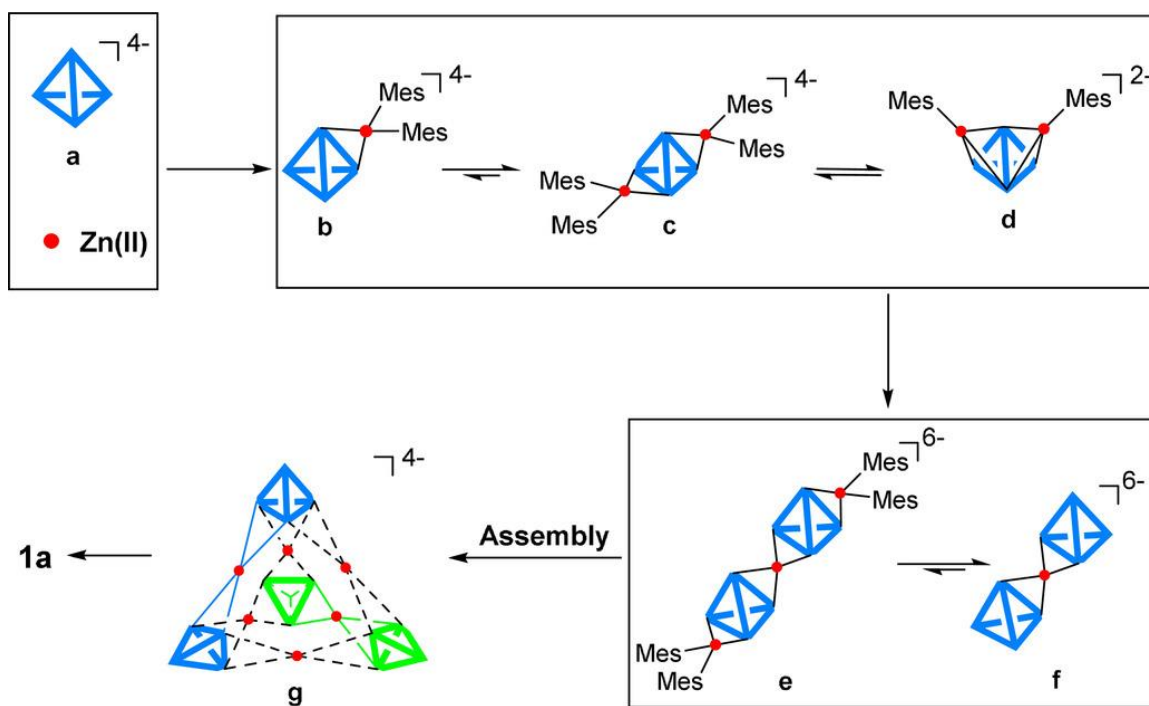


Figure 6-2. The assembly mechanism of tetrahedral cluster $[Zn_6Ge_{16}]^{4-}$. Species that have been observed in the mass spectra are boxed (c, d, e, f, 1a).

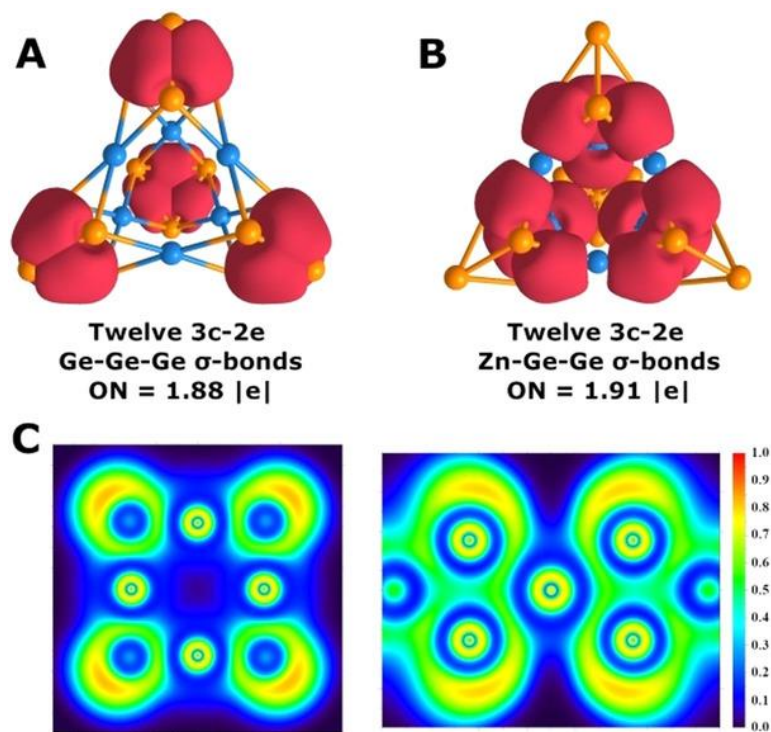


Figure 6-3. A) 3c-2e Ge-Ge-Ge σ -bonds of $[\text{Zn}_6\text{Ge}_{16}]^{4-}$ shown superimposed on the molecular framework (three bonds per Ge_4); B) 3c-2e Zn-Ge-Ge σ -bonds of $[\text{Zn}_6\text{Ge}_{16}]^{4-}$ shown superimposed on the molecular framework (three bonds per Ge_4); C) ELF distribution in rectangular Ge_4Zn fragment (right) and square Zn_4 fragment (left). ON denotes occupation number. The same AdNDP and ELF pictures are identified for $[\text{Cd}_6\text{Ge}_{16}]^{4-}$, both are omitted for clarity.

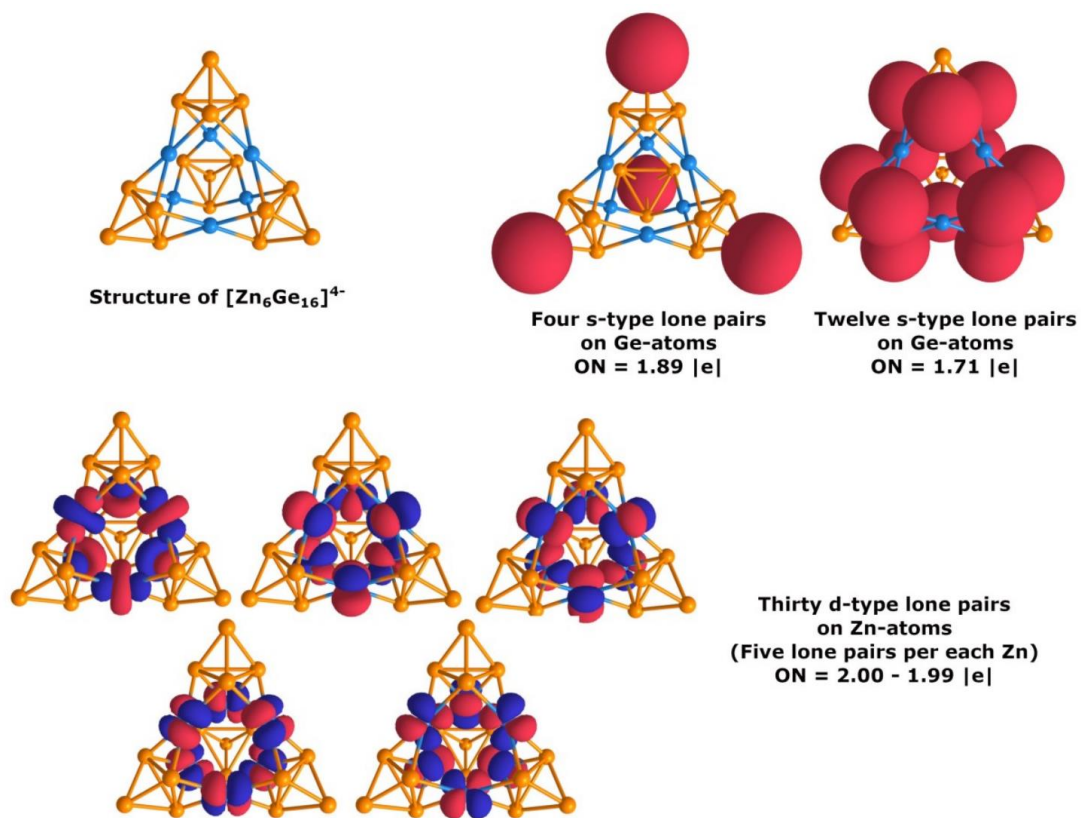


Figure 6-4. Localized lone pairs of $[\text{Zn}_6\text{Ge}_{16}]^{4-}$.

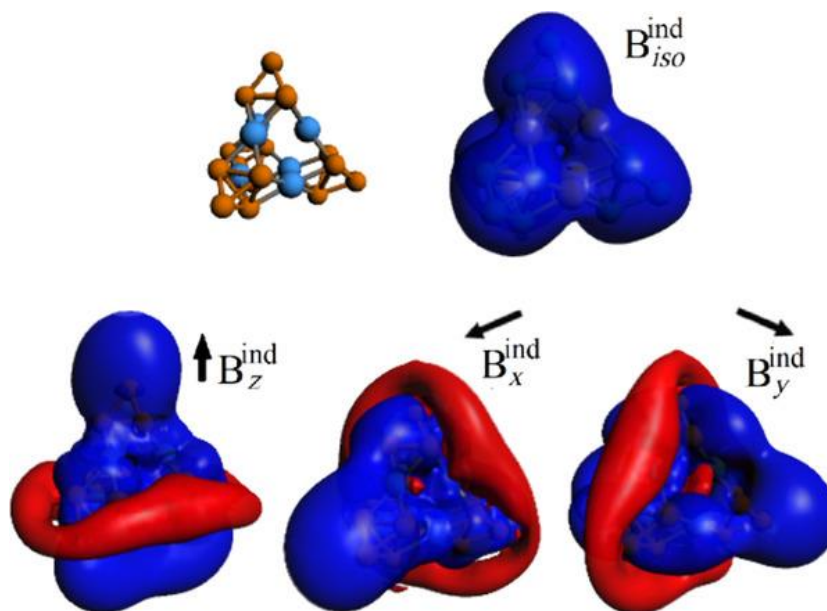


Figure 6-5. Magnetic response properties of $[\text{Zn}_6\text{Ge}_{16}]^{4-}$, given by isotropic term (B_{iso}^{ind}), and under specific orientations of the external field (B_z^{ind} , B_x^{ind} , and B_y^{ind}). Isosurfaces at ± 5 ppm; Blue: shielding; Red: deshielding. The same features are found for $[\text{Cd}_6\text{Ge}_{16}]^{4-}$.

CHAPTER 7
SUPEROCTAHEDRAL TWO-DIMENSIONAL METALLIC BORON WITH
PECULIAR MAGNETIC PROPERTIES¹

Abstract

Among the diversity of new materials, two-dimensional crystal structures have been attracting significant attention from the broad scientific community due to their promising applications in nanoscience. In this study we predict a novel two-dimensional ferromagnetic boron material, which has been exhaustively studied with DFT methods. The relaxed structure of the 2D-B₆ monolayer consists of slightly flattened octahedral units connected with 2c-2e B–B σ -bonds. The calculated phonon spectrum and *ab initio* molecular dynamics simulations reveal the thermal and dynamical stability of the designed material. The calculation of the mechanical properties indicates a relatively high Young's modulus of 149 N m⁻¹. Moreover, the electronic structure indicates the metallic nature of the 2D-B₆ sheets, whereas the magnetic moment per unit cell is found to be 1.59 μ_B . The magnetism in the 2D-B₆ monolayer can be described by the presence of two unpaired delocalized bonding elements inside every distorted octahedron. Interestingly, the nature of the magnetism does not lie in the presence of half-occupied atomic orbitals, as was shown for previously studied magnetic materials based on boron. We hope that our predictions will provide promising new ideas for the further fabrication of boron-based two-dimensional magnetic materials.

¹ Coauthored by Nikolay V. Tkachenko, Dmitriy Steglenko, Nikita Fedik, Natalia M. Boldyreva, Ruslan M. Minyaev, Vladimir I. Minkin, and Alexander I. Boldyrev. Reproduced from *Phys. Chem. Chem. Phys.*, **2019**, *21*, 19764-19771 with permission. Copyright © 2019, Royal Society of Chemistry.

7.1 Introduction

The diversity of boron allotropes is fascinating. Containing one-dimensional, two-dimensional, and three-dimensional structures in its arsenal, boron is one of the most prospective elements for material science. A wide range of structures, such as nanowires, nanotubes, clusters, fullerenes, and 2D sheets, has been studied both theoretically and experimentally in recent years.¹⁻²² Unique electronic properties, such as Dirac cones, were found for several 2D boron allotropes.^{16,19} An even hotter topic is the search for two-dimensional boron structures with magnetic properties due to their potential use in microelectronic and spintronic devices. Although the design of two-dimensional ferromagnetic materials is an extremely interesting and prospective topic, there are still few examples of theoretical²³⁻³⁵ and experimental^{36,37} reports. To the best of our knowledge, only one 2D material made of boron with magnetic properties has been predicted to date.²⁰ However, it was shown that *M*-boron (a monolayer consisting of B₂₀ polyhedrons) should be an antiferromagnetic material with ferromagnetic surface ordering. Following the idea of constructing 2D materials from polyhedrons, we decided to test a monolayer material constructed from boron octahedrons. Three-dimensional bulk materials with octahedral B₆ fragments were experimentally obtained previously. Their crystal structures always include a metal atom (Ca, La, *etc.*)^{38,39} because two electrons should be added to obtain a stable *closo* B₆ structure according to Wade's rules.^{40,41} However, in the current work we predicted a stable superoctahedral magnetic boron material without the inclusion of any metal atoms. Therefore, this material is the second example of magnetic boron and the first example of ferromagnetic two-dimensional boron ever predicted.

7.2 Computational methods

All calculations for the solid state systems were performed using Vienna *Ab initio* Simulation Package⁴² (VASP) code with PAW^{43,44} pseudopotentials. The generalized gradient approximation (GGA) expressed by the PBE functional⁴⁵ was applied. For the structure relaxation, a large 700 eV energy cutoff with a convergence threshold of 10^{-8} eV for the total energy was employed. The Brillouin zone was sampled by the Monkhorst–Pack method⁴⁶ with an automatically generated $31 \times 31 \times 5$ Γ -centered k -point grid. To eliminate the interaction between 2D-B₆ planes, the vacuum space was chosen to be 15 Å. The phonon dispersion was calculated *via* Phonopy code⁴⁷ using a $4 \times 4 \times 1$ supercell and a $7 \times 7 \times 1$ k -mesh. For more accurate calculation of the magnetism in the 2D-B₆ unit cell, the state-of-the-art hybrid functional of Heyd, Scuseria, and Ernzerhof (HSE06)^{48,49} was used. The energy cutoff for these calculations was set to 500 eV, the energy convergence criterion was set to 10^{-6} eV and a $17 \times 17 \times 3$ k -point grid was used. Band structure and DOS calculations for 2D-B₆ were performed at the PBE functional level with an 800 eV energy cutoff. To explore the magnetic ordering within the 2D-B₆ surface, optimization of the $2 \times 2 \times 1$ supercell in nonmagnetic (NM), antiferromagnetic (AFM), and ferromagnetic (FM) configurations was performed.

To evaluate the thermal stability, *ab initio* Born–Oppenheimer molecular dynamics (BOMD) simulations for a $4 \times 4 \times 1$ supercell (96 atoms) were carried out. The time of the simulation was set to 5 ps with a time step of 1 fs. To calculate the molecular dynamics at 300 K, a longer time of 10 ps was set. Temperature control was performed using the Nosé–Hover method.⁵⁰

The solid-state adaptive natural density partitioning (SSAdNDP)⁵¹ algorithm was used to analyze the bonding pattern of the 2D-B₆ structure. SSAdNDP follows an idea of the periodic NBO method⁵² and allowed us to obtain not only classical Lewis elements such as 1c-2e lone pairs and 2c-2e bonds but also delocalized bonding elements (*nc-2e*). A plane-wave calculation was performed using a 400 eV energy cutoff with a convergence threshold of 10⁻⁶ eV for the total energy and a *k*-point grid of 31×31×7. Then, plane-wave density was projected into the cc-pVTZ⁵³ AO basis set. Previously, it was shown that the SSAdNDP is a powerful tool for analyzing chemical bonding in 2D materials.⁵⁴⁻⁶⁵ All optimized geometries and obtained bonding patterns were visualized by Vesta software.⁶⁶

The global minimum of a B₆H₄ cluster was found using the Coalescence Kick algorithm.⁶⁷ Five thousand trial structures were generated and optimized at the PBE0/3-21G level of theory^{68,69} for both singlet and triplet states. All structures within 20 kcal mol⁻¹ from global minimum (GM) were reoptimized at the PBE0/aug-cc-pVTZ level. The bonding pattern was obtained using the AdNDP algorithm⁷⁰ as implemented in the AdNDP 2.0 code.⁷¹ All calculations for molecules were performed using the Gaussian16 program.⁷² All results of molecular calculations were visualized by ChemCraft 1.8 software.

7.3 Results and discussion

The optimized crystal structure of the 2D-B₆ monolayer belongs to the *P*₄/*mmm* crystallographic group. The unit cell consists of six boron atoms ordered in a slightly flattened octahedron. For this type of symmetric structure, we can distinguish two types of equivalent boron atoms (Fig. 7-1b). The B_I-B_I, B_I-B_{II} and B_{II}-B_{II} lengths within the unit cell are 2.08 Å, 1.69 Å, and 1.89 Å, respectively. In turn, the B_{II}-B_{II} length between two neighboring unit cells is 1.62 Å, which is the shortest distance within the whole structure.

The nature of these geometric features will be discussed below. For the magnetic properties, we found both nonmagnetic (NM) and ferromagnetic (FM) configurations of the unit cell. It is noteworthy to mention that the FM state is lower in energy than the NM state by 43 meV per atom; therefore, the former state represents the energetically more stable state of 2D-B₆. However, from the structural point of view, these two configurations almost coincide. For comparison, the lattice constants, total energies, and atomic positions are given in Table 7-1.

Because the magnetic properties of the designed material are our primary interest, we decided to study them at a more sophisticated level of theory. For a more accurate description of the magnetism, the HSE06 functional was used. The calculated magnetic moment per unit cell was found to be 1.59 μ_B . Notably, the magnetic moment is independent of the choice of density functional because almost the same results (1.56 μ_B) were obtained for the PBE functional. The spin charge distribution for the FM 2D-B₆ sheet shows that the spin density is localized not only on the top and bottom boron atoms of the B₆ octahedron but is delocalized through the structure (Fig. 7-2). This type of delocalization may result in the partial 1.59 μ_B magnetic moment per unit cell. To confirm the magnetic surface state, the 2 \times 2 \times 1 supercell of the 2D-B₆ sheet with different magnetic ordering was analyzed (Fig. 7-3). We found that the FM surface state is the most stable configuration; it is 0.10 and 1.02 eV per supercell lower in energy than the AFM and NM states, respectively. Therefore, 2D-B₆ is an exciting example of a ferromagnetic material with ferromagnetic surface ordering.

The dynamic stabilities of the FM and NM configurations of 2D-B₆ were tested by calculating their phonon dispersion curves and phonon densities of states. We showed that

there are no low-lying dispersion curves entering the imaginary region in the whole Brillouin zone for the ferromagnetic configuration (Fig. 7-4). The highest optical mode corresponds to in-plane vibrations and reaches ≈ 40 THz (1334 cm^{-1}), indicating strong B–B interactions. Interestingly, only the ferromagnetic configuration is dynamically stable, while the nonmagnetic state has a large imaginary mode corresponding to the out-of-plane vibrations of B_{II} atoms (Fig. 7-5).

In order to understand the electronic properties of the ferromagnetic 2D- B_6 material, we calculated its electronic band structure and density of states (Fig. 7-6). We found that both the spin up and spin down electrons have bands crossing the zero-energy level. As a result, 2D- B_6 has a nonzero density of states at the Fermi level. These facts prove that the 2D- B_6 sheet is metallic, without any band gap. For comparison, the previously predicted M -boron is an AFM semiconductor with an indirect band gap of 0.43 eV.²⁰

An essential property of a material suitable for practical applications is thermal stability. We performed spin-polarized *ab initio* Born–Oppenheimer molecular dynamics simulations at different temperatures (100 K, 300 K, and 450 K). The Nosé–Hover thermostat was used for temperature control. The time of the simulation was set to 5 ps with a time step of 1 fs. For the 300 K simulation, a longer time of 10 ps was chosen. A periodic $4 \times 4 \times 1$ supercell (96 atoms) was used; this cell size is large enough to demonstrate the structure and magnetic properties during the simulation. In Fig. 7-7, the fluctuations of the total magnetic moment and the temperature are shown as a function of the simulation time. The average total magnetic moment retains a remarkably large value at the end of the simulations (25.4 , 22.7 and $16.7 \mu_B$ for 100, 300, and 450 K, respectively). After 5 ps for the 100 K simulations and 10 ps for the 300 K simulations, we found no significant

structure distortion (Fig. 7-8). However, during the 450 K simulation, the structure was only stable for 3 ps. After that time, drastic structural deformations were observed. Thus, the 2D-B₆ structure is unstable at this high temperature; the octahedral fragments are distorted severely and transformed into planar isomers, leading to a noticeable decrease in the magnetic moment of the material (Fig. 7-7). The root-mean square deviations from the 0 K bond lengths are 0.07, 0.14, and 4.61 Å for 100, 300 and 450 K, respectively. As a result of these calculations, we can declare that the ferromagnetic 2D-B₆ monolayer survives at temperatures up to 300 K, which opens a wide variety of potential applications. However, we should mention that this temperature does not correspond to the Curie temperature because the molecular dynamics simulation does not include spin dynamics. The obtained results indicate the stability of the magnetic state with respect to structural deformations.

Other important aspects of a promising material are its mechanical properties, which characterize the plasticity and elasticity of the material. The elastic constants, Young's modulus, and Poisson's ratio for the 2D-B₆ monolayer are listed in Table 7-2 (only two elastic constants are presented because the structure is isotropic). The Young's modulus and Poisson's ratio were calculated according to the following formulas:

$$Y_{2D} = \frac{c_{11}^2 - c_{12}^2}{c_{11}} \quad (\text{I})$$

$$\nu = \frac{c_{12}}{c_{11}} \quad (\text{II})$$

The question of how to synthesize this material remains open for the moment. However, we hope that we are currently on the right track. Thus, studies on the preparation

of singly charged compounds containing an octahedral B₆ fragment are underway.⁷³ We believe that the results of this research will be helpful for the synthesis of 2D-B₆.

To obtain insight into the chemical bonding of the 2D-B₆ monolayer, we firstly decided to analyze the bonding pattern for a model *D*_{4h}-symmetric B₆H₄ cluster. For the spin state of the model cluster, we chose a triplet as the closest approximation to our ferromagnetic sheet. We should mention that the investigated structure has one imaginary frequency because it was forced to belong to the *D*_{4h} symmetry group. The gradient descending along the imaginary frequency led us to the less symmetric *C*_s structure. However, this distortion is not significant for the exploration of chemical bonding, and in the subsequent discussion, the more symmetric structure will be considered for convenience. The analysis of the potential energy surface *via* the coalescence kick algorithm reveals that the distorted octahedral geometry of B₆H₄ is 5.9 kcal mol⁻¹ higher in energy than the planar global minimum structure. However, the considered structure is still one of the lowest energy isomers for the chosen stoichiometry. In the gas phase, singlet state GM is more favorable than triplet GM by 9.3 kcal mol⁻¹. For the octahedral structures as building blocks for the 2D-B₆ monolayer, the singlet structure is lower in energy by only 1.4 kcal mol⁻¹. Obviously, in the crystal environment, the triplet state is stabilized because the calculated magnetic moment of the unit cell clearly indicates the presence of unpaired electrons; therefore, the bonding pattern for the triplet molecular cluster will be discussed.

The results of the AdNDP analysis are presented in Fig. 7-9. The bonding pattern can be described as four classical two-centered two-electron (2c-2e) B-H σ-bonds with an occupation number (ON) of 1.99 |*e*|, six 6c-2e bonds with ON = 2.00 to 1.96 |*e*|, and two unpaired alpha electrons which form a 2c-1e B-B bond with ON = 0.98 |*e*| and a 6c-1e

bond with $ON = 1.00 |e|$. Unprecedentedly, the 1e bonds are perpendicular to each other; we have never observed this bonding feature before.

Because it is not quite an intuitive result, we decided to build an evolution path of the chemical bonding picture from the well-known $B_6H_6^{2-}$ cluster to the B_6H_4 species. The results can be found in the Supporting Information file of the original manuscript. The obtained bonding patterns for $B_6H_6^{2-}$ and $B_6H_4^{2-}$ as well as the comparison of MO energies pushed us to the conclusion that the presented bonding pattern is correct (Fig. S7–S10, in the Supporting Information file of the original manuscript). It is worth noting that we expected to find two 1c-1e bonds at the top and bottom apexes of the B_6 unit (as was observed for the previously predicted M-boron²⁰). However, during the structure relaxation, we observed a change in the energy of the molecular orbitals which led to the formation of two one-electron bonds perpendicular to each other. These bonds provide a slightly flattened geometry for this cluster. We will see below that similar one-electron bonds were also found in the 2D-B6 monolayer. These bonding elements are responsible for the ferromagnetic properties of this material.

To determine the bonding picture in 2D-B6, we used the Solid State Adaptive Natural Density Partitioning (SSAdNDP) algorithm. Following the ideas extracted from the bonding of the B_6H_4 cluster, we obtained a very cognate bonding pattern for the solid state. The results of the SSAdNDP analysis for the spin up and spin down electrons are presented in Fig. 7-10. Each unit cell is bound with neighboring cells through classical 2c-2e B–B σ -bonds with $ON = 1.93 |e|$ (the equivalent of B–H σ -bonds for the cluster). The remaining electrons form eight delocalized six-centered one-electron bonds, which are responsible for the binding interactions inside each flattened octahedron. For the spin up electrons, we

found a 6c-1e bond with $ON = 0.99 |e|$ (Fig. 7-10b) with a shape similar to the 2c-1e bond found in the B_6H_4 cluster. Indeed, the contributions of the two B_I atoms to the six-centered bond were found to be 97%. Therefore, we can consider it as a pure 2c-1e bond. This chemical bond can cause flattening of the B_6 octahedron. However, although the chemical bonding of the cluster and solid state coincide for several bonding elements, we noted that the last three 6c-1e bonds of the spin down electrons (Fig. 7-10o–q) behave differently. Instead of having one electron on each of the two 6c bonds (Fig. 7-10o and p), as is observed in the case of B_6H_4 , we have almost equal low filling of three 6c bonds. The sum of the occupancies gives us about 2 electrons. This interesting behavior may be associated with more explicit degeneration of these orbitals in the case of the solid state. Despite the described discrepancies in bonding patterns, the calculation of the difference between the spin up and spin down occupancies provides us with a value of $1.58 |e|$, which is in very good agreement with the calculated magnetic moment per unit cell ($1.59 \mu_B$).

7.4 Conclusions

To summarize, we designed and computationally tested a novel ferromagnetic superoctahedral 2D boron material. Based on the phonon spectrum and molecular dynamics simulations, we managed to show that the 2D- B_6 monolayer is dynamically and thermally stable. Moreover, it has substantial magnetic properties, and the calculated magnetic moment per unit cell was found to be $1.59 \mu_B$. The electronic structure indicates that this material is metallic, and its bonding pattern consists of classical 2c-2e bonds between unit cells; the chemical bonding inside of the unit cell almost completely consists of six-centered bonds, which are responsible for the magnetic properties. To the best of our knowledge, the material designed in our work is the second example of a magnetic 2D

sheet and the first example of a ferromagnetic metallic 2D sheet formed from pure boron. Therefore, we believe that this material is of great interest to modern material science, and its thermal and mechanical stabilities promise a wide range of applications once it is experimentally obtained.

References

- (1) B. Albert and H. Hillebrecht, *Angew. Chem., Int. Ed.*, 2009, **48**, 8640.
- (2) A. P. Sergeeva, I. A. Popov, Z. A. Piazza, W. L. Li, C. Romanescu, L. S. Wang and A. I. Boldyrev, *Acc. Chem. Res.*, 2014, **474**, 1349.
- (3) H. J. Zhai, B. Kiran, J. Li and L. S. Wang, *Nat. Mater.*, 2003, **2**, 827.
- (4) N. Gonzalez Szwacki, A. Sadrzadeh and B. I. Yakobson, *Phys. Rev. Lett.*, 2007, **98**, 166804.
- (5) H. Tang and S. Ismail-Beigi, *Phys. Rev. Lett.*, 2007, **99**, 115501.
- (6) D. L. V. K. Prasad and E. D. Jemmis, *Phys. Rev. Lett.*, 2008, **100**, 165504.
- (7) H. Tang and S. Ismail-Beigi, *Phys. Rev. B: Condens. Matter Mater. Phys.*, 2009, **80**, 134113.
- (8) S. Saxena and T. A. Tyson, *Phys. Rev. Lett.*, 2010, **104**, 245502.
- (9) M. Liu, V. I. Artyukhov and B. I. Yakobson, *J. Am. Chem. Soc.*, 2017, **1395**, 2111.
- (10) S. De, A. Willand, M. Amsler, P. Pochet, L. Genovese and S. Goedecker, *Phys. Rev. Lett.*, 2011, **106**, 225502.
- (11) F. Liu, C. Shen, Z. Su, X. Ding, S. Deng, J. Chen, N. Xu and H. Gao, *J. Mater. Chem.*, 2010, **20**, 2197.
- (12) E. S. Penev, S. Bhowmick, A. Sadrzadeh and B. I. Yakobson, *Nano Lett.*, 2012, **12**, 2441.

- (13) X. Wu, J. Dai, Y. Zhao, Z. Zhuo, J. Yang and X. C. Zeng, *ACS Nano*, 2012, **6**, 7443.
- (14) D. V. Steglenko, S. A. Zaytsev, R. M. Minyaev and V. I. Minkin, *Neorg. Khim.*, 2019, **64**, 1.
- (15) H. Liu, J. Gao and J. Zhao, *Sci. Rep.*, 2013, **3**, 3238.
- (16) X. F. Zhou, X. Dong, A. R. Oganov, Q. Zhu, Y. Tian and H. T. Wang, *Phys. Rev. Lett.*, 2014, **112**, 085502.
- (17) X. F. Zhou, A. R. Oganov, X. Shao, Q. Zhu and H. T. Wang, *Phys. Rev. Lett.*, 2014, **113**, 176101.
- (18) H. J. Zhai, Y. F. Zhao, W. L. Li, Q. Chen, H. Bai, H. S. Hu, Z. A. Piazza, W. J. Tian, H. G. Lu, Y. B. Wu, Y. W. Mu, G. F. Wei, Z. P. Liu, J. Li, S. D. Li and L. S. Wang, *Nat. Chem.*, 2014, **6**, 727.
- (19) M. Martinez-Canales, T. R. Galeev, A. I. Boldyrev and C. J. Pickard, *Phys. Rev. B*, 2017, **96**, 195442.
- (20) X. F. Zhou, A. R. Oganov, Z. Wang, I. A. Popov, A. I. Boldyrev and H. T. Wang, *Phys. Rev. B*, 2016, **93**, 085406.
- (21) Z. Zhang, E. S. Penev and B. I. Yakobson, *Chem. Soc. Rev.*, 2017, **46**, 6746.
- (22) Z. Zhang, Y. Yang, E. S. Penev and B. I. Yakobson, *Adv. Funct. Mater.*, 2017, **27**, 1605059.
- (23) J. Zhou and Q. Sun, *J. Am. Chem. Soc.*, 2011, **133**, 15113.
- (24) Y. Liu, S. Bhowmick and B. I. Yakobson, *Nano Lett.*, 2011, **11**, 3113.
- (25) Y. Ma, Y. Dai, M. Guo, C. Niu, Y. Zhu and B. Huang, *ACS Nano*, 2012, **6**, 1695.
- (26) A. Du, S. Sanvito and S. C. Smith, *Phys. Rev. Lett.*, 2012, **108**, 197207.

- (27) Z. Zhang, X. Zou, V. H. Crespi and B. I. Yakobson, *ACS Nano*, 2013, **7**, 10475.
- (28) X. Li, X. Wu and J. Yang, *J. Am. Chem. Soc.*, 2014, **136**, 11065.
- (29) F. Wu, C. Huang, H. Wu, C. Lee, K. Deng and E. Kan, *Nano Lett.*, 2015, **15**, 8277.
- (30) Y. Wang, S. S. Wang, Y. Lu, J. Jiang and S. A. Yang, *Nano Lett.*, 2016, **16**, 4576.
- (31) N. Miao, B. Xu, N. C. Bristowe, J. Zhou and Z. Sun, *J. Am. Chem. Soc.*, 2017, **139**, 11125.
- (32) H. Kumar, N. C. Frey, L. Dong, B. Anasori, Y. Gogotsi and V. B. Shenoy, *ACS Nano*, 2017, **11**, 7648.
- (33) Y. Sun, Z. Zhuo, X. Wu and J. Yang, *Nano Lett.*, 2017, **17**, 2771.
- (34) Y. Zhao, J. J. Zhang, S. Yuan and Z. Chen, *Adv. Funct. Mater.*, 2019, **29**, 1901420.
- (35) X. Zhou, X. Sun, Z. Zhang and W. Guo, *J. Mater. Chem. C*, 2018, **6**, 9675.
- (36) C. Gong, L. Li, Z. Li, H. Ji, A. Stern, Y. Xia, T. Cao, W. Bao, C. Wang, Y. Wang, Z. Qiu, R. Cava, S. G. Louie, J. Xia and X. Zhang, *Nature*, 2017, **546**, 265.
- (37) B. Huang, G. Clark, E. Navarro-Moratalla, D. R. Klein, R. Cheng, K. L. Seyler, D. Zhong, E. Schmidgall, M. A. McGuire, D. H. Cobden, W. Yao, D. Xiao, P. Jarillo-Herrero and X. Xu, *Nature*, 2017, **546**, 270.
- (38) J. Akimitsu, K. Takenawa, K. Suzuki, H. Harima and Y. Kuramoto, *Science*, 2001, **293**, 1125.
- (39) P. H. Schmidt, D. C. Joy, L. D. Longinotti, H. J. Leamy, S. D. Ferris and Z. Fisk, *Appl. Phys. Lett.*, 1976, **29**, 400.
- (40) K. Wade *Chem. Commun.*, 1971, 792.
- (41) K. Wade *Adv. Inorg. Chem. Radiochem.*, 1976, **18**, 1.

- (42) G. Kresse and J. Hafner, *Phys. Rev. B: Condens. Matter Mater. Phys.*, 1993, **47**, 558.
- (43) P. E. Blöchl *Phys. Rev. B: Condens. Matter Mater. Phys.*, 1994, **50**, 17953.
- (44) G. Kresse and D. Joubert, *Phys. Rev. B: Condens. Matter Mater. Phys.*, 1999, **59**, 1758.
- (45) J. P. Perdew, K. Burke and M. Ernzerhof, *Phys. Rev. Lett.*, 1996, **77**, 3865.
- (46) H. J. Monkhorst and J. D. Pack, *Phys. Rev. B: Solid State*, 1976, **13**, 5188.
- (47) A. Togo, F. Oba and I. Tanaka, *Phys. Rev. B: Condens. Matter Mater. Phys.*, 2008, **78**, 134106.
- (48) J. Heyd, G. E. Scuseria and M. Ernzerhof, *J. Chem. Phys.*, 2003, **118**, 8207.
- (49) J. Heyd, G. E. Scuseria and M. Ernzerhof, *J. Chem. Phys.*, 2006, **124**, 219906.
- (50) G. J. Martyna, M. L. Klein and M. Tuckerman, *J. Chem. Phys.*, 1992, **97**, 2635.
- (51) T. R. Galeev, B. D. Dunnington, J. R. Schmidt and A. I. Boldyrev, *Phys. Chem. Chem. Phys.*, 2013, **15**, 5022.
- (52) B. D. Dunnington and J. R. Schmidt, *J. Chem. Theory Comput.*, 2012, **8**, 1902.
- (53) T. H. Dunning *J. Chem. Phys.*, 1989, **90**, 1007.
- (54) A. S. Ivanov, E. Miller, A. I. Boldyrev, Y. Kameoka, T. Sato and K. Tanaka, *J. Phys. Chem. C*, 2015, **119**, 12008.
- (55) H. Zhang, Y. Li, J. Hou, A. Du and Z. Chen, *Nano Lett.*, 2016, **16**, 6124.
- (56) Z. H. Cui, E. Jimenez-Izal and A. N. Alexandrova, *J. Phys. Chem. Lett.*, 2017, **8**, 1224.
- (57) C. Pu, D. Zhou, Y. Li, H. Liu, Z. Chen, Y. Wang and Y. Ma, *J. Phys. Chem. C*, 2017, **121**, 2669.

- (58) Y. Wang, M. Qiao, Y. Li and Z. Chen, *Nanoscale Horiz.*, 2018, **3**, 327.
- (59) I. A. Popov and A. I. Boldyrev, *J. Phys. Chem. C*, 2012, **116**, 3147.
- (60) X. F. Zhou, A. R. Oganov, Z. Wang, I. A. Popov, A. I. Boldyrev and H. T. Wang, *Phys. Rev. B*, 2016, **93**, 085406.
- (61) I. A. Popov, K. V. Bozhenko and A. I. Boldyrev, *Nano Res.*, 2012, **5**, 117.
- (62) M. Martinez-Canales, T. R. Galeev, A. I. Boldyrev and C. J. Pickard, *Phys. Rev. B*, 2017, **96**, 195442.
- (63) L. M. Yang, I. A. Popov, A. I. Boldyrev, T. Heine, T. Frauenheim and E. Ganz, *Phys. Chem. Chem. Phys.*, 2015, **17**, 17545.
- (64) L. M. Yang, I. A. Popov, T. Frauenheim, A. I. Boldyrev, T. Heine, V. Bačić and E. Ganz, *Phys. Chem. Chem. Phys.*, 2015, **17**, 26043.
- (65) L. M. Yang, V. Bačić, I. A. Popov, A. I. Boldyrev, T. Heine, T. Frauenheim and E. Ganz, *J. Am. Chem. Soc.*, 2015, **137**, 2757.
- (66) K. Momma and F. Izumi, *J. Appl. Crystallogr.*, 2011, **44**, 1272.
- (67) A. P. Sergeeva, B. B. Averkiev, H. J. Zhai, A. I. Boldyrev and L. S. Wang, *J. Chem. Phys.*, 2011, **134**, 224304.
- (68) C. Adamo and V. Barone, *J. Chem. Phys.*, 1999, **110**, 6158.
- (69) J. S. Binkley, J. A. People and W. J. Hehre, *J. Am. Chem. Soc.*, 1980, **102**, 939.
- (70) D. Y. Zubarev and A. I. Boldyrev, *Phys. Chem. Chem. Phys.*, 2008, **10**, 5207.
- (71) N. V. Tkachenko and A. I. Boldyrev, *Phys. Chem. Chem. Phys.*, 2019, **21**, 9590.
- (72) M. J. Frisch, *et al.*, Gaussian 16, Revision B.01, Gaussian, Inc., 2016.

- (73) X. Mu, J. C. Axtell, N. Bernier, K. Kirlikovali, D. Jung, A. Umanzor, K. Qian, X. Chen, K. Bay, M. Kirolos, A. L. Rheingold, K. N. Houk and A. Spokoyny, Preprint at ChemRxiv, 201910.26434/chemrxiv.8097542.v1.

Tables and figures

Table 7-1. Lattice constants, atomic positions and total energies of the NM and FM 2D-B₆ monolayers.

Configuration	Type	Atomic positions	a (Å)	b (Å)	c (Å)	Etot (eV per atom)
FM	B _I	(0.5, 0.5, 0.569) (0.5, 0.5, 0.431)	4.292	4.292	14.999	-5.762
	B _{II}	(0.189, 0.5, 0.5) (0.811, 0.5, 0.5)				
		(0.5, 0.189, 0.5) (0.5, 0.811, 0.5)				
NM	B _I	(0.5, 0.5, 0.567) (0.5, 0.5, 0.433)	4.318	4.318	14.823	-5.719
	B _{II}	(0.190, 0.5, 0.5) (0.810, 0.5, 0.5)				
		(0.5, 0.190, 0.5) (0.5, 0.810, 0.5)				

Table 7-2. The calculated elastic constants (c_{ij} , in N m^{-1}), Young's modulus (Y_{2D} , in N m^{-1}), and Poisson's ratio (ν) of the 2D- B_6 monolayer.

Structure	c_{11}	c_{12}	c_{66}	Y_{2D}	ν
2D- B_6	150.06	-12.59	9.84	149.01	-0.08

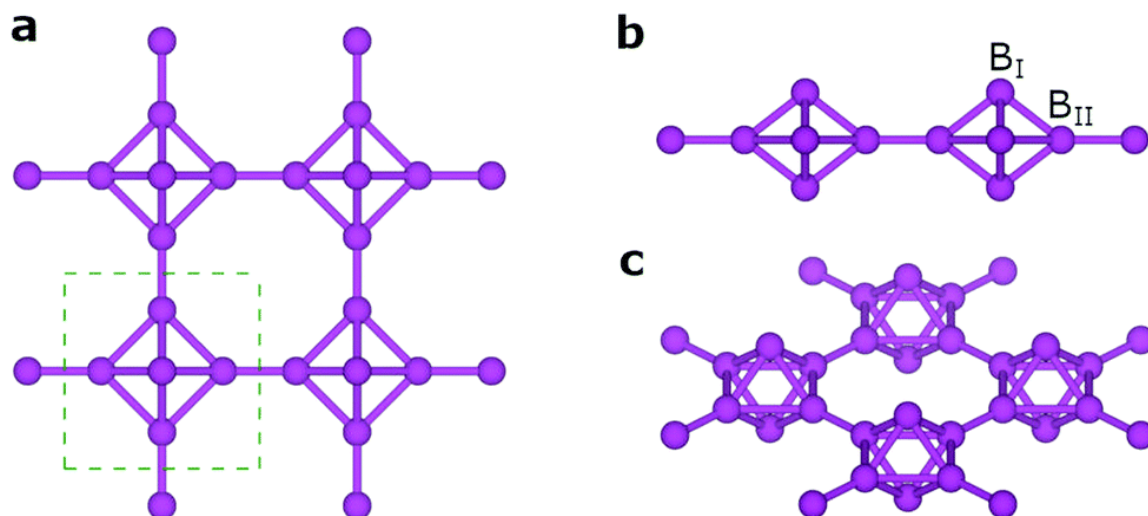


Figure 7-1. (a) The top view of the 2D-B₆ structure. The unit cell is shown with a green dashed square. (b) The side view of the 2D-B₆ structure. The two different types of boron atoms are labeled B_I and B_{II}. (c) The angle view of the 2D-B₆ structure.

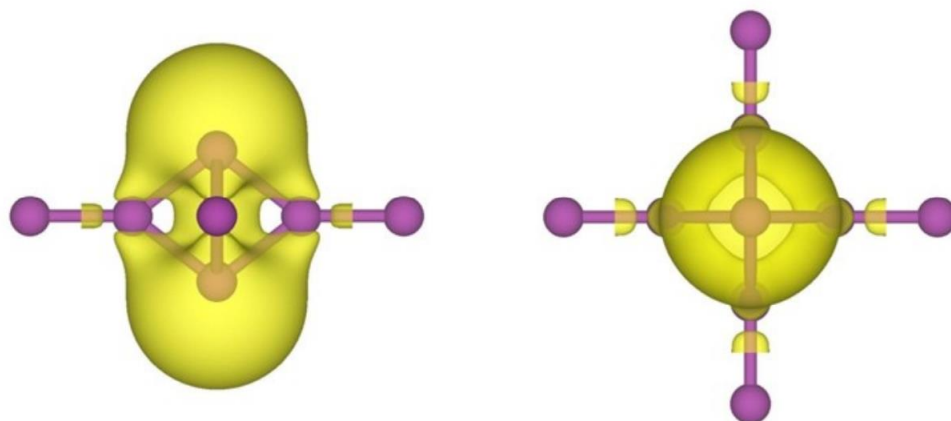


Figure 7-2. Spin charge density distribution with isosurface $0.002 \text{ e}/\text{\AA}^{-3}$ for the ferromagnetic 2D-B₆.

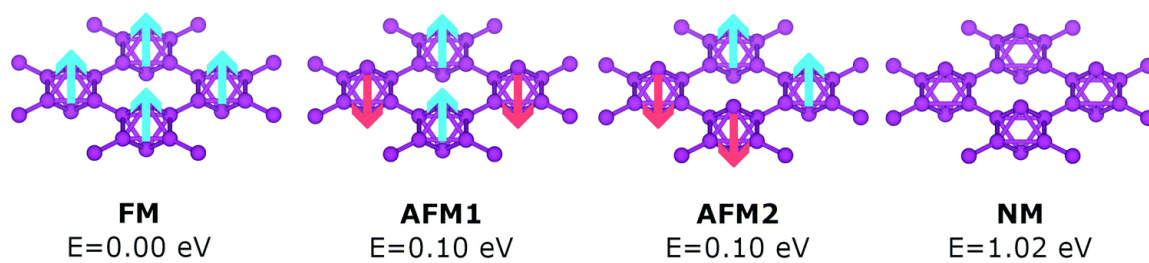


Figure 7-3. Magnetic ordering and relative total energies for the $2 \times 2 \times 1$ supercell of the 2D-B_6 sheet.

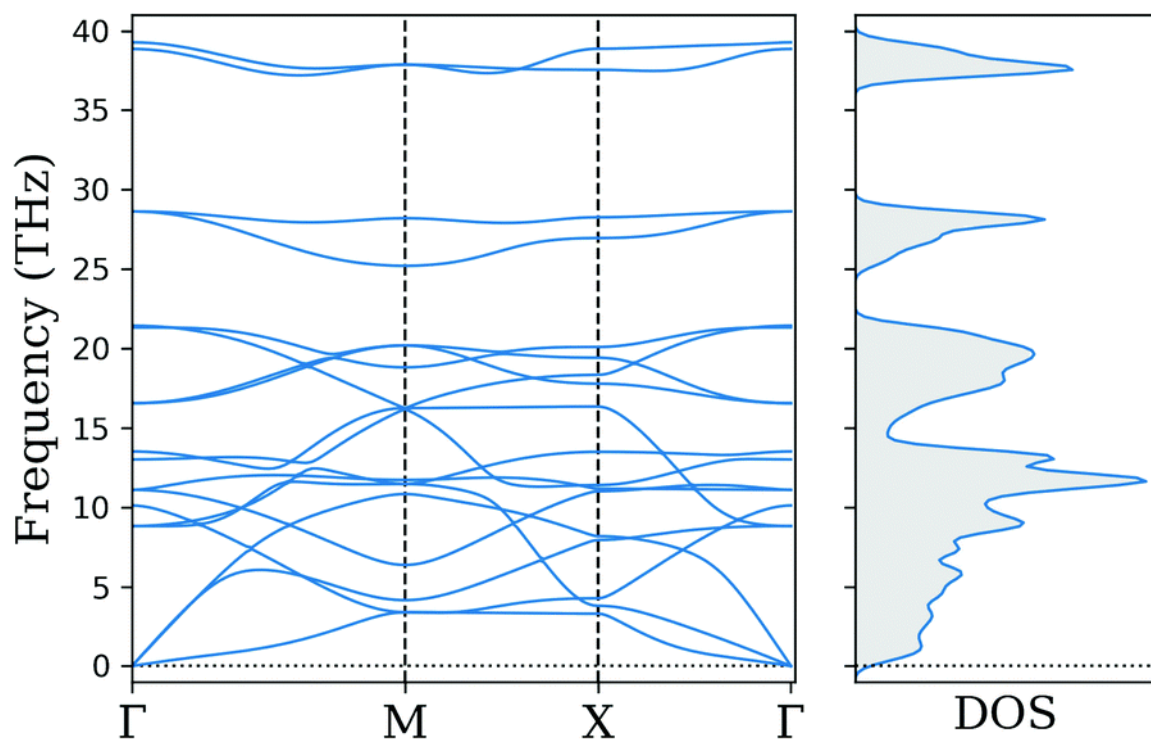


Figure 7-4. Calculated phonon dispersion curves along the Γ -M-X- Γ path and phonon density of states for the ferromagnetic 2D-B₆ material.

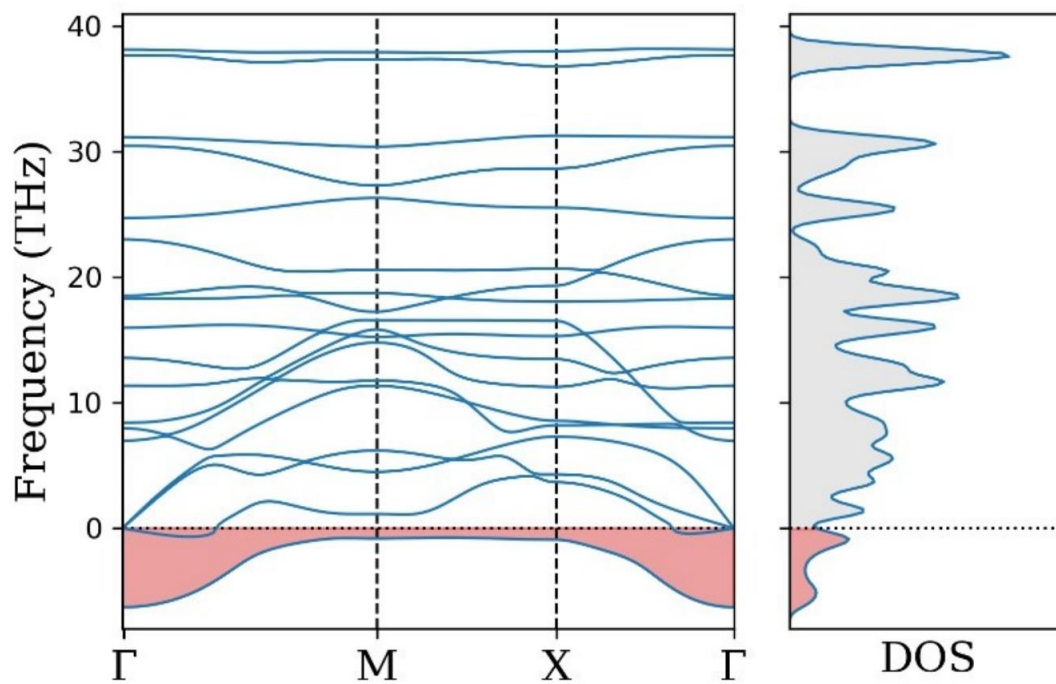


Figure 7-5. Calculated phonon dispersion curves along the Γ -M-X- Γ path and phonon density of states for the nonmagnetic 2D-B₆ material.

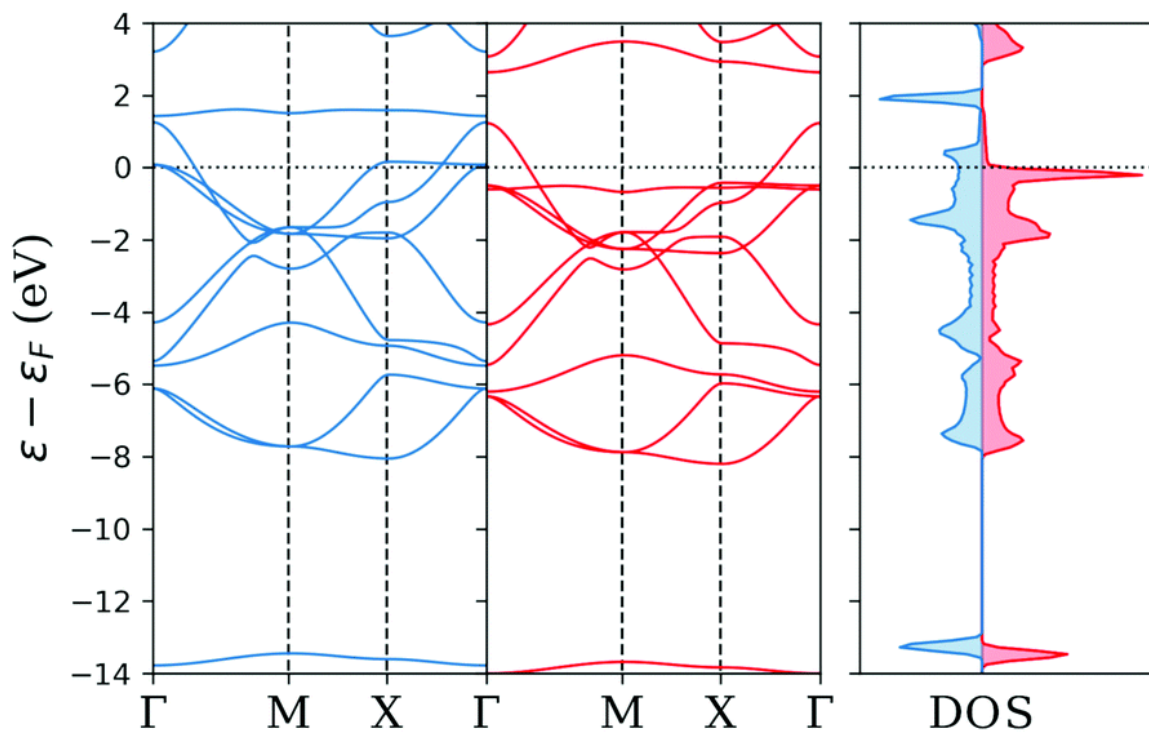


Figure 7-6. Calculated electronic band structure along the Γ -M-X- Γ path and density of states for ferromagnetic 2D-B₆. The red curves correspond to the spin up electrons, while the spin down electrons are illustrated with blue curves. The Fermi level is shown as a horizontal dotted black line.

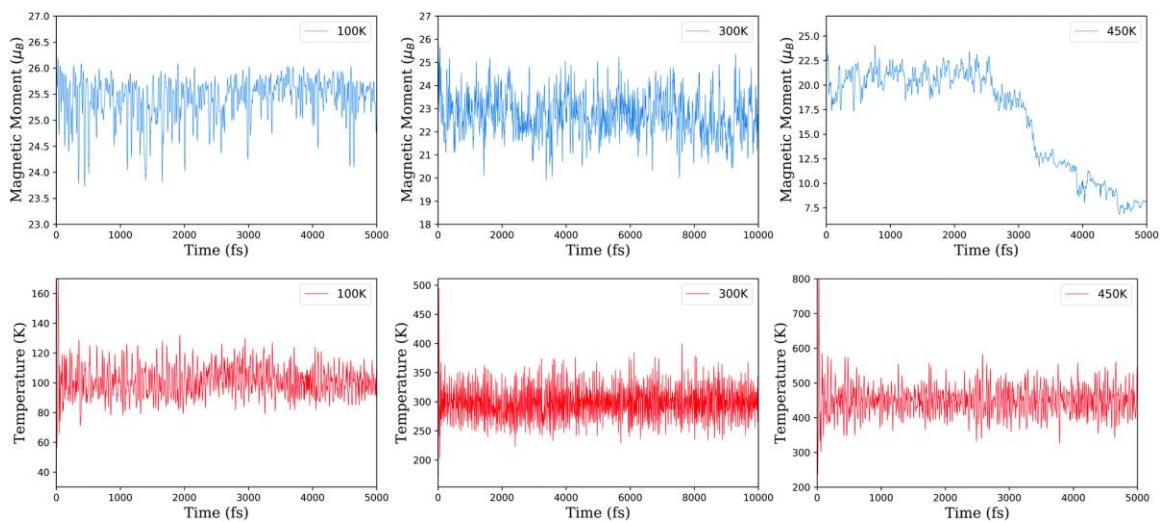


Figure 7-7. Calculated fluctuations of the total magnetic moment and temperature vs. simulation time step at 100 K (left column), 300 K (center column) and 450 K (right column).

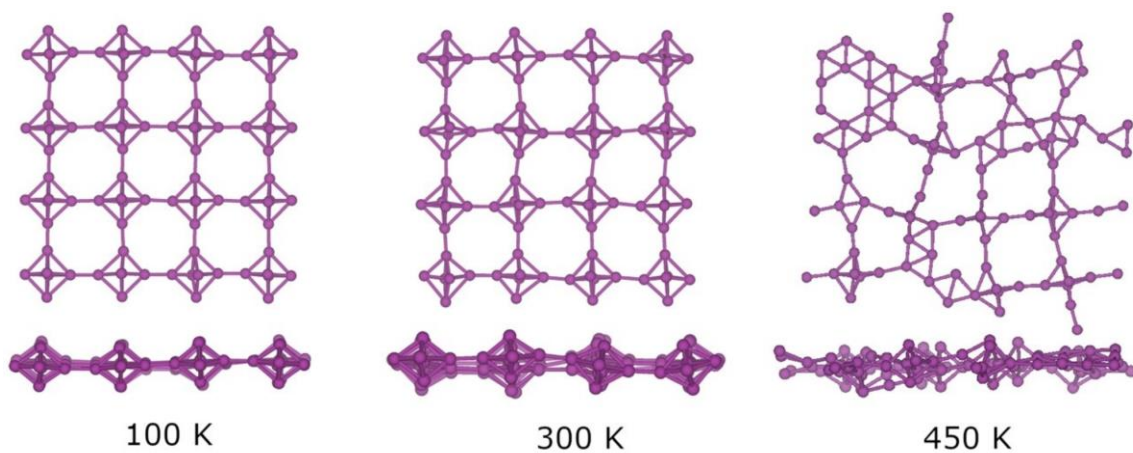


Figure 7-8. Top and side views of final frames of each MD simulation test at different temperatures.

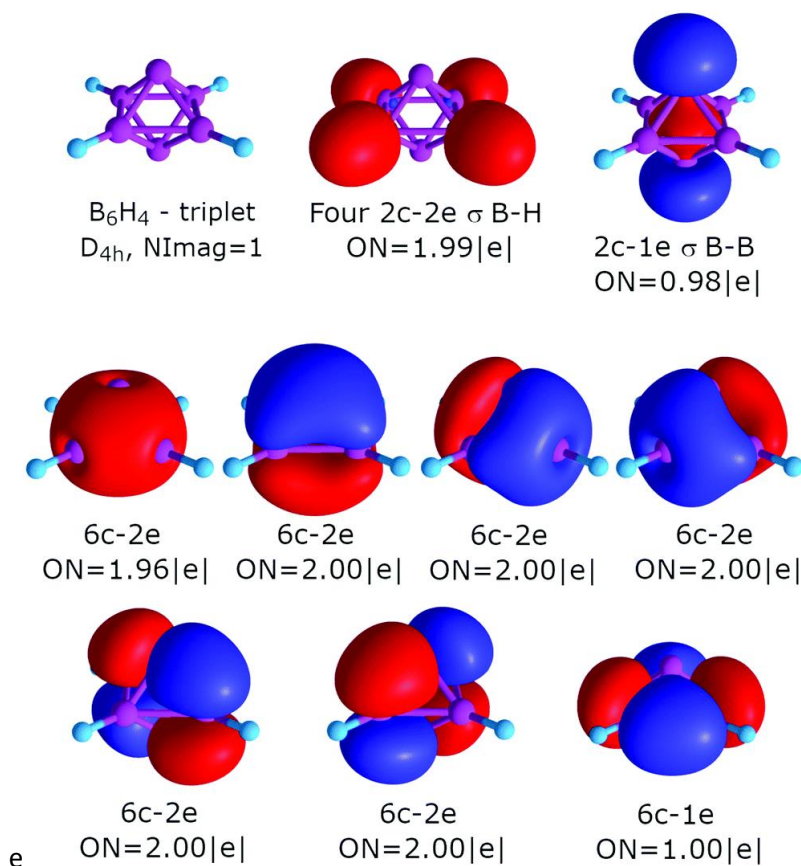


Figure 7-9. Overall chemical bonding picture obtained for the B_6H_4 cluster in the triplet state. The abbreviation ON denotes the occupation number of a certain bond.

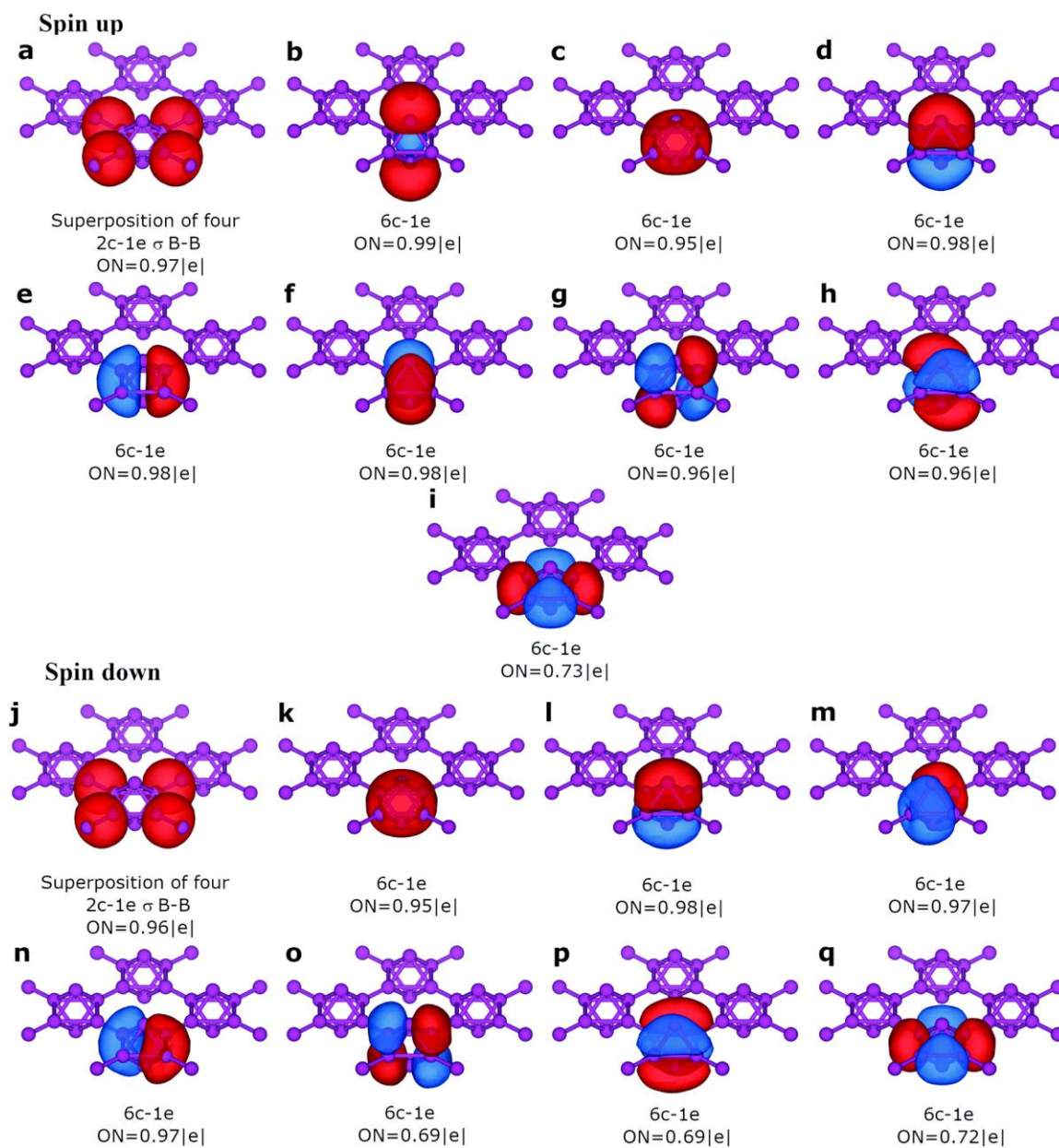


Figure 7-10. Overall chemical bonding picture obtained for the 2D-B₆ sheet. The results for the spin up and spin down electrons are presented separately.

CHAPTER 8

SUMMARY

With the development of computational resources and methods of quantum chemistry, calculations of molecular systems have become an everyday tool in the hands of chemists. Current algorithms have shown their computational affordability and, at the same time, accuracy in predicting chemical and physical properties of molecules. In turn, the language of chemical bonds remains a universal approach understood by all chemists. This fact creates a demand for interpretation of the results obtained from quantum chemical calculations in terms of intuitive chemical bonding description.

This dissertation reports recent advances in the application of the concept of multicenter bonds in chemistry and materials science. The main advancement of this dissertation is the development of a general chemical bonding description of 3D Zintl clusters and cluster-based solids. In the first chapter, the new AdNDP 2.0 program was introduced. This program served as the main tool used in the course of this Ph.D. work. The new version of the program expanded the capabilities of the original method and added new features to the algorithm, such as distance restriction, symmetric direct search, analysis of unrestricted open-shell cases, and analysis of the chemical bond of molecules in excited electronic states. All the features listed above have expanded the possible areas of application of this algorithm. It has also been shown that analysis of the chemical bonding of excited states can predict the subsequent structural deformation that a molecule will undergo. This finding may be useful for photochemistry, photoelectron spectroscopy, electron spectroscopy, and other methods involving electronic excited states.

Using the methods of quantum chemistry and in particular the ADNDP algorithm, in the fourth chapter I deciphered the chemical bonding patterns of nonagermanide clusters - species whose structural motifs are found in a huge number of synthesized complexes and materials. Using structural experimental data, I analyzed several model nonagermanide clusters (C_{4v}/D_{3h} -[Ge₉]⁴⁻, [Ge₉{P(NH₂)₂]₃⁻, Cu[Ge₉{P(NH₂)₂]₃, Cu(NHC)[Ge₉{P(NH₂)₂]₃). As a result of this work, a simple and chemically intuitive picture of the chemical bond was found, which explains the diversity of chemically active sites in nonagermanides and the coexistence of two forms of the Ge₉ cluster (C_{4v} and D_{3h} symmetric).

In the next three chapters, we have tried to extend the application of the chemical bonding models proposed in Chapter 3. In this part of my dissertation, our scientific group worked in close collaboration with experimentalists, in particular with a wonderful and talented synthetic chemist, Professor Zhong-Ming Sun (Nankai University, China). As a logical continuation of the work on nonagermanide clusters, we, as theorists, wanted to find an example of a cluster where two competitive structural motifs (D_{3h} and C_{4v} Ge₉) coexist. Finding such a cluster would further confirm the correctness of our conclusions drawn in Chapter 3. Luckily, Professor Sun's group succeeded in synthesizing a [Ge₂₄]⁴⁻ cluster that contained these two structural motifs. After analyzing the chemical bond of this cluster, we showed the presence of similar bonding patterns that were predicted in our previous work. Moreover, this germanium cluster, at the time of publication, was the largest continuous germanium cluster synthesized, which also serves as an excellent object of study on how the structural transition from medium-sized clusters to solid-state structure occurs.

In Chapter 5, clusters of isoelectronic to germanium element, tin, was studied. Our collaborators synthesized an inverse sandwich-type cluster ($\{[K_2ZnSn_8(ZnMes)]_2\}^{4-}$), where two square antiprismatic Sn_8 fragments were capped with zinc atoms. As in the case of nonagermanides, we found the presence of local sigma aromaticity in Sn_8 fragments and showed that electron delocalization to zinc atoms plays an important role in the stabilization of the antiprismatic fragment. In a follow-up study described in Chapter 6, we also explored the importance of electron delocalization to transition metal atoms in Zintl clusters. In this study, we analyzed the chemical bonding in newly synthesized supertetrahedral clusters $[Zn_6Ge_{16}]^{4-}$ and $[Cd_6Ge_{16}]^{4-}$ that were directly assembled from $[Ge_4]^{4-}$ units and transition metal cations (Zn^{2+} and Cd^{2+}). Using AdNDP, ELF analyses, and DFT calculations, we have shown that the three-center two-electron bonds in Ge_2Zn and Ge_2Cd triangles play a vital role in stabilizing the entire structure. Thus, the stability of the $[Zn_6Ge_{16}]^{4-}$ and $[Cd_6Ge_{16}]^{4-}$ clusters may not be ascribed to pure ionic interactions of metal cations stabilizing the $[Ge_4]^{4-}$ anionic tetrahedra and the appreciable covalent character could be found due to the delocalization over the metal atoms. The self-assembly process, as well as the peculiar picture of chemical bonding, opens up possibilities for the synthesis of new ligand-free metal-framework-base materials.

In the final study of this dissertation, described in Chapter 7, we predicted a new two-dimensional magnetic boron material composed of 3D octahedral B_6 clusters. The monolayer possesses ferromagnetic properties and could be potentially used in spintronic devices. Moreover, the ferromagnetic 2D- B_6 layer is found to be thermally stable up to 300K, representing the first example of ferromagnetic boron material stable at ambient temperature. The ferromagnetic properties of 2D- B_6 are perfectly predicted and explained

via the chemical bonding patterns of their structures, illustrating that the description of solids in terms of chemical bonding is an effective tool for designing new materials with specific properties.

APPENDICES

Appendix A: Permission Letters for Journal Copyright Release

Chemical bonding analysis of excited states using the adaptive natural density partitioning method

N. V. Tkachenko and A. I. Boldyrev, *Phys. Chem. Chem. Phys.*, 2019, **21**, 9590
DOI: 10.1039/C9CP00379G

To request permission to reproduce material from this article, please go to the [Copyright Clearance Center request page](#).

If you are **an author contributing to an RSC publication, you do not need to request permission** provided correct acknowledgement is given.

If you are **the author of this article, you do not need to request permission to reproduce figures and diagrams** provided correct acknowledgement is given. If you want to reproduce the whole article in a third-party publication (excluding your thesis/dissertation for which permission is not required) please go to the [Copyright Clearance Center request page](#).

Read more about [how to correctly acknowledge RSC content](#).

Superoctahedral two-dimensional metallic boron with peculiar magnetic properties

N. V. Tkachenko, D. Steglenko, N. Fedik, N. M. Boldyreva, R. M. Minyaev, V. I. Minkin and A. I. Boldyrev, *Phys. Chem. Chem. Phys.*, 2019, **21**, 19764 DOI: 10.1039/C9CP03786A

To request permission to reproduce material from this article, please go to the [Copyright Clearance Center request page](#).

If you are **an author contributing to an RSC publication, you do not need to request permission** provided correct acknowledgement is given.

If you are **the author of this article, you do not need to request permission to reproduce figures and diagrams** provided correct acknowledgement is given. If you want to reproduce the whole article in a third-party publication (excluding your thesis/dissertation for which permission is not required) please go to the [Copyright Clearance Center request page](#).

Read more about [how to correctly acknowledge RSC content](#).

Multiple local σ -aromaticity of nonagermanide clusters

N. V. Tkachenko and A. I. Boldyrev, *Chem. Sci.*, 2019, **10**, 5761 DOI: 10.1039/C9SC00929A

This article is licensed under a [Creative Commons Attribution 3.0 Unported Licence](#). **You can use material from this article in other publications without requesting further permissions** from the RSC, provided that the correct acknowledgement is given.

Read more about [how to correctly acknowledge RSC content](#).

Symmetry collapse due to the presence of multiple local aromaticity in Ge₂₄₄-**SPRINGER NATURE****Author:** Hong-Lei Xu et al**Publication:** Nature Communications**Publisher:** Springer Nature**Date:** Apr 20, 2022*Copyright © 2022, The Author(s)***Creative Commons**

This is an open access article distributed under the terms of the [Creative Commons CC BY](#) license, which permits unrestricted use, distribution, and reproduction in any medium, provided the original work is properly cited.

You are not required to obtain permission to reuse this article.

To request permission for a type of use not listed, please contact [Springer Nature](#).

10/26/22, 4:48 PM

RightsLink Printable License

JOHN WILEY AND SONS LICENSE
TERMS AND CONDITIONS

Oct 26, 2022

This Agreement between Nikolay Tkachenko ("You") and John Wiley and Sons ("John Wiley and Sons") consists of your license details and the terms and conditions provided by John Wiley and Sons and Copyright Clearance Center.

License Number 5415600995294

License date Oct 24, 2022

Licensed Content Publisher John Wiley and Sons

Licensed Content Publication Angewandte Chemie International Edition

Licensed Content Title [Sn8]6--Bridged Mixed-Valence ZnI/ZnII in {[K2ZnSn8(ZnMes)]2}4- Inverse Sandwich-Type Cluster Supported by a ZnI-ZnI Bond

Licensed Content Author Hong-Lei Xu, Nikolay V. Tkachenko, Alvaro Muñoz-Castro, et al

Licensed Content Date Mar 23, 2021

Licensed Content Volume 60

Licensed Content Issue 18

Licensed 6

10/26/22, 4:48 PM

RightsLink Printable License

Content Pages

Type of use Dissertation/Thesis

Requestor type Author of this Wiley article

Format Print and electronic

Portion Full article

Will you be
translating? NoTitle THE CONCEPT OF MULTICENTER BONDS IN CHEMISTRY AND
MATERIALS SCIENCE

Institution name Utah State University

Expected
presentation
date Apr 2023Requestor
Location Nikolay Tkachenko
 23 Aggie Village, apt. L
 LOGAN, UT 84341
 United States
 Attn: Nikolay TkachenkoPublisher Tax
ID EU826007151

Total 0.00 USD

Terms and Conditions

TERMS AND CONDITIONS

This copyrighted material is owned by or exclusively licensed to John Wiley & Sons, Inc. or one of its group companies (each a "Wiley Company") or handled on behalf of a society with

which a Wiley Company has exclusive publishing rights in relation to a particular work (collectively "WILEY"). By clicking "accept" in connection with completing this licensing transaction, you agree that the following terms and conditions apply to this transaction (along with the billing and payment terms and conditions established by the Copyright Clearance Center Inc., ("CCC's Billing and Payment terms and conditions"), at the time that you opened your RightsLink account (these are available at any time at <http://myaccount.copyright.com>).

Terms and Conditions

- The materials you have requested permission to reproduce or reuse (the "Wiley Materials") are protected by copyright.
- You are hereby granted a personal, non-exclusive, non-sub licensable (on a stand-alone basis), non-transferable, worldwide, limited license to reproduce the Wiley Materials for the purpose specified in the licensing process. This license, **and any CONTENT (PDF or image file) purchased as part of your order**, is for a one-time use only and limited to any maximum distribution number specified in the license. The first instance of republication or reuse granted by this license must be completed within two years of the date of the grant of this license (although copies prepared before the end date may be distributed thereafter). The Wiley Materials shall not be used in any other manner or for any other purpose, beyond what is granted in the license. Permission is granted subject to an appropriate acknowledgement given to the author, title of the material/book/journal and the publisher. You shall also duplicate the copyright notice that appears in the Wiley publication in your use of the Wiley Material. Permission is also granted on the understanding that nowhere in the text is a previously published source acknowledged for all or part of this Wiley Material. Any third party content is expressly excluded from this permission.
- With respect to the Wiley Materials, all rights are reserved. Except as expressly granted by the terms of the license, no part of the Wiley Materials may be copied, modified, adapted (except for minor reformatting required by the new Publication), translated, reproduced, transferred or distributed, in any form or by any means, and no derivative works may be made based on the Wiley Materials without the prior permission of the respective copyright owner. **For STM Signatory Publishers clearing permission under the terms of the [STM Permissions Guidelines](#) only, the terms of the license are extended to include subsequent editions and for editions in other languages, provided such editions are for the work as a whole in situ and does not involve the separate exploitation of the permitted figures or extracts**, You may not alter, remove or suppress in any manner any copyright, trademark or other notices displayed by the Wiley Materials. You may not license, rent, sell, loan, lease, pledge, offer as security, transfer or assign the Wiley Materials on a stand-alone basis, or any of the rights granted to you hereunder to any other person.
- The Wiley Materials and all of the intellectual property rights therein shall at all times remain the exclusive property of John Wiley & Sons Inc, the Wiley Companies, or their respective licensors, and your interest therein is only that of having possession of and the right to reproduce the Wiley Materials pursuant to Section 2 herein during the continuance of this Agreement. You agree that you own no right, title or interest in or to the Wiley Materials or any of the intellectual property rights therein. You shall have no rights hereunder other than the license as provided for above in Section 2. No right, license or interest to any trademark, trade name, service mark or other branding ("Marks") of WILEY or its licensors is granted hereunder, and you agree that you

shall not assert any such right, license or interest with respect thereto

- NEITHER WILEY NOR ITS LICENSORS MAKES ANY WARRANTY OR REPRESENTATION OF ANY KIND TO YOU OR ANY THIRD PARTY, EXPRESS, IMPLIED OR STATUTORY, WITH RESPECT TO THE MATERIALS OR THE ACCURACY OF ANY INFORMATION CONTAINED IN THE MATERIALS, INCLUDING, WITHOUT LIMITATION, ANY IMPLIED WARRANTY OF MERCHANTABILITY, ACCURACY, SATISFACTORY QUALITY, FITNESS FOR A PARTICULAR PURPOSE, USABILITY, INTEGRATION OR NON-INFRINGEMENT AND ALL SUCH WARRANTIES ARE HEREBY EXCLUDED BY WILEY AND ITS LICENSORS AND WAIVED BY YOU.
- WILEY shall have the right to terminate this Agreement immediately upon breach of this Agreement by you.
- You shall indemnify, defend and hold harmless WILEY, its Licensors and their respective directors, officers, agents and employees, from and against any actual or threatened claims, demands, causes of action or proceedings arising from any breach of this Agreement by you.
- IN NO EVENT SHALL WILEY OR ITS LICENSORS BE LIABLE TO YOU OR ANY OTHER PARTY OR ANY OTHER PERSON OR ENTITY FOR ANY SPECIAL, CONSEQUENTIAL, INCIDENTAL, INDIRECT, EXEMPLARY OR PUNITIVE DAMAGES, HOWEVER CAUSED, ARISING OUT OF OR IN CONNECTION WITH THE DOWNLOADING, PROVISIONING, VIEWING OR USE OF THE MATERIALS REGARDLESS OF THE FORM OF ACTION, WHETHER FOR BREACH OF CONTRACT, BREACH OF WARRANTY, TORT, NEGLIGENCE, INFRINGEMENT OR OTHERWISE (INCLUDING, WITHOUT LIMITATION, DAMAGES BASED ON LOSS OF PROFITS, DATA, FILES, USE, BUSINESS OPPORTUNITY OR CLAIMS OF THIRD PARTIES), AND WHETHER OR NOT THE PARTY HAS BEEN ADVISED OF THE POSSIBILITY OF SUCH DAMAGES. THIS LIMITATION SHALL APPLY NOTWITHSTANDING ANY FAILURE OF ESSENTIAL PURPOSE OF ANY LIMITED REMEDY PROVIDED HEREIN.
- Should any provision of this Agreement be held by a court of competent jurisdiction to be illegal, invalid, or unenforceable, that provision shall be deemed amended to achieve as nearly as possible the same economic effect as the original provision, and the legality, validity and enforceability of the remaining provisions of this Agreement shall not be affected or impaired thereby.
- The failure of either party to enforce any term or condition of this Agreement shall not constitute a waiver of either party's right to enforce each and every term and condition of this Agreement. No breach under this agreement shall be deemed waived or excused by either party unless such waiver or consent is in writing signed by the party granting such waiver or consent. The waiver by or consent of a party to a breach of any provision of this Agreement shall not operate or be construed as a waiver of or consent to any other or subsequent breach by such other party.
- This Agreement may not be assigned (including by operation of law or otherwise) by you without WILEY's prior written consent.

10/26/22, 4:48 PM

RightsLink Printable License

- Any fee required for this permission shall be non-refundable after thirty (30) days from receipt by the CCC.
- These terms and conditions together with CCC's Billing and Payment terms and conditions (which are incorporated herein) form the entire agreement between you and WILEY concerning this licensing transaction and (in the absence of fraud) supersedes all prior agreements and representations of the parties, oral or written. This Agreement may not be amended except in writing signed by both parties. This Agreement shall be binding upon and inure to the benefit of the parties' successors, legal representatives, and authorized assigns.
- In the event of any conflict between your obligations established by these terms and conditions and those established by CCC's Billing and Payment terms and conditions, these terms and conditions shall prevail.
- WILEY expressly reserves all rights not specifically granted in the combination of (i) the license details provided by you and accepted in the course of this licensing transaction, (ii) these terms and conditions and (iii) CCC's Billing and Payment terms and conditions.
- This Agreement will be void if the Type of Use, Format, Circulation, or Requestor Type was misrepresented during the licensing process.
- This Agreement shall be governed by and construed in accordance with the laws of the State of New York, USA, without regards to such state's conflict of law rules. Any legal action, suit or proceeding arising out of or relating to these Terms and Conditions or the breach thereof shall be instituted in a court of competent jurisdiction in New York County in the State of New York in the United States of America and each party hereby consents and submits to the personal jurisdiction of such court, waives any objection to venue in such court and consents to service of process by registered or certified mail, return receipt requested, at the last known address of such party.

WILEY OPEN ACCESS TERMS AND CONDITIONS

Wiley Publishes Open Access Articles in fully Open Access Journals and in Subscription journals offering Online Open. Although most of the fully Open Access journals publish open access articles under the terms of the Creative Commons Attribution (CC BY) License only, the subscription journals and a few of the Open Access Journals offer a choice of Creative Commons Licenses. The license type is clearly identified on the article.

The Creative Commons Attribution License

The [Creative Commons Attribution License \(CC-BY\)](#) allows users to copy, distribute and transmit an article, adapt the article and make commercial use of the article. The CC-BY license permits commercial and non-

Creative Commons Attribution Non-Commercial License

The [Creative Commons Attribution Non-Commercial \(CC-BY-NC\) License](#) permits use, distribution and reproduction in any medium, provided the original work is properly cited and is not used for commercial purposes.(see below)

Creative Commons Attribution-Non-Commercial-NoDerivs License

<https://s100.copyright.com/CustomerAdmin/PLF.jsp?ref=308e1385-0538-4efd-9f65-7e5b94b5194d>

5/6

10/26/22, 4:48 PM

RightsLink Printable License

The [Creative Commons Attribution Non-Commercial-NoDerivs License \(CC-BY-NC-ND\)](#) permits use, distribution and reproduction in any medium, provided the original work is properly cited, is not used for commercial purposes and no modifications or adaptations are made. (see below)

Use by commercial "for-profit" organizations

Use of Wiley Open Access articles for commercial, promotional, or marketing purposes requires further explicit permission from Wiley and will be subject to a fee.

Further details can be found on Wiley Online Library
<http://olabout.wiley.com/WileyCDA/Section/id-410895.html>

Other Terms and Conditions:

v1.10 Last updated September 2015

Questions? customercare@copyright.com or +1-855-239-3415 (toll free in the US) or +1-978-646-2777.

10/26/22, 4:49 PM

RightsLink Printable License

JOHN WILEY AND SONS LICENSE
TERMS AND CONDITIONS

Oct 26, 2022

This Agreement between Nikolay Tkachenko ("You") and John Wiley and Sons ("John Wiley and Sons") consists of your license details and the terms and conditions provided by John Wiley and Sons and Copyright Clearance Center.

License Number 5415600930716

License date Oct 24, 2022

Licensed Content
Publisher John Wiley and SonsLicensed Content
Publication Angewandte Chemie International EditionLicensed Content
Title σ -Aromaticity-Induced Stabilization of Heterometallic Supertetrahedral Clusters [Zn₆Ge₁₆]⁴⁻ and [Cd₆Ge₁₆]⁴⁻Licensed Content
Author Zhong-Ming Sun, Alexander I. Boldyrev, Alvaro Muñoz-Castro, et alLicensed Content
Date Aug 13, 2020Licensed Content
Volume 59Licensed Content
Issue 39Licensed Content
Pages 5

10/26/22, 4:49 PM

RightsLink Printable License

Type of use	Dissertation/Thesis
Requestor type	Author of this Wiley article
Format	Print and electronic
Portion	Full article
Will you be translating?	No
Title	THE CONCEPT OF MULTICENTER BONDS IN CHEMISTRY AND MATERIALS SCIENCE
Institution name	Utah State University
Expected presentation date	Apr 2023
Requestor Location	Nikolay Tkachenko 23 Aggie Village, apt. L LOGAN, UT 84341 United States Attn: Nikolay Tkachenko
Publisher Tax ID	EU826007151
Total	0.00 USD
Terms and Conditions	

TERMS AND CONDITIONS

This copyrighted material is owned by or exclusively licensed to John Wiley & Sons, Inc. or one of its group companies (each a "Wiley Company") or handled on behalf of a society with which a Wiley Company has exclusive publishing rights in relation to a particular work (collectively "WILEY"). By clicking "accept" in connection with completing this licensing transaction, you agree that the following terms and conditions apply to this transaction (along with the billing and payment terms and conditions established by the Copyright Clearance Center Inc., ("CCC's Billing and Payment terms and conditions"), at the time that

10/26/22, 4:49 PM

RightsLink Printable License

you opened your RightsLink account (these are available at any time at <http://myaccount.copyright.com>).

Terms and Conditions

- The materials you have requested permission to reproduce or reuse (the "Wiley Materials") are protected by copyright.
- You are hereby granted a personal, non-exclusive, non-sub licensable (on a stand-alone basis), non-transferable, worldwide, limited license to reproduce the Wiley Materials for the purpose specified in the licensing process. This license, **and any CONTENT (PDF or image file) purchased as part of your order**, is for a one-time use only and limited to any maximum distribution number specified in the license. The first instance of republication or reuse granted by this license must be completed within two years of the date of the grant of this license (although copies prepared before the end date may be distributed thereafter). The Wiley Materials shall not be used in any other manner or for any other purpose, beyond what is granted in the license. Permission is granted subject to an appropriate acknowledgement given to the author, title of the material/book/journal and the publisher. You shall also duplicate the copyright notice that appears in the Wiley publication in your use of the Wiley Material. Permission is also granted on the understanding that nowhere in the text is a previously published source acknowledged for all or part of this Wiley Material. Any third party content is expressly excluded from this permission.
- With respect to the Wiley Materials, all rights are reserved. Except as expressly granted by the terms of the license, no part of the Wiley Materials may be copied, modified, adapted (except for minor reformatting required by the new Publication), translated, reproduced, transferred or distributed, in any form or by any means, and no derivative works may be made based on the Wiley Materials without the prior permission of the respective copyright owner. **For STM Signatory Publishers clearing permission under the terms of the [STM Permissions Guidelines](#) only, the terms of the license are extended to include subsequent editions and for editions in other languages, provided such editions are for the work as a whole in situ and does not involve the separate exploitation of the permitted figures or extracts**. You may not alter, remove or suppress in any manner any copyright, trademark or other notices displayed by the Wiley Materials. You may not license, rent, sell, loan, lease, pledge, offer as security, transfer or assign the Wiley Materials on a stand-alone basis, or any of the rights granted to you hereunder to any other person.
- The Wiley Materials and all of the intellectual property rights therein shall at all times remain the exclusive property of John Wiley & Sons Inc, the Wiley Companies, or their respective licensors, and your interest therein is only that of having possession of and the right to reproduce the Wiley Materials pursuant to Section 2 herein during the continuance of this Agreement. You agree that you own no right, title or interest in or to the Wiley Materials or any of the intellectual property rights therein. You shall have no rights hereunder other than the license as provided for above in Section 2. No right, license or interest to any trademark, trade name, service mark or other branding ("Marks") of WILEY or its licensors is granted hereunder, and you agree that you shall not assert any such right, license or interest with respect thereto
- NEITHER WILEY NOR ITS LICENSORS MAKES ANY WARRANTY OR REPRESENTATION OF ANY KIND TO YOU OR ANY THIRD PARTY, EXPRESS, IMPLIED OR STATUTORY, WITH RESPECT TO THE MATERIALS

<https://s100.copyright.com/CustomerAdmin/PLF.jsp?ref=a95539fa-8f3d-426a-b451-3ac6f417451e>

3/6

10/26/22, 4:49 PM

RightsLink Printable License

OR THE ACCURACY OF ANY INFORMATION CONTAINED IN THE MATERIALS, INCLUDING, WITHOUT LIMITATION, ANY IMPLIED WARRANTY OF MERCHANTABILITY, ACCURACY, SATISFACTORY QUALITY, FITNESS FOR A PARTICULAR PURPOSE, USABILITY, INTEGRATION OR NON-INFRINGEMENT AND ALL SUCH WARRANTIES ARE HEREBY EXCLUDED BY WILEY AND ITS LICENSORS AND WAIVED BY YOU.

- WILEY shall have the right to terminate this Agreement immediately upon breach of this Agreement by you.
- You shall indemnify, defend and hold harmless WILEY, its Licensors and their respective directors, officers, agents and employees, from and against any actual or threatened claims, demands, causes of action or proceedings arising from any breach of this Agreement by you.
- IN NO EVENT SHALL WILEY OR ITS LICENSORS BE LIABLE TO YOU OR ANY OTHER PARTY OR ANY OTHER PERSON OR ENTITY FOR ANY SPECIAL, CONSEQUENTIAL, INCIDENTAL, INDIRECT, EXEMPLARY OR PUNITIVE DAMAGES, HOWEVER CAUSED, ARISING OUT OF OR IN CONNECTION WITH THE DOWNLOADING, PROVISIONING, VIEWING OR USE OF THE MATERIALS REGARDLESS OF THE FORM OF ACTION, WHETHER FOR BREACH OF CONTRACT, BREACH OF WARRANTY, TORT, NEGLIGENCE, INFRINGEMENT OR OTHERWISE (INCLUDING, WITHOUT LIMITATION, DAMAGES BASED ON LOSS OF PROFITS, DATA, FILES, USE, BUSINESS OPPORTUNITY OR CLAIMS OF THIRD PARTIES), AND WHETHER OR NOT THE PARTY HAS BEEN ADVISED OF THE POSSIBILITY OF SUCH DAMAGES. THIS LIMITATION SHALL APPLY NOTWITHSTANDING ANY FAILURE OF ESSENTIAL PURPOSE OF ANY LIMITED REMEDY PROVIDED HEREIN.
- Should any provision of this Agreement be held by a court of competent jurisdiction to be illegal, invalid, or unenforceable, that provision shall be deemed amended to achieve as nearly as possible the same economic effect as the original provision, and the legality, validity and enforceability of the remaining provisions of this Agreement shall not be affected or impaired thereby.
- The failure of either party to enforce any term or condition of this Agreement shall not constitute a waiver of either party's right to enforce each and every term and condition of this Agreement. No breach under this agreement shall be deemed waived or excused by either party unless such waiver or consent is in writing signed by the party granting such waiver or consent. The waiver by or consent of a party to a breach of any provision of this Agreement shall not operate or be construed as a waiver of or consent to any other or subsequent breach by such other party.
- This Agreement may not be assigned (including by operation of law or otherwise) by you without WILEY's prior written consent.
- Any fee required for this permission shall be non-refundable after thirty (30) days from receipt by the CCC.
- These terms and conditions together with CCC's Billing and Payment terms and conditions (which are incorporated herein) form the entire agreement between you and WILEY concerning this licensing transaction and (in the absence of fraud) supersedes

all prior agreements and representations of the parties, oral or written. This Agreement may not be amended except in writing signed by both parties. This Agreement shall be binding upon and inure to the benefit of the parties' successors, legal representatives, and authorized assigns.

- In the event of any conflict between your obligations established by these terms and conditions and those established by CCC's Billing and Payment terms and conditions, these terms and conditions shall prevail.
- WILEY expressly reserves all rights not specifically granted in the combination of (i) the license details provided by you and accepted in the course of this licensing transaction, (ii) these terms and conditions and (iii) CCC's Billing and Payment terms and conditions.
- This Agreement will be void if the Type of Use, Format, Circulation, or Requestor Type was misrepresented during the licensing process.
- This Agreement shall be governed by and construed in accordance with the laws of the State of New York, USA, without regards to such state's conflict of law rules. Any legal action, suit or proceeding arising out of or relating to these Terms and Conditions or the breach thereof shall be instituted in a court of competent jurisdiction in New York County in the State of New York in the United States of America and each party hereby consents and submits to the personal jurisdiction of such court, waives any objection to venue in such court and consents to service of process by registered or certified mail, return receipt requested, at the last known address of such party.

WILEY OPEN ACCESS TERMS AND CONDITIONS

Wiley Publishes Open Access Articles in fully Open Access Journals and in Subscription journals offering Online Open. Although most of the fully Open Access journals publish open access articles under the terms of the Creative Commons Attribution (CC BY) License only, the subscription journals and a few of the Open Access Journals offer a choice of Creative Commons Licenses. The license type is clearly identified on the article.

The Creative Commons Attribution License

The [Creative Commons Attribution License \(CC-BY\)](#) allows users to copy, distribute and transmit an article, adapt the article and make commercial use of the article. The CC-BY license permits commercial and non-

Creative Commons Attribution Non-Commercial License

The [Creative Commons Attribution Non-Commercial \(CC-BY-NC\) License](#) permits use, distribution and reproduction in any medium, provided the original work is properly cited and is not used for commercial purposes.(see below)

Creative Commons Attribution-Non-Commercial-NoDerivs License

The [Creative Commons Attribution Non-Commercial-NoDerivs License \(CC-BY-NC-ND\)](#) permits use, distribution and reproduction in any medium, provided the original work is properly cited, is not used for commercial purposes and no modifications or adaptations are made. (see below)

10/26/22, 4:49 PM

RightsLink Printable License

Use by commercial "for-profit" organizations

Use of Wiley Open Access articles for commercial, promotional, or marketing purposes requires further explicit permission from Wiley and will be subject to a fee.

Further details can be found on Wiley Online Library
<http://olabout.wiley.com/WileyCDA/Section/id-410895.html>

Other Terms and Conditions:**v1.10 Last updated September 2015**

Questions? customercare@copyright.com or +1-855-239-3415 (toll free in the US) or +1-978-646-2777.

Appendix B: Permission Letters from Coauthors

Nikolay Tkachenko
Department of Chemistry and Biochemistry
Utah State University
0300 Old Main Hill
Logan, UT 84322-0300

Prof. Dr. Sci. Alexander Boldyrev
Utah State University
Department of Chemistry and Biochemistry
0300 Old Main Hill
Logan, UT 84322-0300
e-mail: a.i.boldyrev@usu.edu

Dear Nikolay Tkachenko,

This letter is to confirm that you have my permission to use the following papers in part or in full for preparation or presentation of your dissertation:

- 1) Tkachenko N.V. and Boldyrev A.I. "Chemical bonding analysis of excited states using the adaptive natural density partitioning method", *Phys. Chem. Chem. Phys.* **2019**, *21*, 9590-9596.
- 2) Tkachenko N.V. and Boldyrev A.I. "Multiple Local σ -Aromaticity of the Nonagermanide Clusters", *Chem. Sci.*, **2019**, *10*, 5761-5765.
- 3) Tkachenko N.V., Steglenko D., Fedik N., Boldyreva N.M., Minyaev R.M., Minkin V. I. and Boldyrev A.I. "Superoctahedral Two-Dimensional Metallic Boron with Peculiar Magnetic Properties", *Phys. Chem. Chem. Phys.*, **2019**, *21*, 19764-19771.
- 4) Xu H.L., Popov I.A., Tkachenko N.V., Wang Z.C., Munoz-Castro A., Boldyrev A.I., and Sun Z.M. " σ -Aromaticity-Induced Stabilization of Heterometallic Supertetrahedral Clusters $[Zn_6Ge_{16}]^{4+}$ and $[Cd_6Ge_{16}]^{4+}$ ", *Angew. Chem. Int. Ed.*, **2020**, *59*, 17286-17290.
- 5) Xu H.L., Tkachenko N.V., Munoz-Castro A., Boldyrev A.I., and Sun Z.M. " $[Sn_8]^{6-}$ -bridged mixed-valence Zn(I)/Zn(II) in $\{[K_2ZnSn_8(ZnMes)]_2\}^{4+}$ Inverse Sandwich-Type Cluster Supported by Zn^I-Zn^I Bond", *Angew. Chem. Int. Ed.*, **2021**, *60*, 9990-9995.
- 6) Xu H.L., Tkachenko N.V., Szczepanik D., Popov I.A., Muñoz-Castro A., Boldyrev A.I., Sun Z.M. "Symmetry Collapse due to the Presence of Multiple Local Aromaticity in Ge_{24}^{4-} ", *Nat. Commun.*, **2022**, *13*, 2149.

Sincerely,

Alexander Boldyrev



10/24/2022

Nikolay Tkachenko
Department of Chemistry and Biochemistry
Utah State University
0300 Old Main Hill
Logan, UT 84322-0300

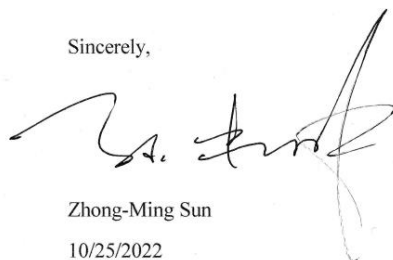
Prof. Dr. Zhong-Ming Sun
School of Materials Science and Engineering
Nankai University
Tianjin 300350, China

Dear Nikolay Tkachenko,

This letter is to confirm that you have my permission to use the following papers in part or in full for preparation or presentation of your dissertation:

- 1) Xu H.L., Popov I.A., Tkachenko N.V., Wang Z.C., Munoz-Castro A., Boldyrev A.I., and Sun Z.M. "σ-Aromaticity-Induced Stabilization of Heterometallic Supertetrahedral Clusters $[Zn_6Ge_{16}]^{4+}$ and $[Cd_6Ge_{16}]^{4+}$ ", *Angew. Chem. Int. Ed.*, **2020**, *59*, 17286-17290.
- 2) Xu H.L., Tkachenko N.V., Munoz-Castro A., Boldyrev A.I., and Sun Z.M. " $[Sn_8]^{6-}$ -bridged mixed-valence Zn(I)/Zn(II) in $\{[K_2ZnSn_8(ZnMes)_2]_2\}^{4+}$ Inverse Sandwich-Type Cluster Supported by Zn^I-Zn^I Bond", *Angew. Chem. Int. Ed.*, **2021**, *60*, 9990-9995.
- 3) Xu H.L., Tkachenko N.V., Szczepanik D., Popov I.A., Muñoz-Castro A., Boldyrev A.I., Sun Z.M. "Symmetry Collapse due to the Presence of Multiple Local Aromaticity in Ge_4^{4+} ", *Nat. Commun.*, **2022**, *13*, 2149.

Sincerely,



Zhong-Ming Sun

10/25/2022

Nikolay Tkachenko
Department of Chemistry and Biochemistry
Utah State University
0300 Old Main Hill
Logan, UT 84322-0300

Dr. Dmitriy Steglenko
Institute of Physical and Organic Chemistry
Southern Federal University
Stachka Avenue 194/2
Rostov-on-Don, Russian Federation, 344090

Dear Nikolay Tkachenko,

This letter is to confirm that you have my permission to use the following paper in part or in full for preparation or presentation of your dissertation:

1) Tkachenko N.V., Steglenko D., Fedik N., Boldyreva N.M., Minyaev R.M., Minkin V. I. and Boldyrev A.I. "Superoctahedral Two-Dimensional Metallic Boron with Peculiar Magnetic Properties", *Phys. Chem. Chem. Phys.*, **2019**, *21*, 19764-19771.

Sincerely,

Dmitriy Steglenko



10/24/2022

Nikolay Tkachenko
Department of Chemistry and Biochemistry
Utah State University
0300 Old Main Hill
Logan, UT 84322-0300

Prof. Dr. Sci. Ruslan Minyaev
Institute of Physical and Organic Chemistry
Southern Federal University
Stachka Avenue 194/2
Rostov-on-Don, Russian Federation, 344090

Dear Nikolay Tkachenko,

This letter is to confirm that you have my permission to use the following paper in part or in full for preparation or presentation of your dissertation:

1) Tkachenko N.V., Steglenko D., Fedik N., Boldyreva N.M., Minyaev R.M., Minkin V. I. and Boldyrev A.I. "Superoctahedral Two-Dimensional Metallic Boron with Peculiar Magnetic Properties", *Phys. Chem. Chem. Phys.*, **2019**, *21*, 19764-19771.

Sincerely,



Ruslan Minyaev

10/25/2022

Nikolay Tkachenko
Department of Chemistry and Biochemistry
Utah State University
0300 Old Main Hill
Logan, UT 84322-0300

Dr. Natalia Boldyreva
Institute of Physical and Organic Chemistry
Southern Federal University
Stachka Avenue 194/2
Rostov-on-Don, Russian Federation, 344090

Dear Nikolay Tkachenko,

This letter is to confirm that you have my permission to use the following paper in part or in full for preparation or presentation of your dissertation:

1) Tkachenko N.V., Steglenko D., Fedik N., Boldyreva N.M., Minyaev R.M., Minkin V. I. and Boldyrev A.I. "Superoctahedral Two-Dimensional Metallic Boron with Peculiar Magnetic Properties", *Phys. Chem. Chem. Phys.*, **2019**, *21*, 19764-19771.

Sincerely,

Natalia Boldyreva



10/24/2022

Nikolay Tkachenko
Department of Chemistry and Biochemistry
Utah State University
0300 Old Main Hill
Logan, UT 84322-0300

Dr. Nikita Fedik
Center for Non-Linear Studies (CNLS)/T-1 division
Los Alamos National Laboratory
Los Alamos, NM 87545

Dear Nikolay Tkachenko,

This letter is to confirm that you have my permission to use the following paper in part or in full for preparation or presentation of your dissertation:

1) Tkachenko N.V., Steglenko D., Fedik N., Boldyreva N.M., Minyaev R.M., Minkin V. I. and Boldyrev A.I. "Superoctahedral Two-Dimensional Metallic Boron with Peculiar Magnetic Properties", *Phys. Chem. Chem. Phys.*, **2019**, *21*, 19764-19771.

Sincerely,
Nikita Fedik



10/24/2022

Nikolay Tkachenko
Department of Chemistry and Biochemistry
Utah State University
0300 Old Main Hill
Logan, UT 84322-0300

Prof. Dr. Ivan Popov
Department of Chemistry
The University of Akron
Akron, OH 44325-3601

Dear Nikolay Tkachenko,

This letter is to confirm that you have my permission to use the following papers in part or in full for preparation or presentation of your dissertation:

- 1) Xu H.L., Popov I.A., Tkachenko N.V., Wang Z.C., Munoz-Castro A., Boldyrev A.I., and Sun Z.M. " σ -Aromaticity-Induced Stabilization of Heterometallic Supertetrahedral Clusters $[\text{Zn}_6\text{Ge}_{16}]^{4+}$ and $[\text{Cd}_6\text{Ge}_{16}]^{4+}$ ", *Angew. Chem. Int. Ed.*, **2020**, *59*, 17286-17290.
- 2) Xu H.L., Tkachenko N.V., Szczepanik D., Popov I.A., Muñoz-Castro A., Boldyrev A.I., Sun Z.M. "Symmetry Collapse due to the Presence of Multiple Local Aromaticity in Ge_{24}^{4+} ", *Nat. Commun.*, **2022**, *13*, 2149.

Sincerely,
Ivan Popov



10/24/2022

Nikolay Tkachenko
Department of Chemistry and Biochemistry
Utah State University
0300 Old Main Hill
Logan, UT 84322-0300

Dr hab. Dariusz W. Szczepanik
Department of Theoretical Chemistry
Faculty of Chemistry, Jagiellonian University
Gronostajowa 2, 30-387 Kraków, Poland

Dear Nikolay Tkachenko,

This letter is to confirm that you have my permission to use the following paper in part or in full for preparation or presentation of your dissertation:

1) Xu H.L., Tkachenko N.V., Szczepanik D., Popov I.A., Muñoz-Castro A., Boldyrev A.I., Sun Z.M. "Symmetry Collapse due to the Presence of Multiple Local Aromaticity in Ge_2^{4+} ", *Nat. Commun.*, **2022**, *13*, 2149.

Sincerely,

Dariusz Szczepanik

10/24/2022



Nikolay Tkachenko
Department of Chemistry and Biochemistry
Utah State University
0300 Old Main Hill
Logan, UT 84322-0300

Dr. Zi-Chuan Wang
School of Materials Science and Engineering
Nankai University
Tianjin 300350, China

Dear Nikolay Tkachenko,

This letter is to confirm that you have my permission to use the following paper in part or in full for preparation or presentation of your dissertation:

1) Xu H.L., Popov I.A., Tkachenko N.V., Wang Z.C., Munoz-Castro A., Boldyrev A.I., and Sun Z.M. "σ-Aromaticity-Induced Stabilization of Heterometallic Supertetrahedral Clusters $[Zn_6Ge_{16}]^{4-}$ and $[Cd_6Ge_{16}]^{4-}$ ", *Angew. Chem. Int. Ed.*, **2020**, 59, 17286-17290.

Sincerely,

Zi-Chuan Wang

10/24/2022

Zi-Chuan Wang
ZC

Nikolay Tkachenko
Department of Chemistry and Biochemistry
Utah State University
0300 Old Main Hill
Logan, UT 84322-0300

Prof. Dr. Alvaro Muñoz-Castro
Universidad San Sebastián
Santiago, Chile

Dear Nikolay Tkachenko,

This letter is to confirm that you have my permission to use the following papers in part or in full for preparation or presentation of your dissertation:

- 1) Xu H.L., Popov I.A., Tkachenko N.V., Wang Z.C., Muñoz-Castro A., Boldyrev A.I., and Sun Z.M. “ σ -Aromaticity-Induced Stabilization of Heterometallic Supertetrahedral Clusters $[\text{Zn}_6\text{Ge}_{16}]^{4+}$ and $[\text{Cd}_6\text{Ge}_{16}]^{4+}$ ”, *Angew. Chem. Int. Ed.*, **2020**, *59*, 17286-17290.
- 2) Xu H.L., Tkachenko N.V., Muñoz-Castro A., Boldyrev A.I., and Sun Z.M. “[Sn_8]⁶⁻-bridged mixed-valence Zn(I)/Zn(II) in $\{[\text{K}_2\text{ZnSn}_8(\text{ZnMes})_2]_2\}^{4+}$ Inverse Sandwich-Type Cluster Supported by $\text{Zn}^{\text{I}}\text{-Zn}^{\text{I}}$ Bond”, *Angew. Chem. Int. Ed.*, **2021**, *60*, 9990-9995.
- 3) Xu H.L., Tkachenko N.V., Szczepanik D., Popov I.A., Muñoz-Castro A., Boldyrev A.I., Sun Z.M. “Symmetry Collapse due to the Presence of Multiple Local Aromaticity in Ge_{24}^{4+} ”, *Nat. Commun.*, **2022**, *13*, 2149.

Sincerely,

Alvaro Muñoz-Castro



10/24/2022

Nikolay Tkachenko
Department of Chemistry and Biochemistry
Utah State University
0300 Old Main Hill
Logan, UT 84322-0300

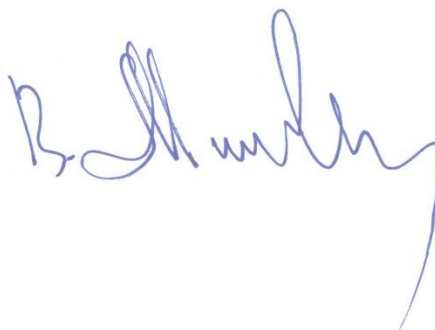
Prof. Dr. Sci. Vladimir Minkin
Institute of Physical and Organic Chemistry
Southern Federal University
Stachka Avenue 194/2
Rostov-on-Don, Russian Federation, 344090

Dear Nikolay Tkachenko,

This letter is to confirm that you have my permission to use the following paper in part or in full for preparation or presentation of your dissertation:

1) Tkachenko N.V., Steglenko D., Fedik N., Boldyreva N.M., Minyaev R.M., Minkin V. I. and Boldyrev A.I. "Superoctahedral Two-Dimensional Metallic Boron with Peculiar Magnetic Properties", *Phys. Chem. Chem. Phys.*, **2019**, *21*, 19764-19771.

Sincerely,
Vladimir Minkin



10/24/2022

Nikolay Tkachenko
Department of Chemistry and Biochemistry
Utah State University
0300 Old Main Hill
Logan, UT 84322-0300

Hong-Lei Xu
School of Materials Science and Engineering
Nankai University
Tianjin 300350, China

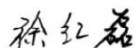
Dear Nikolay Tkachenko,

This letter is to confirm that you have my permission to use the following papers in part or in full for preparation or presentation of your dissertation:

- 1) Xu H.L., Popov I.A., Tkachenko N.V., Wang Z.C., Munoz-Castro A., Boldyrev A.I., and Sun Z.M. “ σ -Aromaticity-Induced Stabilization of Heterometallic Supertetrahedral Clusters $[\text{Zn}_6\text{Ge}_{16}]^+$ and $[\text{Cd}_6\text{Ge}_{16}]^{4+}$ ”, *Angew. Chem. Int. Ed.*, **2020**, *59*, 17286-17290.
- 2) Xu H.L., Tkachenko N.V., Munoz-Castro A., Boldyrev A.I., and Sun Z.M. “[Sn_8]⁶⁻-bridged mixed-valence Zn(I)/Zn(II) in $\{[\text{K}_2\text{ZnSn}_3(\text{ZnMes})]_2\}^+$ Inverse Sandwich-Type Cluster Supported by $\text{Zn}^{\text{I}}\text{-Zn}^{\text{I}}$ Bond”, *Angew. Chem. Int. Ed.*, **2021**, *60*, 9990-9995.
- 3) Xu H.L., Tkachenko N.V., Szczepanik D., Popov I.A., Muñoz-Castro A., Boldyrev A.I., Sun Z.M. “Symmetry Collapse due to the Presence of Multiple Local Aromaticity in Ge_{24}^{4+} ”, *Nat. Commun.*, **2022**, *13*, 2149.

Sincerely,

Hong-Lei Xu



10/31/2022

CURRICULUM VITAE (February 2, 2023)
Nikolay Tkachenko

CONTACT INFORMATION

e-mails: nikolay.tkachenko@usu.edu; nikolay.tkachenko95@gmail.com

Web Page: <http://ion.chem.usu.edu/~boldyrev/nikolay.html>

Tel: 435-512-7462

EDUCATION

08/2018-Present: Ph.D. (expected 04/2023), Physical Chemistry, Utah State University, Logan, Utah, USA (GPA = 4.0)

09/2013-07/2018: Specialist degree, Fundamental and Applied Chemistry major, Novosibirsk University, Novosibirsk, Russia (GPA = 4.0 (summa cum laude))

09/2011-05/2013 High school diploma, Educational and Scientific Center of Novosibirsk University, Novosibirsk, Russia

SCIENTIFIC INTERESTS

Quantum Computing; Quantum Chemistry; Computational Materials Design; Computational Catalysis; Chemical Bonding; Adiabatic and Non-Adiabatic Molecular Dynamics Simulations.

AWARDS

College of Science PhD Student Researcher of the Year Award 2023, given to a student, who has demonstrated outstanding research and academic achievements. Utah State University | February 2023 (USU College of Science Competition, success rate: < 1% or 1 Awardee out of ~150 students)

Oppenheimer Distinguished Postdoctoral Fellow appointment at Los Alamos National Laboratory; recognizes outstanding individuals whose research aligns with the Laboratory's mission | December 2022 (International Competition, success rate < 0.25% or 1 Awardee out of ~400 postdocs)

ACS Utah Outstanding Graduate Student Award 2022, recognizes the research, mentorship, leadership, and public outreach of an outstanding chemistry graduate student in Utah | October 2022 (State Competition, success rate < 0.5% or 1 Awardee out of ~250 students)

Claude E. ZoBell Scholarship, a support for the graduate student pursuing degrees in biology, chemistry and biochemistry, geology, or physics. Utah State University | June 2022 (USU College of Science Competition, success rate: < 1% or 1 Awardee out of ~150 students)

Stephen Bialkowski Award in Environmental Chemistry, a support of a specific environmental chemistry research at the Department of Chemistry and Biochemistry, Utah State University | April 2020 (Departmental Competition, success rate: < 3% or 1 Awardee out of ~35 students)

The Early Research Progress in Chemistry Award for outstanding research progress at Utah State University | April 2020 (Departmental Competition, success rate: < 15% or 1 Awardee out of ~7 students)

Marjorie H. Gardner Teaching Award for outstanding work as a teaching assistant at Utah State University | March 2019 (Departmental Competition, success rate: < 10% or 3 Awardees out of ~35 students)

British Petroleum Scholarship Award for High Academic Standing and Outstanding Leadership Qualities || 2017, 2016 (University Competition, success rate: < 5% or 10 Awardees out of ~250 students)

1st Degree Diploma of the “*VII International Natural Sciences Tournament*” – Individual Competition || November 2016 (International Competition, success rate: < 7% or 7 Awardees out of ~100 students)

1st Degree Diploma of the International Forum of Young Scientists “*Science Game*” – Team Competition || May 2016 (National Competition, success rate: < 5% or 1 Team Awardee out of ~20 teams)

CITATION METRICS AND PUBLICATIONS

Total citations: 479

h-index: 14; **i10-index:** 18

42) Rublev P., Tkachenko N.V., Pozdeev A.S., Boldyrev A.I. “Tinning the Carbon: Hydrostannanes Strike Back”, *Dalton Trans.*, **2022**, Accepted DOI: 10.1039/D2DT03545F. (Featured on the Front Cover Page, highlighted as “Dalton Transactions HOT Articles”) (IF = 4.57, citations = 0)

41) Tkachenko N.V., Sun Z.M., Boldyrev A.I., Munoz-Castro A. “Advances in Cluster Bonding: Bridging Superatomic Building Blocks via Intercluster Bonds”, In *Atomic Clusters with Unusual Structure, Bonding and Reactivity*, **2023**, Elsevier, pp. 321-332, DOI: 10.1016/B978-0-12-822943-9.00010-3 (Invited Chapter, citations = 0).

- 40)** Tkachenko N.V., Rublev P., Dub P.A. “The Source of Proton in the Noyori–Ikariya Catalytic Cycle”, *ACS Catal.*, **2022**, Accepted DOI: 10.1021/acscatal.2c03540. (IF = 13.70, citations = 0)
- 39)** Getmanskii I.V., Koval V.V., Tkachenko N.V., Zaitsev S.A., Boldyrev A.I., Minyaev R.M. “Ultralight Supertetrahedral Aluminum: Stability at Various Temperatures”, *MRS Bull.* **2022**, Accepted, DOI 10.1557/s43577-022-00383-6. (IF = 4.88, citations = 0)
- 38)** Tkachenko N.V., Zhang Y., Cincio L., Boldyrev A.I., Tretiak S., Dub P.A. “Quantum Davidson Algorithm for Excited States”, *ArXiv*, **2022**, 2204.10741. Under Review in *PRX Quantum*. (IF = 7.51, citations = 6)
- 37)** Tkachenko N.V., Chen W.X., Morgan H.W.T., Muñoz-Castro A., Boldyrev A.I., Sun Z.M. “Sn₃₆⁸⁻: A 2.7 nm Naked Aromatic Tin Rod”, *Chem. Commun.*, **2022**, 58, 6223-6226. (IF = 6.07, citations = 0)
- 36)** Xu H.L., Tkachenko N.V., Szczepanik D., Popov I.A., Muñoz-Castro A., Boldyrev A.I., Sun Z.M. “Symmetry Collapse due to the Presence of Multiple Local Aromaticity in Ge₂₄⁴⁺”, *Nat. Commun.* **2022**, 13, 2149. (IF = 17.69, citations = 2)
- 35)** Rublev P., Tkachenko N.V., Boldyrev A.I. “Overlapping electron density and the global delocalization of π -aromatic fragments as the reason of conductivity of the biphenylene network”, *J. Comp. Chem.* **2022**, Accepted DOI: 10.1002/jcc.26854. (IF = 3.67, citations = 0)
- 34)** Tkachenko N.V., Rublev P., Boldyrev A.I., Lehn J.M. “Superalkali Coated Rydberg Molecules”, *Front. Chem.* **2022**, 10, 880804. (IF = 5.22, citations = 0)

- 33)** Yokelson D., Tkachenko N.V., Robey R., Li Y.W., Dub P.A. “Performance Analysis of CP2K Code for Ab Initio Molecular Dynamics”, *J. Chem. Inf. Model* **2022**, *62*, 2378-2386. (IF = 6.16, citations= 3)
- 32)** Chen W.X., Tkachenko N.V., Munoz-Castro A., Boldyrev A.I., Sun Z.M. “Ruthenium-mediated assembly and enhanced stability of heterometallic polystannides $[\text{Ru}_2\text{Sn}_{19}]^{4-}$ and $[\text{Ru}_2\text{Sn}_{20}]^{6-}$ ”, *Nano Res.*, **2022**, *15*, 5705–5711. (IF = 9.24, citations = 0)
- 31)** Minkin V.I., Ivakhnenko E.P., Knyazev P.A., Starikov A.G., Demidov O.P., Tkachenko N.V., Boldyrev A.I. “Electronic isomerism (electromerism) of 6,8-di-tert-butyl-3H-phenoxazin-3-one oxime radical”, *Russ. Chem. Bull.*, **2022**, *1*, 30-37. (IF = 1.57, citations = 2)
- 30)** Zhang W.Q., Tkachenko N.V., Qiao L., Boldyrev A.I., Sun Z.M. “Synthesis and structure of binary copper/silver–arsenic clusters derived from Zintl ion As_7^{3-} ”, *Chin. J. Chem.*, **2022**, *40*, 65-70. (IF = 5.56, citations = 4)
- 29)** Tkachenko N.V., Munoz-Castro A., Boldyrev A.I. “Occurrence of Double Bond in π -Aromatic Rings: An Easy Way to Design Doubly Aromatic Carbon-Metal Structures”, *Molecules*, **2021**, *26*, 7232. (IF = 4.93, citations = 4)
- 28)** Tkachenko N.V., Tkachenko A.A., Kulyukin V.A., and Boldyrev A.I. “DFT Study of Microsolvated $[\text{NO}_3 \cdot (\text{H}_2\text{O})_n]^-$ ($n = 1-12$) Clusters and Molecular Dynamics Simulation of Nitrate Solution”, *J. Phys. Chem. A*, **2021**, *40*, 8899–8906. (IF = 2.94, citations = 1)
- 27)** Tkachenko N.V., Popov I.A., Kulichenko M., Fedik N., Sun Z.M., Munoz-Castro A., and Boldyrev A.I., “Bridging Aromatic/Antiaromatic Units. Recent Advances in Aromaticity and Antiaromaticity in Main-group and Transition-metal Clusters From

Bonding and Magnetic Analyses”, *Eur. J. Inorg. Chem.*, **2021**, *41*, 4239-4250. (IF = 2.55, citations = 3)

26) Xu Y.H., Tkachenko N.V., Popov I.A., Qiao L., Munoz-Castro A., Boldyrev A.I., and Sun Z.M. “Ternary aromatic and anti-aromatic clusters derived from the hypophosphite species $[\text{Sn}_2\text{Sb}_5]^{3-}$ ”, *Nat. Commun.*, **2021**, *12*, 4465. (IF = 17.69, citations = 5)

25) Dub P.A., and Tkachenko N.V. “Mechanism of Potassium tert-Butoxide-Catalyzed Ketones Hydrogenation in the Solution Phase”, *J. Phys. Chem. A*, **2021**, *125*, 5726-5737. (IF = 2.94, citations = 8)

24) Tkachenko N. V., Sud J., Zhang Y., Tretiak S., Anisimov P. M., Arrasmith A. T., Coles P. J., Cincio L., and Dub P. A. “Correlation-Informed Permutation of Qubits for Reducing Ansatz Depth in the Variational Quantum Eigensolver” *PRX Quantum*, **2021**, *2*, 020337. (IF = 7.51, citations = 35)

23) Kulichenko M., Fedik N., Tkachenko N. V., Munoz-Castro A., Sun Z.-M., and Boldyrev A. I. “Spherical aromaticity in inorganic chemistry” In *Aromaticity: Modern Computational Methods and Applications*, **2021**, Ed. Israel Fernandez, Elsevier, ISBN: 9780128227237, pp. 447-488. (Invited Chapter, citations = 1)

22) Dub P. A., Tkachenko N. V., Vyas V. K., Wills M., Smith J. S., and Tretiak S., “Enantioselectivity in the Noyori-Ikariya Asymmetric Transfer Hydrogenation of Ketones”, *Organometallics*, **2021**, *40*, 1402-1410. (IF = 3.84, citations = 16)

21) Xu H. L., Tkachenko N. V., Munoz-Castro A., Boldyrev A. I., and Sun Z.-M. “[Sn_8]⁶⁻-bridged mixed-valence Zn(I)/Zn(II) in $\{[\text{K}_2\text{ZnSn}_8(\text{ZnMes})_2]\}^{4-}$ Inverse Sandwich-Type

Cluster Supported by Zn^I-Zn^I Bond”, *Angew. Chem. Int. Ed.*, **2021**, *60*, 9990-9995. (IF = 16.82, citations = 7)

20) Semenok D. V., Zhou D., Kvashnin A. G., Huang X., Galasso M., Kruglov I. A., Ivanova A. G., Gavriiliuk A. G., Chen W., Tkachenko N. V., Boldyrev A. I., Troyan I., Oganov A. R., and Cui T. “Novel Strongly Correlated Europium Superhydrides”, *J. Phys. Chem. Lett.*, **2021**, *12*, 32-40. (IF = 6.89, citations = 26)

19) Xu H.-L., Tkachenko N. V., Wang Z.-C., Chen W.-X., Qiao L., Munoz-Castro A., Boldyrev A. I., and Sun Z.-M. “A Sandwich-Type Cluster Containing Ge@Pd₃ Planar Fragment Flanked by Aromatic Nonagermanide Caps”, *Nat. Commun.*, **2020**, *11*, 5286. (IF = 17.69, citations = 13)

18) Narendrapurapu B. S., Bowman M. C., Xie Y., Schaefer III H. F., Tkachenko N. V., Boldyrev A. I., and Li G. “Dibridged, Monobridged, Vinylidene-Like, and Linear Structures for the Alkaline Earth Dihydrides Be₂H₂, Mg₂H₂, Ca₂H₂, Sr₂H₂, and Ba₂H₂. Proposals for Observations”, *Inorg. Chem.*, **2020**, *59*, 10404-10408. (IF = 5.44, citations = 2)

17) Xu H. L., Popov I. A., Tkachenko N. V., Wang Z. C., Munoz-Castro A., Boldyrev A. I., and Sun Z.-M. “σ-Aromaticity-Induced Stabilization of Heterometallic Supertetrahedral Clusters [Zn₆Ge₁₆]⁴⁺ and [Cd₆Ge₁₆]⁴⁺”, *Angew. Chem. Int. Ed.* **2020**, *59*, 17286-17290. (IF = 16.82, citations = 19)

16) Wang Z. C., Tkachenko N. V., Qiao L., Matito E., Muñoz-Castro A., Boldyrev A. I., and Sun Z.-M. “All-Metal σ-Antiaromaticity in Dimeric Cluster Anion {[CuGe₉Mes]₂}⁴⁻”, *Chem. Commun.*, **2020**, *56*, 6583-6586. (IF = 6.07, citations = 17)

- 15) Steglenko D. V., Tkachenko N. V., Boldyrev A. I., Minyaev R. M., and Minkin V. I. “Stability, electronic and optical properties of two-dimensional phosphoborane”, *J. Comp. Chem.*, **2020**, *41*, 1456-1463. (IF = 3.67, citations = 14)
- 14) Tkachenko N. V., Zhang X. W., Qiao L., Shu C. C., Steglenko D., Munoz-Castro A., Sun Z.-M., and Boldyrev A. I. “Spherical aromaticity of all-metal $[\text{Bi}@\text{In}_8\text{Bi}_{12}]^{3-/5-}$ clusters”, *Chem. Eur. J.*, **2020**, *26*, 2073-2079. (IF = 5.02, citations = 14)
- 13) Tkachenko N. V., Song B., Steglenko D., Minyaev R. M., Yang L. M., and Boldyrev A. I. “Computational Prediction of the Low Temperature Ferromagnetic Semiconducting Two-Dimensional SiN Monolayer”, *Phys. Status Solidi B*, **2020**, *257*, 1900619. (IF = 1.78, citations = 11)
- 12) Tkachenko N. V., Steglenko D., Fedik N., Boldyreva N. M., Minyaev R. M., Minkin V. I., and Boldyrev A. I. “Superoctahedral Two-Dimensional Metallic Boron with Peculiar Magnetic Properties”, *Phys. Chem. Chem. Phys.*, **2019**, *21*, 19764-19771. (IF = 3.95, citations = 30)
- 11) Tkachenko N. V., Sun Z.-M., and Boldyrev A. I. “Record Low Ionization Potentials of Alkali Metal Complexes with Crown Ethers and Cryptands”, *ChemPhysChem*, **2019**, *20*, 2060-2062. (Highlighted as Very Important Paper, featured on the Front Cover Page, highlighted in ChemViews Magazine) (IF = 3.52, citations = 20)
- 10) Tkachenko N. V., and Boldyrev A. I. “Multiple Local σ -Aromaticity of the Nonagermanide Clusters”, *Chem. Sci.*, **2019**, *10*, 5761-5765. (IF=9.97, citations = 25)
- 9) Liu C., Tkachenko N. V., Popov I. A., Fedik N., Min X., Xu C. Q., Li J., McGrady J. E., Boldyrev A. I., and Sun Z.-M. “Structure and Bonding in $[\text{Sb}@\text{In}_8\text{Sb}_{12}]^{3-}$ and

[Sb@In₈Sb₁₂]⁵⁻”, *Angew. Chem. Int. Ed.*, **2019**, *58*, 8367-8371. (Featured on the Inside Cover Page) (IF = 16.82, citations = 26)

8) Tkachenko N. V., and Boldyrev A. I. “Chemical bonding analysis of excited states using the adaptive natural density partitioning method”, *Phys. Chem. Chem. Phys.*, **2019**, *21*, 9590-9596. (IF = 3.95, citations = 60)

7) Tkachenko N. V., and Scheiner S. “Optical Stability of 1,1'-Binaphthyl Derivatives”, *ACS Omega*, **2019**, *4*, 6044-6049. (IF = 4.13, citations = 11)

6) Tkachenko N. V., and Bryliakov K. P. “Transition Metal Catalyzed Aerobic Asymmetric Coupling of 2-Naphthols”, *Mini Rev. Org. Chem.*, **2019**, *16*, 392-398. (IF = 2.16, citations = 7)

5) Salnikov G. E., Genaev A. M., Shernyukov A. V., Zhu Z., Tkachenko N. V., and Koltunov K. Y. “Configurational Stability of 1,1'-Bi-2-naphthol in Superacid System HSO₃F–SbF₅–SO₂ClF”, *Russ. J. Org. Chem.*, **2018**, *54*, 792-794. (IF=0.70, citations = 6)

4) Tkachenko N. V., Lyakin O. Y., Zima A. M., Talsi E. P., and Bryliakov K. P. “Effect of Different Carboxylic Acids on the Aromatic Hydroxylation with H₂O₂ in the Presence of an Iron Aminopyridine Complex”, *J. Organomet. Chem.*, **2018**, *871*, 130-134. (IF=2.35, citations = 7)

3) Lyakin O. Y., Zima A. M., Tkachenko N. V., Bryliakov K. P., and Talsi E. P. “Direct Evaluation of the Reactivity of Nonheme Iron(V)-Oxo Intermediates toward Arenes”, *ACS Catalysis*, **2018**, *8*, 5255-5260. (IF = 13.70, citations = 35)

2) Tkachenko N. V., Ottenbacher R. V., Lyakin O. Yu., Zima A. M., Samsonenko D. G., Talsi E. P., and Bryliakov K. P. “Highly Efficient Aromatic C-H Oxidation with H₂O₂ in the Presence of Iron Complexes of the PDP Family”, *ChemCatChem*, **2018**, *10*, 4052-4057. (IF=5.50, citations = 24)

1) Tkachenko N. V., Lyakin O. Y., Samsonenko D. G., Talsi E. P., and Bryliakov K. P. “Highly Efficient Asymmetric Aerobic Oxidative Coupling of 2-Naphthols in the Presence of Bioinspired Iron Aminopyridine Complexes”, *Catal. Comm.*, **2018**, *104*, 112-117. (IF=3.63, citations = 15)

CONFERENCES AND INVITED TALKS

Invited seminar at Computer Science Department, Utah State University “Quantum Computing and Its Applications in Quantum Chemistry” | 30 November **2022**, Logan, USA

Invited seminar at Stanford University “Exploring the Electronic-Structure Problem with Quantum Computers and Deciphering Exotic Chemical Bonding in Clusters and Solids” | 8 September **2022**, Stanford, USA

Invited talk at International Conference on Chemical Bonding, “Simulating Electronic Structure on Quantum Computers with PermVQE and QDavidson Algorithms” | 11-17 August **2022**, Kauai (Hawaii), USA

ACS National Meeting & Expo, Oral Presentation, the symposium on "Synergy Between Quantum Computing and High-Performance Computing in Quantum Chemistry and Materials Science" | 5-16 April **2021**, USA

ACS National Meeting & Expo, Physical Chemistry Poster Session, Sci-Mix Session || 25-29 August **2019**, San Diego (CA), USA

27th International Chugaev Conference on Coordination Chemistry, Oral Presentation, “Physicochemical Methods in Coordination Chemistry” || 2-6 October **2017**, Nizhny Novgorod, Russia

IV Scientific Conference Boreskov Readings dedicated to the 110th anniversary of Academician Georgii K. Boreskov, Poster Session || 19-21 April **2017**, Novosibirsk, Russia

EMPLOYMENT HISTORY

01/2021-**Present** **Research Assistant, *Utah State University, USA***

05/2019-12/2019

Responsibilities:

08/2018-12/2018

Collecting and analyzing the data obtained during the computational research work; writing scientific papers; conceiving and designing of scientific projects.

01/2022-**Present** **LANL Student Contractor, Utah State University, USA**

01/2021-09/2022

Responsibilities:

Collecting and analyzing the data obtained during the computational/theoretical research work; writing scientific papers; conceiving and designing of scientific projects.

06/2020-08/2020 **Graduate Research Assistant, *Los Alamos National Laboratory, USA***

Responsibilities:

Collecting and analyzing the data obtained during the computational research work; writing scientific papers; conceiving and designing of scientific projects.

08/2020-12/2020 **Teaching Assistant, *Utah State University, USA***

01/2020-04/2020

Responsibilities:

01/2019-04/2019

Conducting General Chemistry Recitations, Chemical Principles Laboratories, and Physical Chemistry; Grading students' works.

06/2016-07/2018 **Research Assistant, *Borshkov Institute of Catalysis, Russia***

Responsibilities:

Collecting and analyzing the data obtained during the experimental research work; writing scientific papers.

06/2015-05/2016 **Research Assistant, *Nikolaev Institute of Inorganic Chemistry, Russia***

Responsibilities:

Collecting and analyzing the data obtained during the experimental research work.

GRANTS AND SPECIAL ACTIVITIES

Spring 2021 – Fall 2022 Participating in Los-Alamos National Laboratory sub-contract with Utah State University on the topic “Quantum Chemistry on Quantum Computers”

Summer 2020 Participating in Los-Alamos National Laboratory Graduate Research Assistantship program. “Quantum Chemistry on Quantum Computers”, DR project.

Summer 2018 – Fall 2019 Participating in National Science Foundation grant CHE-1664379

SKILLS

Programming using the following languages: Python 3, C++;

Developing scientific software: AdNDP 2.0, DFT-driven-PSO;

Expertise in QC software: Gaussian, ORCA, VASP, CP2K; AdNDP; AdNDP 2.0; SSAdNDP; MultiWFN;

Group website administration;